Chris Helmut Sala, BSc

Novel Sulfur-rich Molybdenum Scorpionate Complexes - Synthesis and Theory

MASTERARBEIT

zur Erlangung des akademischen Grades

Diplom-Ingenieurin

Masterstudium Biochemie und Molekulare Biomedizin

eingereicht an der

Technischen Universität Graz

Betreuerin

Univ.-Prof. Dipl.-Chem. Dr. rer. nat. Nadia Carmen Mösch-Zanetti

Institut für Chemie (Anorganische Chemie)
Karl-Franzens-Universität Graz

Ao.-Univ.-Prof. Dr. phil. Alexander Sax
Institut für Chemie (Physikalische und Theoretische Chemie)

Graz, Juni 2014
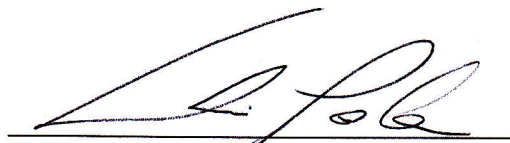
EIDESSTATTLICHE ERKLÄRUNG

AFFIDAVIT

Ich erkläre an Eides statt, dass ich die vorliegende Arbeit selbstständig verfasst, andere als die angegebenen Quellen/Hilfsmittel nicht benutzt, und die den benutzten Quellen wörtlich und inhaltlich entnommenen Stellen als solche kenntlich gemacht habe. Das in TUGRAZonline hochgeladene Textdokument ist mit der vorliegenden Masterarbeit identisch.

I declare that I have authored this thesis independently, that I have not used other than the declared sources/resources, and that I have explicitly indicated all material which has been quoted either literally or by content from the sources used. The text document uploaded to TUGRAZonline is identical to the present master's thesis.

17. 06. 2014
_____
Datum / Date

_____
Unterschrift / Signature

"Chemists are a strange class of mortals, impelled by an almost maniacal impulse to seek their pleasures amongst smoke and vapour, soot and flames, poisons and poverty, yet amongst all these evils I seem to live so sweetly that I would rather die than change places with the King of Persia."

by Johann Joachim Becher, Physica subterranea (1667)

Acknowledgement

Abstract

This project focussed on the synthesis of novel pyridazine and methimazole based scorpionate Mo complexes. Established methods were applied in ligand synthesis, modifications introduced if necessary. Reduction of the water content in the formation of the 6-*tert*-butylpyridazine-3-one precursor increased the yield from 17 to >60 %. The use of toluene as solvent in the synthesis of pyridazine based scorpionate ligands resulted in irreproducible ranging of yields from 0 to >90 %. The reaction of the pyridazine scorpionate ligand Tn^{tBu} with the low valent $[Mo(CO)_3(MeCN)_3]$ (**1**) precursor yielded the unexpected dimeric Mo complex **8a** with two pyridazines as bridging units, instead of the desired scorpionate complex. A variety of differently substituted, pyridazinones and pyridazinthiones were reacted with NaH to yield the respective sodium salts in high yields. It could be shown, that **8a** was also accessible from the reaction of **1** with the sodium salt of 6-*tert*-butylpyridazine-3-thione.

The procedure for the synthesis of $Li[PhBH_3]$ was modified by dissolving $PhB(OH)_2$ in THF/Et_2O, allowing a more controlled addition to $LiAlH_4/Et_2O$ solution. The phenyl substituted methimazole scorpionate ligand PhTm was synthesized from $Li[PhBH_3]$ with an excess of methimazole. The attempt to synthesize the pyridazine based counterpart $PhTn^{tBu}$ by the same route was not successful. The reaction of **1** with PhTm resulted in the formation of an air-sensitive complex **7e**, in which only two of three sulfur atoms were coordinated to the Mo central atom. Unexpectedly, four carbonyls were coordinated to the Mo atom, despite starting from a $[Mo(CO)_3]$ fragment. The mechanism of the carbonyl transfer was not within the scope of this thesis. Cation exchange from Li^+ to $[NBu_4]^+$ facilitated the isolation and crystallisation of another novel complex **8e**.

The unexpected degradation reaction of the pyridazine based scorpionate ligand was subject to an investigation using DFT. A comparison of the shared electron numbers of the $B-N$ bond suggested an only marginally weaker $B-N$ bond in Tn^{tBu} (2-6 %). There were hardly any differences in the formation reactions of the ligands and complexes from a thermodynamical point of view.

In case of a dissociation the negative charge would reside at the cleaved methimazole or pyridazine moiety. A second dissociation step of the formed neutral boron species was significantly less likely. The presence of THF solvent molecules in close proximity to neutral and positively charged dissociation products was found to have an stabilizing effect. A stepwise bond stretch revealed energy barriers with a maximum of roughly 150 kJ/mol at a $B-N$ distance of 2.7 Å for both ctTm and $ctTn^{tBu}$ in presence of a THF molecule.

Consideration of the thione-thiol tautomerism showed, that the thiol form had significant lower contribution in case of methimazole. If the thiol tautomer was an intermediate in the degradation process, this result would be a possible explanation for the instability of the Tn^{tBu} ligand in the presence of an Mo compound.

Zusammenfassung

Das Projekt war auf die Synthese neuartiger Pyridazin- und Methimazol-basierten Mo Skorpionatkomplexen fokussiert. Etablierte Methoden wurden in der Ligandensynthese angewandt, Modifikationen eingeführt, falls notwendig. Eine Reduktion des Wassergehalts bei der Bildung von 6-*Tert*-butylpyridazin-3-on steigerte die Ausbeute von 17 auf >60 %. Die Verwendung von Toluol als Lösungsmittel für die Synthese Pyridazin basierter Skorpionatliganden führte zu stark schwankenden Ausbeuten zwischen 0 und >90 %.

Die Reaktion des Pyridazin Skorpionatligands Tn^{tBu} mit der niedervalenten $[Mo(CO)_3(MeCN)_3]$ (**1**) Vorläuferverbindungen führte zu dem unerwarteten, dimeren Mo Komplex **8a** mit zwei verbrückenden Pyridazinen, anstatt des gewünschten Skorpionatkomplexes. Eine Reihe unterschiedlich substituierter Pyridazinone und Pyridazinthione wurden mit Nah umgesetzt, um die jeweiligen Natriumsalze in hoher Ausbeute zu isolieren. Es konnte gezeigt werden, dass **8a** auch durch die Reaktion von **1** mit dem Natriumsalz von 6-*Tert*-butylpyridazin-2-thion zugänglich war.

Die Syntheseprozedur von $Li[PhBH_3]$ wurde durch Lösen von $PhB(OH)_2$ in THF/Et_2O modifiziert, wodurch eine kontrolliertere Zugabe zur $LiAlH_4/Et_2O$ Lösung erlaubt war. Der Phenyl substituierte Methimazol Skorpionatligand PhTm wurde ausgehend von $Li[PhBH_3]$ mit einem Überschuss an Methimazol synthetisiert. Der Versuch das Pyridazin basierte Pendant $PhTn^{tBu}$ nach der gleichen Methode zu synthetisieren, war nicht erfolgreich. Die Reaktion von **1** mit PhTm resultierte in der Bildung des luftempfindlichen Komplexes **7e**, in dem nur zwei der drei Schwefelatome ans Mo Atom koordinierten. Unerwarteterweise waren vier Carbonyle an das Mo Atom koordiniert, obwohl ein $[Mo(CO)_3]$ Fragment eingesetzt wurde. Der Mechanismus des Carbonyltransfers war nicht Gegenstand dieser Abschlussarbeit. Kationenaustausch von Li^+ zu $[NBu_4]^+$ erleichterte die Isolierung und Kristallisation eines weiteren neuen Komplexes **8e**.

Die unerwartete Abbaureaktion des Pyridazin basierten Skorpionatliganden war Gegenstand der Untersuchung mittels DFT. Ein Vergleich der shared electron numbers der $B-N$ Bindungen wies auf eine marginal schwächere $B-N$ Bindung in Tn^{tBu} hin (2-6 %). Vom thermodynamischen Standpunkt aus betrachtet, gab es kaum Unterschiede in den Bildungsreaktionen der Liganden und Komplexe.

Im Falle einer Dissoziation würde sich die negative Ladung an der abgespalten Methimazol oder Pyridazin aufhalten. Eine zweite Dissoziation der gebildeten neutralen Borspezies war deutlich unwahrscheinlicher. Die Anwesenheit von THF Lösungsmittelmolekülen in räumlicher Nähe hatte einen stabilisierenden Effekt auf neutrale oder positiv geladene Dissoziationsprodukte. Eine schrittweise Bindungsdehnung zeigte eine Energiebarriere mit einem Maximum von etwa $150\,\mathrm{kJ/mol}$ bei einer $B-N$ Distanz von $2{,}7\,\text{Å}$ für ctTm und $ctTn^{tBu}$ in Anwesenheit eines THF Moleküls.

Die Betrachtung der Thion-Thiol Tautomerie zeigte, dass die Thiolform einen deutlich geringeren Anteil im Falle von Methimazol hat. Sollte das Thiol Tautomer ein Intermediat im Abbauprozess sein, so wäre dieses Ergebnis eine mögliche Erklärung für die Instabilität des Tn^{tBu} in Gegenwart einer Mo Verbindung.

Contents

Chapter 1

Introduction

Molybdenum (Mo), element number 42, is a second row transition metal in group 6 of the periodic table. Elemental Mo was first isolated by P.J. Hjelm in 1782. There are seven natural isotopes (A = 92, 94, 95, 96, 97, 98 and 100) with a relative abundance between $9.25\,\%$ ($^{94}_{42}$Mo) and $24.13\,\%$ ($^{98}_{42}$Mo).[1]

Mo is a hard but ductil metal with a melting point of $2620\,^{\circ}$C and a density of $10.28\,$g·cm^{-3}. The most important and stable oxidation state in Mo chemistry is +VI. Its high number of oxidation states (-II to +VI) and different possible coordination numbers (4 to 8) allow a versatile chemistry, becoming apparent in its key roles in biological systems as well as manifold applications in industrial processes.[1]

1.1 Industrial Applications

In nature Mo can be found in different ores, but only molybdenite (MoS_2) is of economical interest.[2] The mined ore is being milled to reach the desired grain size of 3-10 μm. Flotation and if necessary acid leaching reduces undesired impurities and yields a concentrate of up to $92\,\%$ MoS_2.[3]

The next step is a roasting process, in which MoS_2 is converted to MoO_3 using atmospheric oxygen at temperatures between 500-600°C in special furnaces. The reactions are shown in equations 1.1-1.3[3]

$$2\,MoS_2 + 7\,O_2 \longrightarrow 2\,MoO_3 + 4\,SO_2 \tag{1.1}$$

$$MoS_2 + 6\,MoO_3 \longrightarrow 7\,MoO_2 + 2\,SO_2 \tag{1.2}$$

$$2\,MoO_2 + O_2 \longrightarrow 2\,MoO_3 \tag{1.3}$$
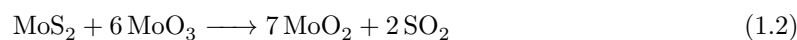
A large fraction (30-40 %) of the so-called technical Mo-oxide is mixed with Fe-oxide. The thermite reaction with aluminium yields Ferromolybdenum (FeMo), an alloy, which is mainly used in "high-strength-low-alloy" (HSLA) steels.[4] Products with higher purity are accessible via sublimation or wet chemical processes. Among the latter dissolution in NH_4OH followed by filtration and/or extraction has been found to be a successful way to yield pure ammoniumdimolybdate $(NH_4)_2Mo_2O_7$ (ADM).[3]

ADM is used as starting material for other Mo based compounds as well as Mo metal. Depending on the starting material, the metal production is a two or three step process (equations 1.4-1.6).

$$(\text{NH}_4)_2\text{Mo}_2\text{O}_7 \longrightarrow 2\,\text{NH}_3 + 2\,\text{MoO}_3 + \text{H}_2\text{O} \tag{1.4}$$

$$\text{MoO}_3 + \text{H}_2 \xrightarrow{450\text{-}650^\circ\text{C}} \text{MoO}_2 + \text{H}_2\text{O} \tag{1.5}$$

$$\text{MoO}_2 + 2\,\text{H}_2 \xrightarrow{1000\text{-}1100^\circ\text{C}} \text{Mo} + 2\,\text{H}_2\text{O} \tag{1.6}$$
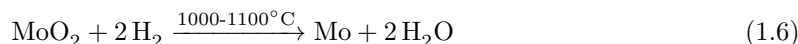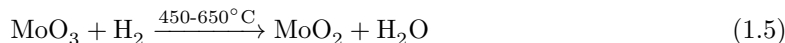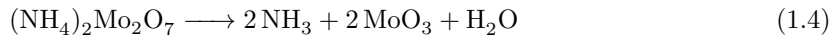
Single step reduction at temperatures of 1000-1100°C is not desirable, due to substantial losses of MoO_3 through evaporation above 800°C. Additionally side reactions forming different lower Mo-oxides (e.g. equation 1.7), accompanied by sintering processes, lead to products of lower quality. [5]

$$2\,\text{MoO}_3 + \text{Mo} \longrightarrow 3\,\text{MoO}_2 \tag{1.7}$$

Owing its special physical and chemical properties Mo has found widespread use in different types of steels and alloys. In stainless steels (>10.5 % Cr) Mo contents of up to 6.1 % increase the corrosion resistance, especially in chloride-containing environments, making these steels favorable for maritime applications. In addition alloys containing Mo feature enhanced hardness, ductility, chemical resistance and heat stability. Therefore Mo alloys can be found in mining drills, cars, ships and aircrafts as well as in the chemical and pharmaceutical industry. [4]

Another important field is the use of MoS_2 as hydrodesulfurisation catalyst in oil and petrol industry. Additionally its layered structure, temperature and pressure resistance allows it to be used as a high performance lubricant in engines. Different molybdates are used in pigments, as smoke suppressants and corrosion inhibitors as well as co-catalysts in selective oxidation reactions. [4]

1.2 Physiological Relevance

Mo is considered an essential trace element. It is ubiquitous, therefore can be found in every living organism. The general opinion is, that natural levels of Mo in the environment pose no health risks.

Due to the growing interest in Mo, studies, concerning the concentration of Mo in the environment, are manifold. An average of 1.2-1.3 mg·kg^{-1} with great deviations has been reported in U.S. soils. Concentrations between 0.2-5 mg·kg^{-1} are considered to be in a normal range. Significantly higher values were measured in areas in proximity to mines and steel industry. [2]

The levels of different Mo species in water are subject to great deviations. While most natural surface waters contain around 1 μg·L^{-1}, anthrophogenic influences result in up to several thousandfold times higher concentrations. [2] The *predicted no effect concentration* (PNEC) for freshwater introduced in the REACH dossiers is 12.7 mg·L^{-1}. [6]

1.2.1 Molybdenum in the human body

The daily intake of Mo strongly depends on the habitual residence, the diet and water consumed. Food accounts for the major part of resorbed Mo. Amounts range from 50-500 μg·d^{-1}, the mean value being around 100 μg·d^{-1}. [2,7] The recommended dietary allowance is 45 μg·d^{-1}, the tolerable upper intake level 2000 μg·d^{-1}. [8] Mo is distributed throughout the body, the highest concentrations

are found in the liver and kidneys with 0.5-1 $\mu g \cdot g^{-1}$ and 0.25 $\mu g \cdot g^{-1}$ wet weight, respectively. Excretion happens mainly via urine.

Its role as an essential metal can be traced back to the fact, that Mo is present in three different enzymes (xanthine dehydrogenase, sulfite oxidase and aldehyde oxidase) in the human body. A more detailed description of Mo based enzymes follows in the section below.

In general a dose-response curve for essential substances can be divided into three areas: an optimal concentration range, a deficiency region at too low concentrations and a toxical level, if a certain threshold concentration is exceeded.[2]

In the case of Mo assigning these regions has been subject to many studies. Friberg and co-workers' review[9] shows, that determining distinct levels is hardly possible. Due to the great dependency on the tested species, extrapolation is difficult to achieve.[8]

Mo is considerably less toxic than many other heavy metals. So far there are no reported cases of acute toxicity caused by an overdose of Mo in human beings. Available data is based on studies on different animals. It could be shown, that ruminating animals, such as cattle, exhibit a higher sensitivity towards increased Mo doses. Nevertheless these results can not be utilized for risk assessment for humans due to great difference of the gastrointestinal tracts.[8] Effects such as reduced growth, infertility or anemia were observed in different laboratory animals but not in humans.[10]

A deficiency in Mo based enzymes causes a severe metabolic dysfunction. The survival rate of newborn children is low, the surviving ones suffering from grave neurological defects. Owing the great Mo absorption efficiency deficiency due to dietary reason has only been observed in a single case.[8]

1.3 Molybdenum based enzymes

The essential role of Mo in living organisms is emphasized by its appearance in over 50 enzymes.[11] These enzymes are responsible for several redoxreactions in different metabolic pathways. Except for in the nitrogenase all Mo is bound to a pterin based compound (pyranopterin), referred to as molybdenum-cofactor (Moco, see Figure 1.1).

A short description of the major Mo based enzymes follows in the paragraphs below. Structural and mechanistic details will be discussed in the context of model compounds in sections 1.4.1 and 1.5.
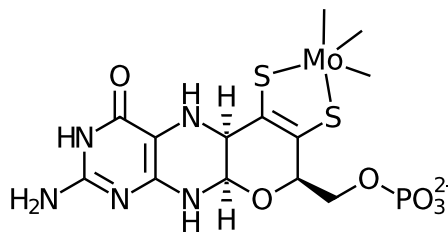
Figure 1.1: Molybdenum-cofactor

Nitrogenase

This Mo and Fe based enzyme enables a few prokaryotic organisms to conduct the process of nitrogen fixation (see equation 1.8).[12] The great importance of the nitrogenase is reflected by numerous publications, focussing on the mechanistic details[12–14] and structure[15,16], which has not been solved until recently.

$$N_2 + 8\,H^+ + 8\,e^- + 16\,MgATP \longrightarrow 2\,NH_3 + H_2 + 16\,MgADP + 16\,P_i \qquad (1.8)$$
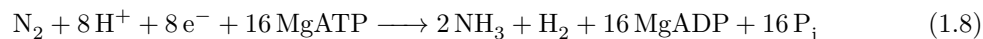
The Xanthine Oxygenase Family

Enzymes belonging to the xanthine oxygenase (XO) family are involved in oxidative hydroxylation reactions of the general type shown in equation 1.9.[17] In the human metabolism xanthine dehydrogenases are present in the purine degradation metabolism and the formation of uric acid from hypoxanthine via xanthine (see Scheme 1.1).[18]

$$R{-}H + H_2O \longrightarrow ROH + 2\,H^+ + 2\,e^- \qquad (1.9)$$
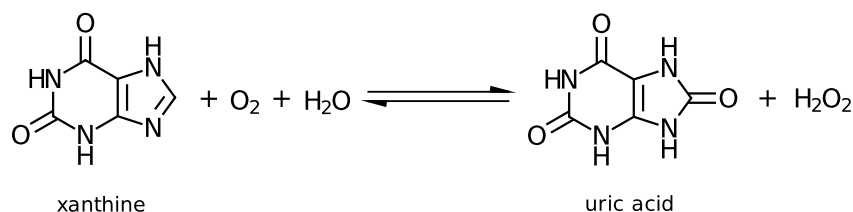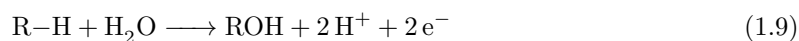
Scheme 1.1: Formation of uric acid from xanthine

Sulfite Oxidase Family

Enzymes, such as the sulfite oxidases (SO) catalyze the oxidation of sulfite to sulfate as shown in equation 1.10. This reaction is of great physiological importance due to the toxicity of SO_3^{2-}. Sulfite dehydrogenase, a member of the SO family, enables certain bacteria to utilize the reaction of thiosulfate to sulfite as energy source.[19]

$$SO_3^{2-} + H_2O \longrightarrow SO_4^{2-} + 2\,H^+ + 2\,e^- \qquad (1.10)$$
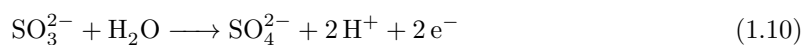
DMSO Reductase Family

The third major Mo depended enzyme family are the DMSO reductases (DMSOR). Members of the DMSOR appear in bacteria and archaea and the Mo central atom is the only redox active center in the enzyme. The overall reaction based on DMSO as substrate is shown in equation 1.11.[17] A broad variety of possible ligands at the active site makes the DMSOR the most diverse Mo based enzyme family.[20]

$$(CH_3)_2SO + 2\,H^+ + 2\,e^- \longrightarrow (CH_3)_2S + H_2O \qquad (1.11)$$
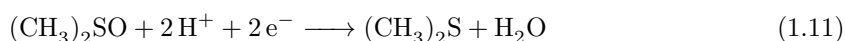
1.3.1 Mechanistic Details

Despite differences in their active sites, the general mechanisms of three major Mo based enzyme families proceed in a similar manner. The general features will be explained using the example of DMSOR (see Scheme 1.1).
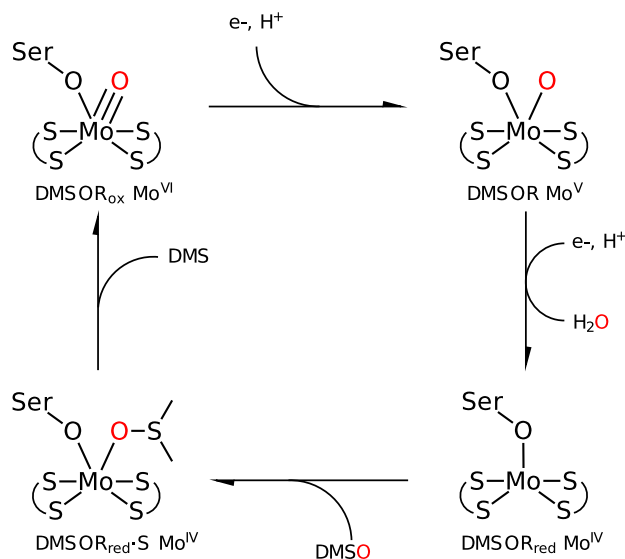
Scheme 1.1: Postulated catalytic mechanism of the DMSOR[a]

The biological relevant oxidation states of the enzymes are +IV to +VI. The catalytic cycle can be divided into an oxidative and reductive half cycle. The substrate binds via its oxygen atom to the reduced Mo^{IV} in the active site. The Mo^{IV} is oxidized to Mo^{VI} and the deoxygenated product is released. Subsequently, a first single electron reduction step leads to an EPR-active Mo^{V} species, a second one regenerates the active Mo^{IV} and eliminates H_2O as by-product. This commonly accepted cycle is shown in Scheme 1.1.[21]

An interesting fact is, that the high concentrations of dimethylsulfide (DMS) generated in *in-vitro* experiments reverse the oxidative step, since DMS is able to bind to the terminal oxo group. This intermediate has been isolated and its crystal structure solved in 1998.[22]

XO Family The mechanism of the XO has been studied thoroughly, using experimental techniques, such as EPR spectroscopy or kinetic experiments, as well as theoretical calculations.

It could be shown, that H_2O rather than molecular O_2 acted as oxygen donor.[23] ^{18}O-labeling experiments under single turnover conditions provided evidence for the transfer of a catalytical site's oxygen atom and subsequent regeneration using H_2O.[24]

1.4 Model systems for Moco based enzymes

Studying enzymes is a very challenging task due to the size and sensitivity of the molecules. The synthesis of model compounds is demanded in order to elucidate the reaction mechanism. Generally, synthetic analogues can be divided in structural and functional models.

The aim of structural models is to match the active site of the respective enzyme as close as possible. Based on crystallographic and spectroscopic data information about the electronic and structural details, such as oxidation state, ligand binding and stereochemistry, is accessible.

Functional models execute the same type of reaction in a catalytic or at least stoichiometric manner. A great advantage of these models is the possibility to investigate the effect of manipulations at ligands directly coordinated to the the catalytically active center. Kinetic and spectroscopic studies of different well defined model compounds facilitate the elucidation of mechanistic details.

These two groups will be described in more detail in the following sections.

1.4.1 Structural Models

This section is focussed on structural models. First models were developed to mimic the coordination of the molybdopterin over its two sulfur atoms. The model ligands are shown in Figure 1.2.
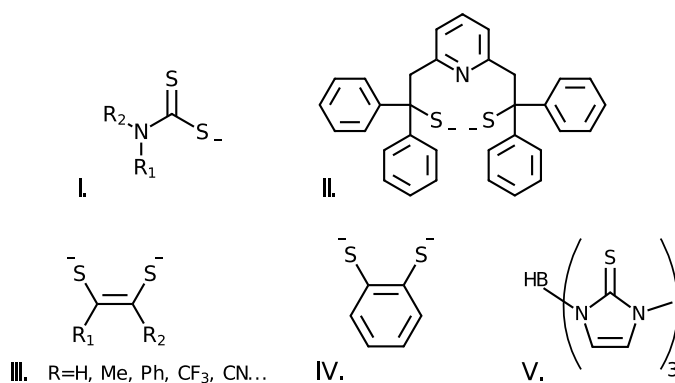
Figure 1.2: Ligands and model complexes

The early models were based on different dithiocarbamate ligands (see Figure 1.2 I).[25,26] Despite being also active in oxygen atom transfer (OAT), these type of systems were not considered to be good model compounds, since they were prone to dimerisation reactions (see equation 1.12) and the ligand did not resemble the binding situation of the dithiolene moiety of the pyranopterin cofactor because of a different bite angle.[27] So-called LNS$_2$ system were the second important group of non dithiolene ligands (see Figure 1.2 II).

$$Mo^zO_aL_n + Mo^{z+2}O_{a+1}L_n \rightleftharpoons (L_nMo^{z+1}O_a)_2O \qquad (1.12)$$

The best way to simulate the binding situation of the pyranopterin cofactor were dithiolene ligands. These systems were either based on ene-1,2-dithiolates or on benzene-1,2-dithiolate with a broad variety of substituents (see Figure 1.2 III and IV).

An example of so-called soft scorpionate ligands is shown in Figure 1.2 V. Since this type of ligand was assigned the central role in this work, it will be described in more detail in section 1.7.

1.4.2 Structural Models of the XO Family

The active site of XO is shown in Figure 1.3a. Synthesis of models for the XO family featuring a *cis*-[Mo$^{\text{VI}}$OS] moiety proved to be difficult, due high reactivity of the sulfido group.

(a) Active site   (b) Structural Model

Figure 1.3: Active site and model compound of the XO family

Some of the only stable models exhibiting a *cis*-[Mo$^{\text{VI}}$OS] fragment were reported by Thapper *et al.*[28] in 1999. This models were stabilized by bulky, differently substituted phenanthrolines (see Figure 1.3b). Thus far, the synthesis of a model compound, featuring both the *cis*-[Mo$^{\text{VI}}$OS] fragment and a dithiolene ligand, has not been accomplished.

1.4.3 Structural Models of the SO Family

The active side of the SO family is shown in Figure 1.4. The *cis*-[MoO$_2$] fragment proved to be less challenging than the [MoO(S)] core of the XO family.
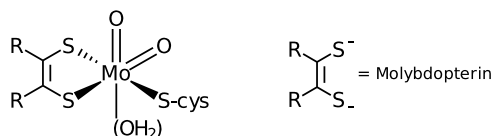
Figure 1.4: Active site of the SO family

Two of the SO models are shown in Figure 1.5. The first one was an example for a non-dithiolene system, similar to Figure 1.2 II, mimicking the EPR active Mo$^{\text{V}}$ intermediate.[29] Dithiolene systems as in Figure 1.5 II were more successful, due to their better resemblance of the actual coordination sphere.[30]
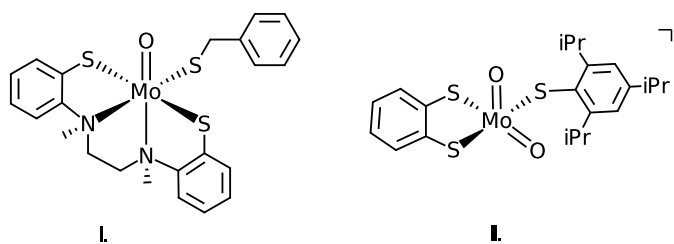
Figure 1.5: Structural models of the SO family

In 1994 a complex in the form of [Mo$^{\text{VI}}$O$_2$(mnt)$_2$]$^{2-}$ with the CN$^-$ substituted ene-1,2-dithiolate (mnt) was synthesized by Das and co-workers. The ever-present dimersation in solution, as described in equation 1.12 was not observed.[31]

1.4.4 Structural Models of the DMSOR Family

The structure of DMSOR was first solved by Schindelin *et al.* in 1996 and it was shown, that the Mo atom in the active site is coordinated by two pyranopterin ligands, an oxo group and the side chain of an aminoacid.[32] The active site is shown in Figure 1.6.
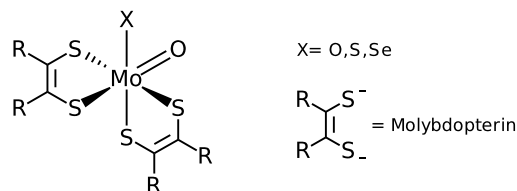
Figure 1.6: Active site of the DMSOR family

The use of dithiolene ligands allowed DMSOR models of type I and II in Figure 1.7. They are accessible via the reaction with the respective Ni complex (see equation 1.13) and subsequent replacement of the two labile CO groups.[33]
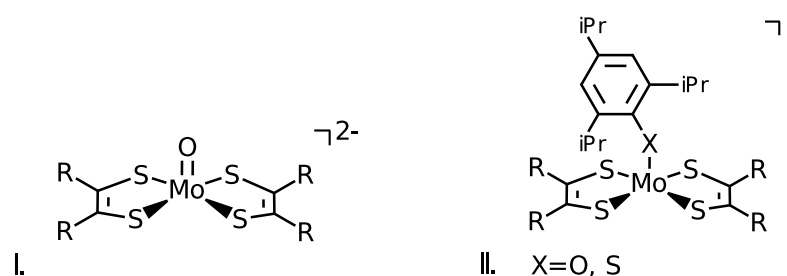
Figure 1.7: Structural models of the DMSOR family

$$[Mo(CO)_3(MeCN)_3] + 2\,[Ni(S_2C_2R_2)_2] \longrightarrow [Mo(CO)_2(S_2C_2R_2)_2] + 2\,[Ni_2^{II}(S_2C_2R_2)_2]_x$$
$$+ CO + 3\,MeCN \quad (1.13)$$
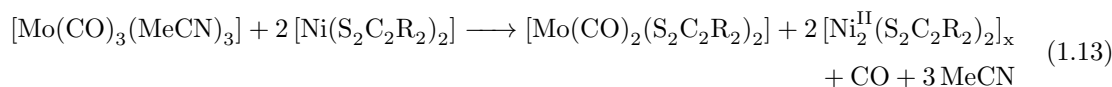
Since only one of the ligands of $[Ni(S_2C_2R_2)_2]$ is transferred, it was assumed, that one ligand is present as a dithiolene and the other one as a dithioketone ligand (see Figure 1.8).[33]
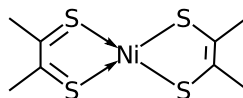
Figure 1.8: Structure of $[Ni(S_2C_2R_2)_2]$

Complexes such as Figure 1.7 I resembled the reduced active site and were active in oxygen atom transfer. A 2-adamantyl group instead of the 2,4,6-triisopropylphenyl moiety in Figure 1.7 II stabilizes X=Se and represents a structural model of DMSOR enzymes featuring a seleno-cysteine moiety.[34] The greater the steric demand of the substituent on X the slower the OAT reaction.[35]

1.5   Functional Models

The aim of functional models is to catalyze the same reaction as the respective enzymes. This reactivity is often gained at the expense of structural similarity. The Holy Grail of bioinorganic chemistry is a model combining both functionality and structural similarity.

Oxygen atom transfer reactions from or to a substrate are also of great economical importance. A comprehensive review article on homogeneous catalysis of olefin epoxidation was recently published by KÃ¼hn and co-workers ranking the most active catalysts up to date.[36] Among these catalysts a complex of the type $[MoO_2L_2]$, with L being 5-(2'-hydroxyphenyl)pyrazole, was published by Mösch-Zanetti and co-workers, featuring excellent yields and a high turnover number of 5000.[37] Research was focussed on the synthesis of systems, that catalyze primary OAT (see equation 1.14). Mo Complexes active in OAT change their oxidation state from +IV to +VI and feature a single terminal oxo group in their reduced state.[27]

$$Mo^{IV}OL_n + XO \rightleftharpoons Mo^{VI}O_2L_n + X \tag{1.14}$$
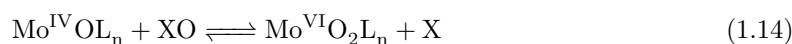
Complexes featuring the ligands described in section 1.4.1 could oft be considered functional models too. Another type of ligand forming functional models are the intensively studied 3,5-disubstituted trispyrazolylborates. These so-called scorpionate complexes will be discussed in more detail in section 1.6.

1.5.1   Functional Models of the XO Family

The synthesis of *cis*-[MoO(S)] complexes remains a challenging task. Only a few relatively stable structural models have been reported and even less functional models thus far. However, a model compound featuring a 3,5-disubstituted trispyrazolylborate and a $[MoO(S)]^{2+}$ center transferred its sulfur rather than its oxygen atom to the substrate. The significance of this will be discussed in more detail later on. A novel functional model has been reported recently. The complex generated *in-situ* could not be isolated, but experimental data points towards $[Et_4N]_2[Mo^{VI}O(S)L_2]$ with L being 1,2-dicarbomethoxyethylene-1,2-dithiolate.[38]

1.5.2   Functional Models of the SO Family

Synthesis of functional models for the SO family was significantly more successful, due to greater stability of the $[MoO_2]$ center.

In 1985 Berg and Holm published complexes of the type $[MoO_2LNS_2]$ (see also Figure 1.9 I), with LNS_2 being tridentate pyridine based ligands with either hydroxy or thiol groups (see Figure 1.2 II).[39] The crystal structure suggested, that the spacial orientation of the phenyl moieties inhibited dimerisation reactions. Complexes of the type $[MoO_2LNS_2]$ catalyzed the oxidation of tertiary phosphines with DMSO as oxygen source (see equation 1.15), but a reorientation of the ligand allowed dimerisation after the OAT.[11]

$$R_3P + DMSO \longrightarrow R_3PO + DMS \tag{1.15}$$

Despite being active in OAT, the model described above was not considered a good functional models, since it was incapable of oxidizing SO_3^{2-} to SO_4^{2-}. However, the most interesting feature

of the SO model $[Mo^{VI}O_2(mnt)_2]^{2-}$ (see Figure 1.9 II) was its ability to oxidize SO_3^{2-} to SO_4^{2-}, hence being a structural and functional model of the active site of the SO. Additionally structural analoga with the biological relevant +V und +IV oxidation states were accessible in the form of $[Mo^VOCl(mnt)_2]^{2-}$ and $[Mo^{IV}O(mnt)_2]^{2-}$, making this system even more valuable.[31]
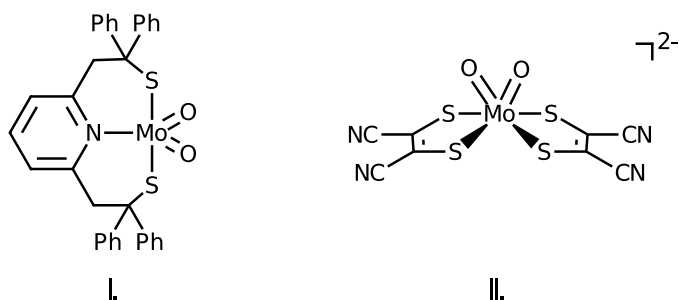
Figure 1.9: Functional models of the SO family

1.5.3 Functional Models of the DMSOR Family

The model given in Figure 1.10 I exhibited slow, but clean primary OAT. This system was subject to many studies, since bulkier ligands, such as shown in Figure 1.7 II, impeded the necessary oxidation step.[11] A review focussing on biomimetic chemistry on DMSOR has been published recently by Schulzke.[40]

A second more reactive model is shown in Figure 1.10 II. The bdtCl$_2$ ligand is able to stabilize the important oxidation states +IV, +V and +VI of Mo. Additionally OAT to Ph$_3$P could be observed
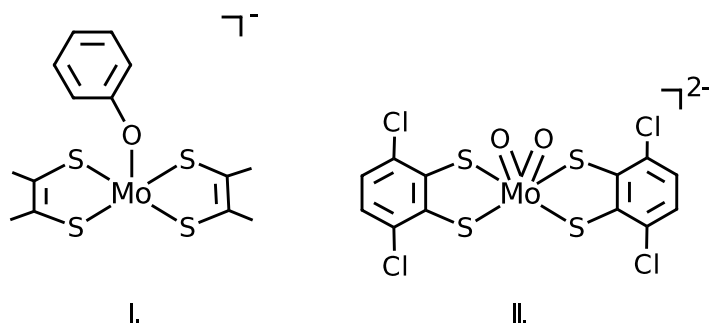
Figure 1.10: Functional models of the DMSOR family

1.6 Scorpionate Ligands and Complexes

The importance of the so-called scorpionate ligands has been indicated in the previous sections. As this project focusses on developing novel scorpionate based Mo complexes, this class of ligands will be described in more detail.

In 1966 polypyrazoyl- and polyazolylborates were introduced as new ligand class by Swiatoslaw Trofimenko. The stability of the derivatives of borates against H_2O induced decomposition was remarkably high and the ligand system reacted with a broad range of metals across the periodic table. As the coordination of these ligands resembled the pincers and sting of a scorpion, this group of ligands was soon to be known as scorpionate ligands (see Figure 1.11[b]).
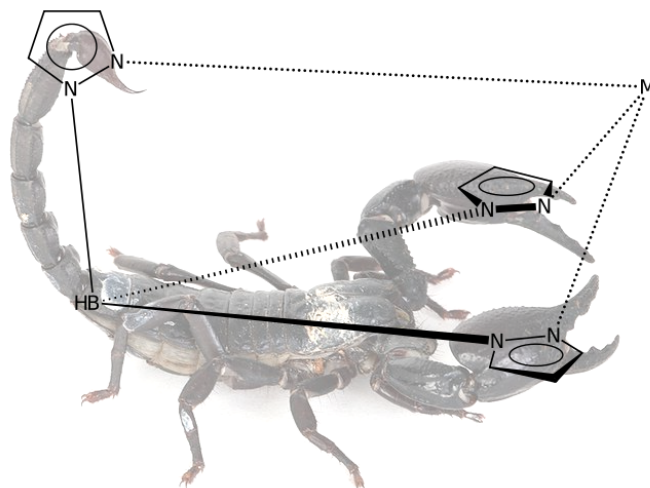
Figure 1.11: Scorpion-like coordination of hydrotrispyrazolylborate (Tp)

1.6.1 Nomenclature

The broad variety of ligands made it necessary to introduce a systematic notation. Moieties bound to the boron atom are abbreviated, e.g. pyrazole = pz or p. The number of moieties bound to the boron atom is denoted by capital letters. T stands for *tris*; B stands for *bis* and is used in heteroscorpionates. Substituents are expressed in a special manner. The numbering scheme of pz is shown in Figure 1.12. Generally, the substituent in 3-position of the pz moiety is denoted as a superscript.
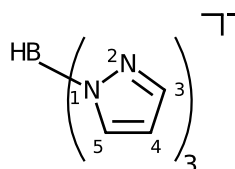
Figure 1.12: Numbering Scheme

---

[b]modified from http://ampest.typepad.com/american-pest-control/2013/11/trivia-time-do-you-know-this-scorpion.html

If a 3→5 spacial rearrangement takes place, it is denoted by a "*". Tp^{Me*} is the shortform of $[HB(3\text{-}Mepz)_2(5\text{-}Mepz)]^-$. Tp* with three 3,5-dimethylpyrazol-1-yl substituent is an exception, because of the importance of this ligand. If there are two different substituents in 3- and 5-position, 5-R is denoted after the 3-R separated by a comma. Two identical substituents are followed by a subscripted 2 (e.g. Tp^{R_2}). The fourth substituent preceedes the symbol (e.g. PhTp = phenyltris-1-pyrazolylborate). These are only some of the rules introduced by Curtis and co-workers[41,42] in order to create a unified notation.[43]

1.6.2 Homo- vs. heteroscorpionate ligands

Generally, there are two classes of scorpionate complexes, namely homo- and heteroscorpionates. In polypyrazolylborate complexes of the general formula $[RR'B(\mu-pz^x)_2ML_n]$ the nature of R' is the crucial factor (see Figure 1.13). If R'= pz^x the complex is considered to be a homoscorpionate with a local C_{3v} symmetry. If R' is not identical to the pz^x moieties, due to e.g. a different substituent (pz^y) or a different moiety altogether, the respective complex belongs to the class of heteroscorpionates with C_s being the highest possible local symmetry.[44] Another possible classification is to distinguish between hard and soft scorpionates. The differences will be considered in the following sections.
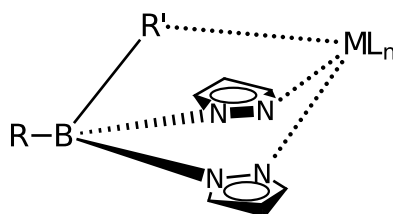
Figure 1.13: R' dependent classification of scorpionates

Trofimenko's pyrazole based scorpionate ligands are often called 1st generation scorpionates. The introduction of bulky substituents R on the pyrazole moiety marks the 2nd generation.[45,46] Scorpionates belonging to the 3rd generation feature a functionalized moiety as the non-coordinating fourth substituent on the boron atom.[47]

1.6.3 Synthesis

The original synthetical pathway published by Trofimenko is based on the addition of the respective borate (e.g. KBH_4) as the limiting factor to a melt of the (substituted) pyrazole (pz^x). Reaction progress can be monitored by measuring the amount of H_2 evolved.[48] The substitution is a stepwise process, that can be controlled precisely by regulation of the temperature of the melt. Depending on the stoichiometry of the reactants the mono-, di-, tri- or tetrasubstituted borates can be isolated after work-up and recrystallization.[46,48]

An alternative method is refluxing the starting materials in dry solvents, such as toluene, xylene or THF. This synthetic pathway is the method of choice when using starting materials, which decompose upon melting or feature high melting temperatures, making a reaction in the melt uncontrollable.

Boron based systems are by far the most common scorpionate ligands. Over the time C, N or

P based ligands have been developed. Changing the bridging atom leads to the neutral and cationic counterparts of the borate based scorpionates and further increases the spectrum of possible compounds. The general method, when synthesizing non boron based scorpionates, is to react respective halides in the desired stoichometry with the heterocycles.[49–52]

1.6.4 General Features

The tridentante scorpionate ligands act as six e$^-$-donors. The sterical demand, number of donated electrons and charge resemble the well established cyclopentadienyl (Cp) ligand. Indeed it was shown, that complexes of the type [LM(CO)$_3$] or [L$_2$M], which were known with Cp ligands, were also accessible, when using scorpionate ligands.[53–56]

Scorpionates coordinating via nitrogen or oxygen, such as polypyrazolylborates and similar ligands are considered to be hard in terms of the HSAB concept. Donor properties can be finetuned to some extent by varying the substituents at the pyrazolyl moieties. The effect of different substituents is manifested in a change of the CO stretching frequencies in carbonyl complexes.[57]

Comparison of Tm, Tp and Cp In contrast to Tp, the so-called soft methimazole based scorpionate ligand Tm coordinated via three sulfur atoms. Soft scorpionate ligands will be described in more detail in section 1.7, since they are of central interest in this thesis.

Nitrosyl complexes of Mo and W were accessible by the reaction of [TmM(CO)$_3$]$^-$ with NOBF$_4$. A theoretical comparison of the structural Cp and Tp analogues confirmed the trends observed in experiments. The IR signals for the C=O stretching frequencies were shifted to lower wavenumbers from Cp to Tm. The better donor properties of the soft Tm ligand enhanced the backbonding into the antibonding $\pi*$ C=O orbital, decreasing the C=O bond strength.[56]

1.6.5 Coordination modes

The great advantage of scorpionate ligands lies in the possibility of tuning their sterical demand and electronic properties by introducing additional or different heteroatoms into the ring system or by using bulkier substituents.

The broad variety of different ligands results in a vast number of different coordination modes. Bi- and tridentate modes are the most common, but even a hexadentate ligand[58] is described in the literature.[44,59–61]

Figure 1.14 shows a selection of different coordination modes. If the sterical demand of the scorpionate ligand and the remaining ligands of the metal fragment is low to moderate, a κ^3-N,N',N" coordination is formed (see Figure 1.14 I).[60] Trofimenko and co-workers[62] reported a Co^{II} complex featuring two different scorpionate ligands (see Figure 1.14 II). The comparably large phenyl moieties prevent the standard κ^3-N,N',N" and result in a κ^3-N,N',H coordination with an agostic B-H-M bond. A κ^2-N,N' mode is the result of the protonation of the respective κ^3-N,N',N" complex (see Figure 1.14 III).[63]

Another unusual coordination is the κ^2-N,H of 1.14 IV. The reason for this mode is still unknown, though it is believed, that steric hindrance plays the central role.[64]

The most abundant coordination mode in soft scorpionate ligands is κ^3-S,S,S with roughly 84 % followed by κ^3-S,S,H (11.5 %), a coordination mode often found in Bm^R-systems. Other modes, such as κ^2-S,S are fairly uncommon.[65]
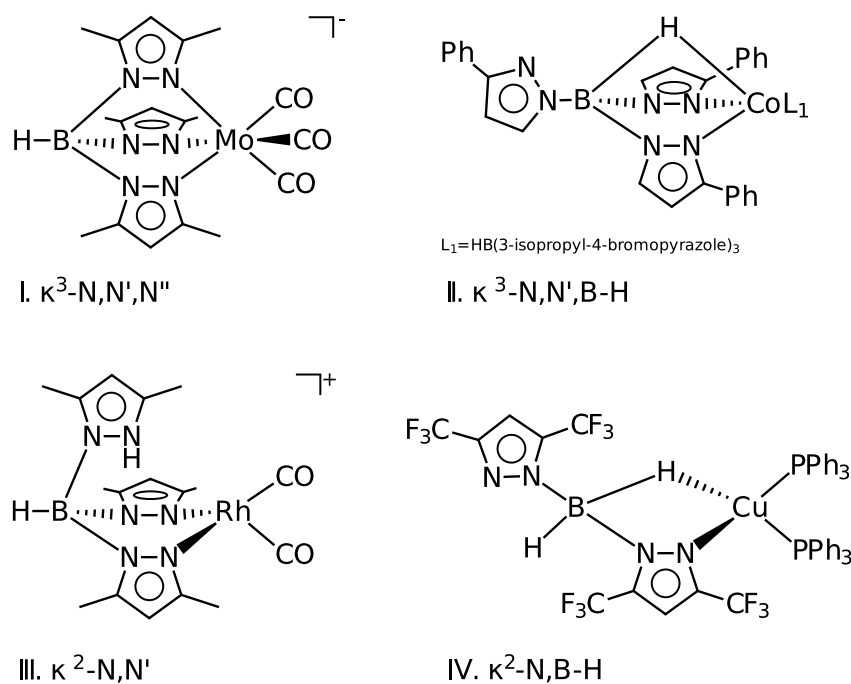
Figure 1.14: Examples for different coordination modes

1.6.6 Mo and W complexes with hard scorpionate ligands

Owing its many oxidation states and possible coordination numbers the first Mo-scorpionate complexes were synthesized shortly after the development of the Tp and Tp* ligands. The broad variety of ligands lead to a plethora of different Mo based complexes. Kisala *et al.* reported the synthesis of low valent Mo complexes with a hydrotris(3-(2-thienyl)-5-methylpyrazolyl)-borate ($Tp^{Th,Me}$) ligand. It was shown that $Tp^{Th,Me}$ acted as a hard ligand and did not coordinate via the sulfur atoms of the thiophen moieties (Th) (see Figure 1.15 I).[66]

The first Mo based scorpionate complexes exhibiting B-H-Mo three center two electron bonds caused by a κ^3-N,N',H coordination mode were published by Kosky and co-workers (see Figure 1.15 II).[67]
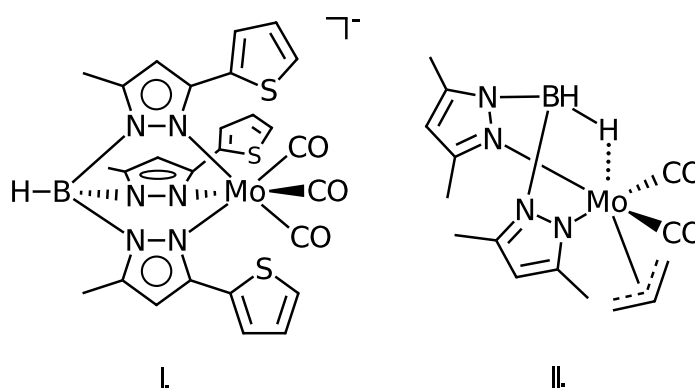
Figure 1.15: Examples for hard Mo scorpionate complexes

A common precursor is $[Mo(CO)_6]$ resulting in $[Mo(CO)_3]$ or $[Mo(CO)_4]$ fragments depending on the dentacity of the scorpionate. The great advantage of these low valent species is simple introduction of other ligands, such as NO^+, Cl^-, ArN_2^+,... by substitution of the remaining carbonyl groups.[68,69]

Just like Mo also tungsten (W) has been found to be present in the active site of enzymes in thermophilic bacteria featuring a pterin moiety.[70] Among the first models were the complexes $[Tp^*W^{VI}O(S)Cl]$ and $[Tp^*W^{VI}S_2Cl]$.[71] Complexes of the type $[Tp^*W^{VI}S_2X]$ react with alkynes to give the respective ene-1,2-dithiolate ligand.[72]

The first W-scorpionate complex featuring a *cis*-dioxotungsten center was $[Tp^*WO_2Cl]$.[71] As discussed in section 1.3.1, the catalytic cycle of Mo and W based enzymes proceeded via two single electron reductions. A drawback of most *cis*-$[M^{VI}O_2]^{2+}$ (M= Mo, W) systems was the formation of $[Mo^VO]^{3+}$ or $[Mo^V2O_3]^{4+}$ species upon single electron reduction, rather than stable *cis*-$[M^VO_2]^+$ centers. By introducing Tp^* ligands, the generation of the desired $[W^VO_2]^+$ species could be accomplished.[73]

The utilization of CO and CO_2 as basic building blocks for chemicals has gained increasing attention due to the negative environmental impact of these compounds. Carbonyloxo-species are believed to be key intermediates in processes such as the industrial methanol synthesis.[74,75] Young and co-workers were able to synthesize a series of tungsten complexes of the type $[Tp^*W(CO)_2X]$ (X=Cl,Br,I), that readily reacted with O_2 to yield the respective $[Tp^*WO(CO)X]$ complexes (see equation 1.16).[76–78]

$$[Tp^*W(CO)_2X] + O_2 \longrightarrow [Tp^*WO(CO)X] + CO_2 \qquad (1.16)$$
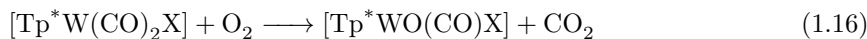
1.6.7 Hard scorpionates as functional models

Different Mo complexes with hard scorpionate ligands were found to be functional models for the OAT. In this section the most important models as well as the catalytical cycle of the SO will be discussed in more detail.

A proposed mechanism for the SO family is illustrated in Scheme 1.2. The first step is the reaction of sulfite with an oxo group of the active site, resulting in an enzyme-product complex $(1 \rightarrow 2)$. Hydrolysis and a first internal electron transfer (IET) forms the EPR-active intermediate $(2 \rightarrow 3)$. A second IET regenerates the initial state $(3 \rightarrow 1)$.[17]

The order of hydrolysis and IET is subject to ongoing discussions in the literature. An IET preceding hydrolysis (via 4) is in accordance with the significant higher IET rates compared to the turnover rates. A pathway via 5 seems possible due to high sulfite concentrations in the experiments. Full proof for either route has yet to be provided.[79]
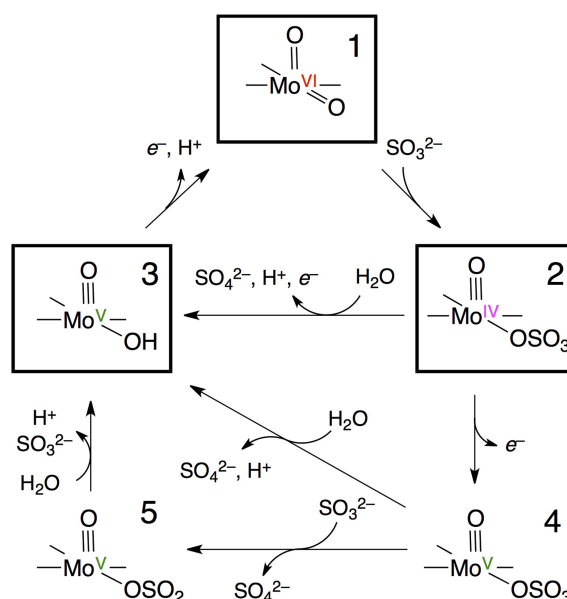
Scheme 1.2: Postulated catalytic mechanism of the SO[c]

The possibility to finetune the steric and electronic properties of Tp made this system cut out for modeling the active site of enzymes. Over the years different models for the key states of enzymatic OAT, covering Mo^{VI}, Mo^{V} and Mo^{IV} species, were synthesized and characterized.[80,81] Finding a fully functional model remained elusive, especially the regeneration of the active $[MoO_2]^{2+}$ center by two single one-electron transfers proved to be a great challenge.

In 1992 Young, Enemark and Wedd presented the complex $[Tp^*Mo^{VI}O_2(SPh)]$, the very first system providing all steps of the catalytic cycle as shown in Scheme 1.3.[82]
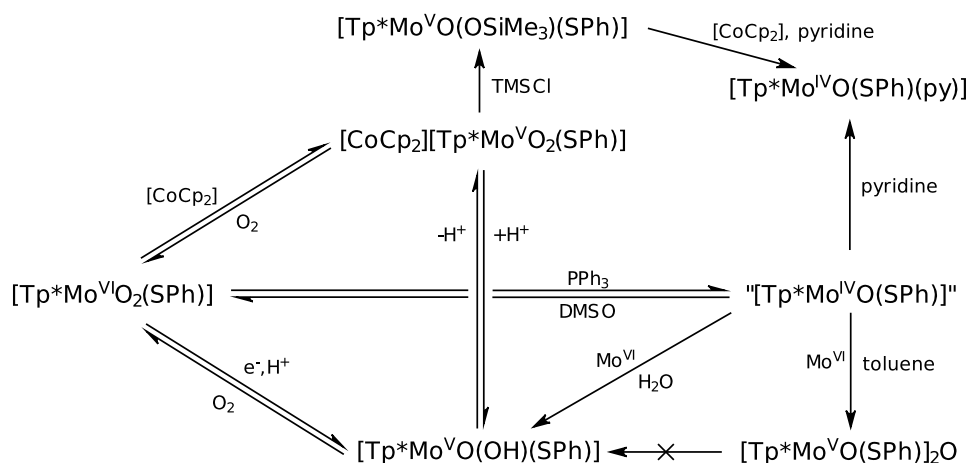
Scheme 1.3: Reactions of $[Tp^*Mo^{VI}O_2(SPh)]$[d]

Starting from $[Tp^*Mo^{VI}O_2(SPh)]$ one of the oxo groups was easily transferred to PPh_3 and the presumably coordinatively unsaturated Mo^{IV} species could be trapped using pyridine. The OAT

---

[c]Reprinted from Klein, E. L. *et al.* Coord. Chem. Rev. **2013**, 257, 110-118., Copyright (2012), with permission from Elsevier.

[d]Adapted with permission from Xiao, Z. *et al.* J. Am. Chem. Soc. **1992**, 114, 9194-9195. Copyright (1992) American Chemical Society.

was highly reversible; the oxidation reaction with DMSO yielded over 90 % of the starting material and was equivalent to the reoxidation of the enzyme's active site. In addition the previously often inaccessible two single electron oxidations/reductions were achieved. [82]

In 2008 Basu and co-workers provided the crystal structures and other spectroscopical data of $[Tp^*MoO(SPh)(OPMe_3)]$ and $[Tp^*MoO(SPh)(CH_3CN)]$, two key intermediates in the OAT of the $[Tp^*MoO_2(SPh)]$ system. [83]

The scorpionate complex $[Tp^{iPr}MoO(S)(OPh)]$ showed an interesting property. While being a disulfido bridged dimer in solid state, a monomeric complex was found in solution. [11] The reaction with CN^- in presence of H_2O yields SCN^- and $[Tp^{iPr}MoO_2(OPh)]$. This behavior is similar to the CN^- induced deactivation of XO enzymes. [84]

The latest work in the field of functional models includes the challenge to isolate the reactive intermediates such as the oxo(aqua)-Mo(V) or oxo(hydroxo)-Mo(IV) species. These compound are supposedly key intermediates in the catalytic cycles of the Mo based enzymes. Since these enzymes are active in the aqueous environments, a change to aqueous conditions is desirable in order to promote and stabilize the formation of these complexes. Watersoluble ligands such as tris(pyrazolyl)methanesulfonate ligands (Tpms, see Figure 1.16) have been reported in litera-ture. [85,86] Another approach involves stabilization caused by hydrogen bonds. Up until now these approaches have been successful only for several first row metals, e.g. Ni, Co and Mn complexes with $Tp^{COOEt,Me}$ [87], but not for Mo. [88]
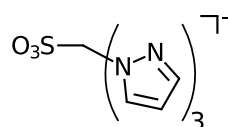
Figure 1.16: Watersoluble scorpionate ligands

1.7   Soft Scorpionates

Hard scorpionate ligands were successfully applied in the modelling of functional compounds for Mo based enzymes. The major drawback of these systems was their inability to mimic the sulfur rich environment of the enzyme's active site.

Introducing "soft" sulfur instead of "hard" nitrogen was first achieved in 1994. The ligand system was based on thioethers (see Figure 1.18 I) and used to mimic the sulfur-rich environment in molybdoenzymes. [89]

The main difference to the established scorpionate ligands was, that it coordinated via the sulfur atoms of the thioethers. Sulfur is less electronegative, has a larger atomic radius and polarisability than nitrogen or oxygen and is considered to be soft in terms of the HSAB concept. Scorpionate ligands can thus be classified in terms of "hard" or "soft" scorpionates. [90,91]

1.7.1   Tautomerism of methimazole

The "workhorse" among the soft scorpionates hydrotris(methimazolyl)borate (Tm) was developed by Garner and co-workers in 1996 (see Figure 1.17).
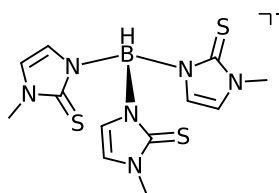
Figure 1.17: The Tm ligand

Methimazole (1-methyl-3H-imidazole-2-thione, mtH) is a heterocyclic compound, in which a thione and thiol form, in analogy to a keto-enol tautomerism, is possible. Depending on the location of the acidic hydrogen the formation of a B−N or B−S bond could be possible. It was shown, that the hydrogen atom was located at the N rather than the S atom. The tautomeric thione and thiol form are shown in Scheme 1.4.[90]
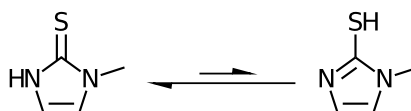
Scheme 1.4: Tautomeric forms of methimazole

1.7.2   Synthesis

The original synthesis of the methimazole based ligands involved the established solvent-free reaction in the melt. Nevertheless the high melting point of methimazole did not allow a controlled stepwise substitution, but rather resulted directly in the trisubstituted product "Tm" (see Figure 1.18 II). A more controlled route of synthesis was stirring in solvents (under reflux). The monosubstituted form was accessible by the reaction in THF at rt,[92] the bisubstituted form at temperatures from 50-110 °C in toluene or THF[93] and the Tm ligand under reflux conditions in toluene.[94] Unlike in the case of pyrazolyl scorpionates tetrakis-substituted form was inaccessible due to a thermal degradation at T > 180 °C.[65]

One of the reasons for the success of the methimazole based scorpionates lied in the easy modification of the moiety by substituting the N-Methyl group and hence controlling the steric demand in analogy to different substituents of Tp^x. Common substituents were Et[95], tBu[96], Ph[94], *p*-iPrPh[96] or Bz[95], but also bulkier ligands such as 4-((2-methoxyphenyl)-1-piperazinyl)butyl[92] were possible.

Several soft scorpionate complexes were prone to degradation reactions (see section 1.7.4). An approach avoiding this kind of degradation was the use alkyl- or arylborohydrides as starting materials. The formed scorpionate ligands of the type RTm (R= e.g. Me[97], Ph[97] or *n*Bu[65] were found to be quite stable against hydrolysis or aerial oxidation.[97] Soft phenyl substitued scorpionate ligands will be in the focus of this project.

1.7.3   Different soft systems

Other soft scorpionates based on thiazolidine-2-thione or benzothiazole-2-thione (see Figure 1.18 III and IV) were synthesized to investigate the influence of the pK_a-value and melting point of the respective thiones. By measuring the amount of generated H_2 it could be shown, that the reaction was less favored with increasing melting temperatures of the substrates.[98]

Ligands featuring moieties like Figure 1.18 V[99] (Tt) and VI[100] are referred to as "Janus ligands", since they possess the ability to coordinate via the soft S- or the hard N- atoms depending on the nature of the central atom. This becomes obvious, when comparing the structures of $[Na(Tt)(dmf)_3]$ and $[Sn(Tt)Cl_3]$. The sodium ion is stabilized by the three nitrogen atoms of Tt, the larger Sn^{IV} by the three sulfur atoms, despite its high charge.
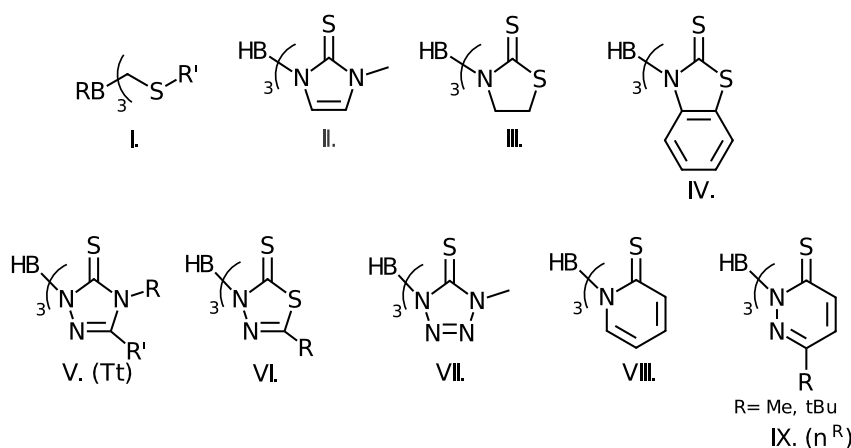
Figure 1.18: Different soft scorpionate ligands

In 2005 Wang, Cao and Bi investigated the chemistry of thioxotetrazoles (see Figure 1.18 VII) as possible models for the active sites of liver alcohol dehydrogenases.[101]

A new class of soft scorpionates was introduced by Owen *et al.* in 2009. Scorpionates based on 2-thiopyridines are considered to be more electron rich than the established Tm system, since the aromatic thiolate tautomer results in a higher electron density on the S atoms.[102] It is also possible to synthesize heteroscorpionates by reaction Bm with one equivalent of 2-thiopyridine yielding a soft scorpionate with two methimazole and one 2-thiopyridine moiety. Attempts to synthesize the analogue with two 2-thiopyridines and a single methimazole group were unsuccessful.[103]

Only recently a thiopyridazine based system has been developed by Mösch-Zanetti and co-workers (see Figure 1.18 IX).[104] Thus far only Co, Ni and Cu complexes have been characterized. The full potential of this system has yet to be tested and its reactivity will be one of the major points of interest in this work.

1.7.4   Degradation reactions of soft scorpionate ligands/complexes

A major drawback of the soft systems is the redox activity of the thione groups. Under oxidizing conditions an oxidative degradation of the ligand with concomitant reduction of the metal precursor can be observed. A possible mechanism involves the formation of disulfides, accompanied by a B-N bond cleavage. The reaction of $CuCl_2$ with NaTm, yielding $[Cu^{I}Cl(mtH)(\mu-mtH)]_2$, a

dimeric complex bridged over free mtH moieties as main product, is an example for the oxidative degradation of the ligand concomitant to metal reduction (see Figure 1.19).[65]
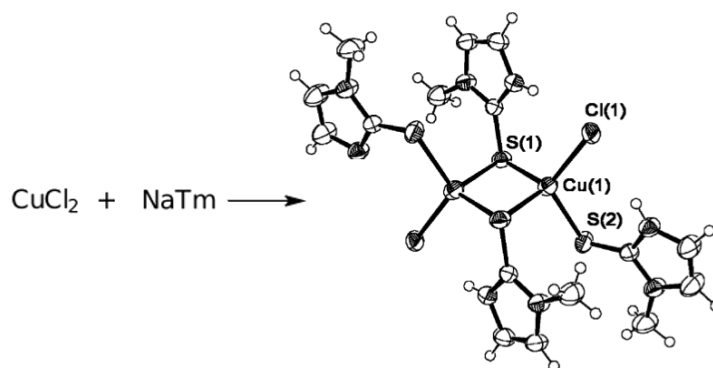
Figure 1.19: Bridged Cu^I dimer[e]

The compound shown in 1.20 was isolated as a by-product in reactions of Tm with CH_2Cl_2 as solvent. This type of side reaction has to be considered in the choice of solvent.[105]
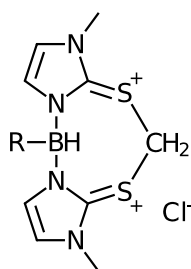
Figure 1.20: Examples for ligand reactions

The lability of the B-H bond manifests in the formation of so-called metallaboratranes after hydride elimination. The structure of a copper boratrane, reported by Mösch-Zanetti and co-workers with the novel pyridazine based scorpionate ligand, is shown in Figure 1.21.[106] Metallaboratranes have been reported for several elements, e.g. for Cu, Ru[107] or Pt[108] and are still discussed in literature due to the interesting bonding situation.[109]
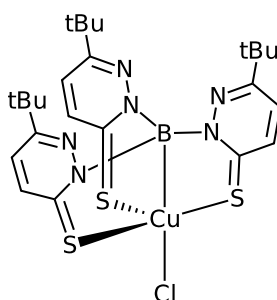
Figure 1.21: A copper boratrane as degradation product

1.7.5 Mo and W complexes with soft scorpionate ligands

The first successful approach in modelling a soft environment providing a coordination mode similar to Tp based ligands was the synthesis of $[Mo(CO)_3(B(CH_2SMe)_4)]^-$ (see equation 1.17). Protonation with HBF_4 results in the air-sensitive neutral $[MoH(CO)_3(B(CH_2SMe)_4)]$ compound.[89]

$$[(C_7H_8)Mo(CO)_3] + [NBu_4][B(CH_2SMe)_4] \longrightarrow C_7H_8 + [NBu_4][Mo(CO)_3(B(CH_2SMe)_4)] \quad (1.17)$$
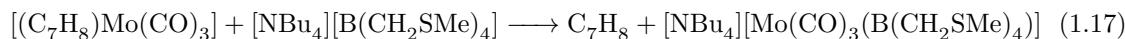
The field of soft Mo and W scorpionate complexes is dominated by their carbonyl compounds. Nevertheless the structure of the central species of Scheme 1.5 $[TmM(CO)_3]^-$ has yet to be been determined. Available IR data in the solid state revealed the unexpected number of four strong C=O stretching frequencies.[110] This suggested a symmetry lower than C_3 caused by solid state effects and/or close ion pairing. In THF and CH_2Cl_2 solutions the number of C=O frequencies was reduced to three. Scheme 1.5 summarizes the synthesis of Tm based carbonyl complexes of Mo and W.[65]
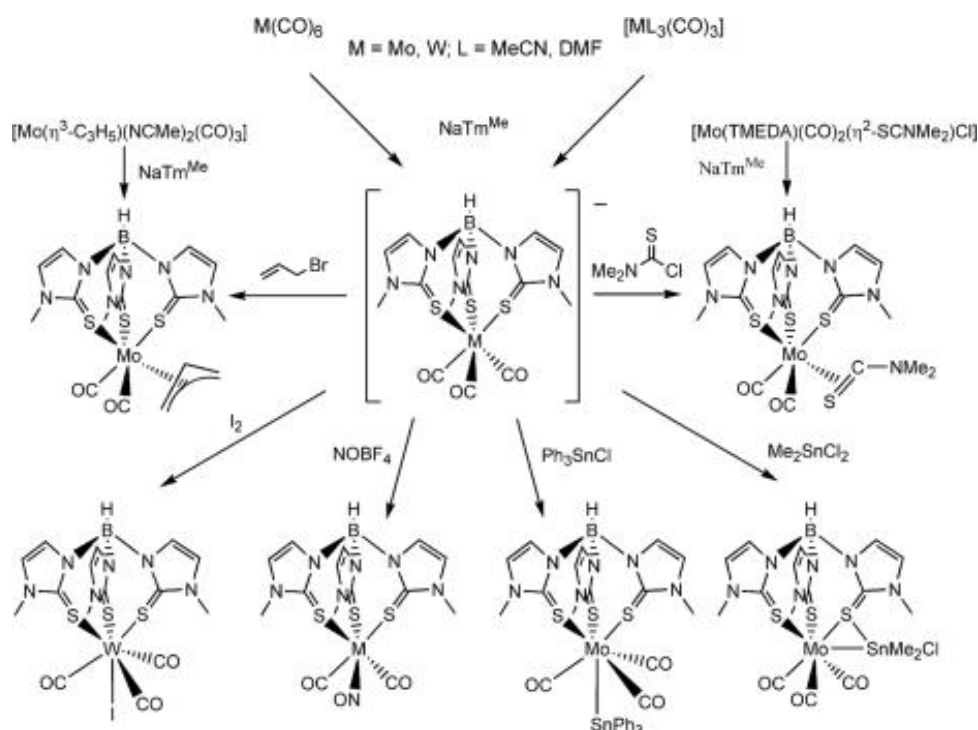
Scheme 1.5: Summarized Tm^R complexes of Mo- and W-carbonyls[f]

The first Tm complexes of Mo and W were synthesized in 2001, starting from $[Mo(CO)_6]$ and $[W(CO)_3(CH_3CN)_3]$. The Mo complex was isolated in form of $[TmMo(CO)_2(\eta^3-allyl)]$ after the reaction with allyl bromide, the reaction of the W analogue with I_2 yielded a sevenfold coordinated complex.

An interesting observation is the fact, that there is only on set of signals in the ^{1}H-NMR for the three methimazole moieties in $[TmMo(CO)_2(\eta^3-allyl)]$. The signals are somewhat broadened, suggesting a high degree of flexibility or ligand exchange on the timescale of a NMR-measurement.[54]

Foreman *et al.* reported differently substituted complexes of the type $[TmW(\equiv CR)(CO)_2]$. The formation of boratranes by hydride transfer to the respective alkylidyne ligand in the same manner as in $[TmRu(R)(CO)_2]$ complexes was not observed.[111]

Treatment of $[TmMo(CO)_3]^-$ with N,N-dimethylthiocarbamoyl chloride leads to the formation of $[TmMo(CO)_2(\eta^2-SCNMe_2)]$ in 87 % yield (see Scheme 1.5).[110]

The reaction of $[MI_2(CO)_3(CH_3CN)_2]$ with $PhC\equiv CPh$ or $MeC\equiv CMe$ and subsequent addition of NaBm or NaTm yields κ^3-S,S',H and κ^3-S,S',S'' coordinated complexes with elongated alkyne $C\equiv C$ bond lengths (around 130 pm).[112]

In 2008 improved synthetic routes for new Mo- and W-nitrosyl complexes were reported and increasing the yield from approx. 15 % to up to 80 %.[113]

1.7.6 Soft scorpionates as functional and structural models

The oxidation states of biological interest are +IV, +V and +VI. The first investigation of soft Mo-scorpionate complexes in these oxidation states was conducted in 2007 by Tran and Carrano. Using $[Mo^{IV}OCl(CNC(CH_3)_3)_4]$, $MoCl_5$ and $[(pyH)_2MoOCl_5]$ as starting point the complexes $[TmMo^{IV}O(CNC(CH_3)_3)_2]PF_6$, $[TmMo^VOCl_2]$ and $[TmMo^{VI}O_2Cl]$ were prepared (see Figure 1.22 I-III). $[TmMo^{VI}O_2Cl]$ is active in OAT with PPh_3 as substrate and DMSO as oxygen donor. The formation of a dimeric $[TmMoOCl]_2O$ species can be observed after letting the catalyst/PPh_3/DMSO mixture stand for several days.[114]

The synthesis of $[TmMo^{VI}O_2Cl]$ had been reported independently by Spicer and co-workers. It was shown, that the complex was able to catalytically oxidize SO_3^{2-} to SO_4^{2-} in the presence of DMSO. This reaction was typical for the sulfite oxidase and the voltammogram showed values closer to the enzyme than previous functional models.[115]

The ability of this system to catalyze OAT reactions classified it as functional model. In addition the sulfur-rich environment made this compound a valuable structural model for Mo dependent enzymes.
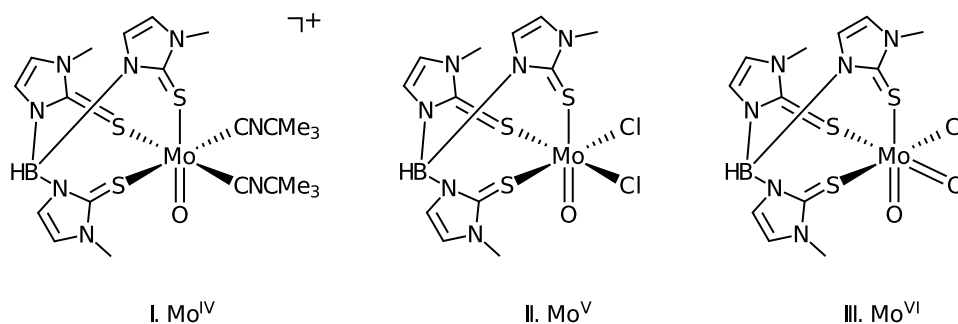
Figure 1.22: Structural and functional models featuring a Tm ligand

1.8 Scope of the thesis

The first part of this thesis covers the synthesis of soft pyridazine and methimazole based scorpionate ligands according to published methods. While methimazole based scorpionates are well established (see section 1.4.2), first examples of their pyridazine derived counterparts (see Figure 1.23) have been reported only recently.[104,106] Their reactions with different Mo precursors is investigated. The possibility to introduce different substituents in 6-position of the pyridazine moiety allows finetuning of sterical and electronical properties in the same manner as with methimazole moieties with a focus on low valent Mo compounds. A metal precursor in a low oxidation state should minimize the chance of degradation by redox reactions similar to formation of dimers (see Figure 1.19) as reported in literature.[65] Obtained complexes may prove to be a suitable starting point for a new class of biomimetic compounds for the active centers of Mo depended enzymes.

In the second section DFT calculations are used to gain further insight into the nature of the boron-nitrogen bond of two homo- and two heteroscorpionate ligands. The comparison of the B-N bonds in terms of dissociation energy, bond force constant and polarity of the bond should provide valuable information for the explanation of different stabilities of the respective ligands.

The influence of solvents is considered by the comparison of gas phase calculations and calculations with the COSMO-model simulating a solvent cavity.

In order to explain and support experimental results and conclusions the reaction enthalpies of the formation of (hypothetical) scorpionate complexes are calculated and compared to each other.
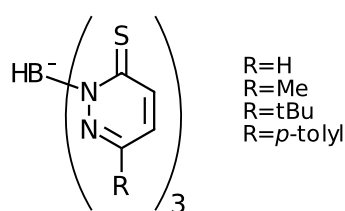
Figure 1.23: Pyridazine based scorpionate ligands

Chapter 2

Results

2.1 Synthesis of ligands and complexes

Synthesis of 3a The synthesis of 6-*tert*-butylpyridazine-3-thione **3a** (see Scheme 2.1) was performed according to published methods.[116,117] The major drawback of this route of synthesis was the low overall yield of 17%[116]) of the first two steps.

The pH-value on the outcome of the first reaction to **1a** was investigated by adding 1M HCl and 1M NaOH. Changing the pH-value did not result in the desired increase of yield. Partially removing H_2O from the glyoxylic acid at the rotary evaporator prior to the reaction had a significant impact on the yield, increasing it up to 60.8%. Decreasing the H_2O content resulted in the formation of a single phase instead of two after the first reflux step. Furthermore **2a** was isolated using a separation funnel with CH_2Cl_2/H_2O to work up the reaction solution. The results are summarized in Table 2.1.

The reaction from **2a** to **3a** according to a published procedure resulted in the formation of yellow microcrystalline product in 48.7% yield.[117]
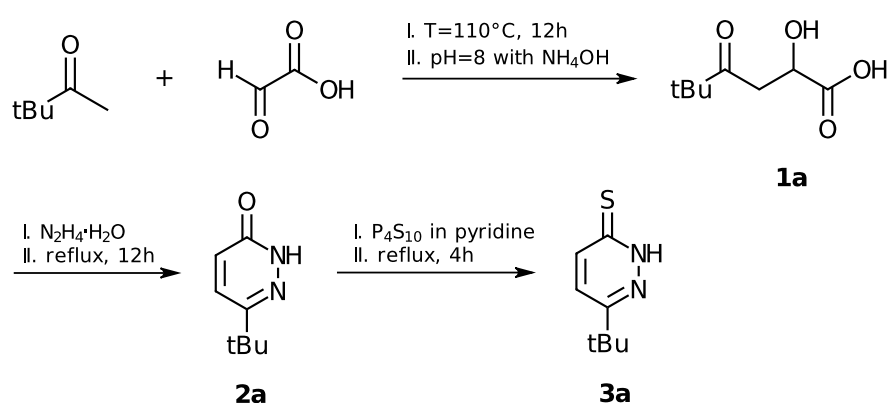
Scheme 2.1: Synthesis of **3a**

Table 2.1: Optimization of the synthesis of **2a**

test	H_2O removed	H^+/OH^-	mL added	yield [%]
1	yes	-	-	**60.8** (modified)
2	yes	H^+	0.4	26.2
3	yes	OH^-	1.0	16.7
4	no	-	-	**15.4** (original)
5	no	H^+	0.2	6.8
6	no	OH^-	0.2	11.3

Synthesis of 3b   The synthesis of 6-methylpyridazine-3-thione **3b** was performed according to published methods (see Scheme 2.2).[117,118] The product was isolated in 53 % yield and ^{1}H NMR signals matched the signals reported in literature only recently.[104]
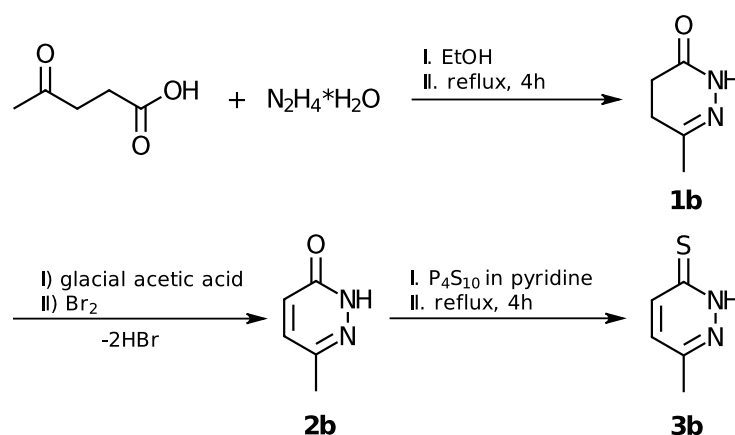
Scheme 2.2: Synthesis of **3b**

Synthesis of 4a The formation of the scorpionate ligand **4a** (see Scheme 2.3) was greatly influenced by changing the solvent from diphenylmethane (60 %[104]) to toluene. The yields varied irreproducibly from no conversion to >90 %. Testing different conditions showed, that dry toluene as solvent resulted in yields of only a few percent in the best cases. However, with technical grade toluene higher yields up to quantitative conversion were achieved. Nevertheless strong deviations depending on the solvent batch were observed. The outcome of the reaction seemed to be sensitive to the water content. Unreacted pyridazine could be extracted, using hot cyclohexane as reported by Mösch-Zanetti and co-workers.[106]
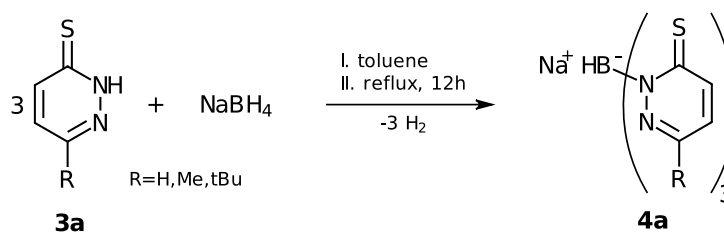
Scheme 2.3: Synthesis of **4a**

Synthesis of Mo precursor 1   Two low valent Mo precursor were used in the synthesis of novel complexes. $[Mo(CO)_6]$ had the disadvantage of longer reaction times under reflux conditions. Hence the more reactive $[Mo(CO)_3(MeCN)_3]$ (**1**) was synthesized according to Scheme 2.4.[119] An advantage of this air sensitive compound was the simple crystallization of **1***cdot*MeCN by vapor diffusion of pentane into a concentrated **1**/MeCN solution at -25 °C.

$$[Mo(CO)_6] \xrightarrow[\text{II. reflux, 12h}]{\text{I. CH}_3\text{CN}} [Mo(CO)_3(MeCN)_3]$$
$$\textbf{1}$$
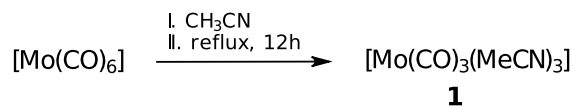
Scheme 2.4: Synthesis of **1**

Synthesis of 8a from 4a   The reaction of precursor **1** with pyridazine based scorpionate ligand **4a** results in an immediate color change to dark brown/orange (see Scheme 2.5). Direct removal of the solvent allowed no isolation of a defined compound.^{1}H NMR spectroscopy revealed serveral resonances, which could not be assigned unequivocally.
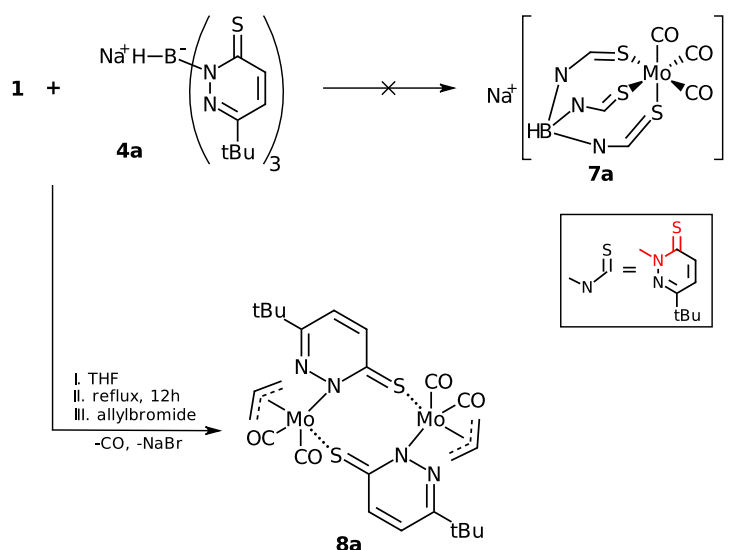
Scheme 2.5: Synthesis of **8a** from **4a**

In order to facilitate the isolation, allyl bromide was added similar to a procedure published by Reglinski and Spicer[54] for the precipitation of $[TmMo(CO)_2(\eta^3-allyl)]$. This led to the precipitation of NaBr, which was removed by filtration. Subsequent careful removal of the solvent led to the isolation of an orange powder (**8a**) in in poor yield (5.9 %) in one attempt. Due to the small amount obtained, the compound was not characterized in solution. However, single crystals suitable for X-ray analysis were obtained by vapor diffusion of Et_2O into a concentrated solution of **8a** at -25 °C under inert conditions. This confirmed the formation of the dimeric compound **8a** (see Figure fig:8a), instead of the desired mononuclear scorpionate complex **7a**. Unfortunately, the reaction was not reproducible.

Synthesis of the sodium salts 6a, 6b, 6b2, 6c and 6d   In order to test if the dimeric complex **8a** was directly accessible by the reaction of **1** with **6a**, the sodium salts of the different pyridazine-3-thiones **3c**[a], **2b**, **3b**, **3a** and 6-*p*-tolyl-pyridazine-3-one **2d**[a] were prepared in high yields (>85 %) using NaH (see Scheme 2.6). A slight excess of NaH (1.1 equiv, estimated concentration 55 %) was used in the reaction due to a broad concentration specification of 50-60 %. A reaction of possible residual NaH (H$_2$-gas formation) in subsequent reactions could not be observed, suggesting that all NaH had been consumed in the formation reaction.

3a ⟶	**6a**	X=S, R=tBu	
2b ⟶	**6b**	X=O, R=Me	
3b ⟶	**6b2**	X=S, R=Me	
3c ⟶	**6c**	X=S, R=H	
2d ⟶	**6d**	X=O, R=*p*-tolyl	
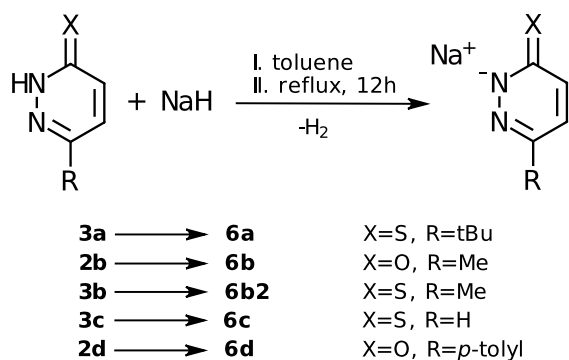
Scheme 2.6: Synthesis of **6a**, **6b**, **6b2**, **6c** and **6d**

Synthesis of 8a from 6a   Complex **8a** was also accessible by the reaction of **1** with the sodium salt **6a** (see Scheme 2.7), albeit in low yield (16.0 %). Single crystals suitable for X-ray analysis by vapor diffusion of Et$_2$O into a concentrated solution of **8a** in THF at -25 °C under inert conditions. confirmed the formation of **8a**. A molecular view of **8a** is displayed in Figure 2.1. Selected angles, distances and torsion angles are given in Table 2.2. Additionally, the reaction of the other sodium salts **6b**, **6b2**, **6c** and **6d** with **1** were tested, but no products could be isolated.
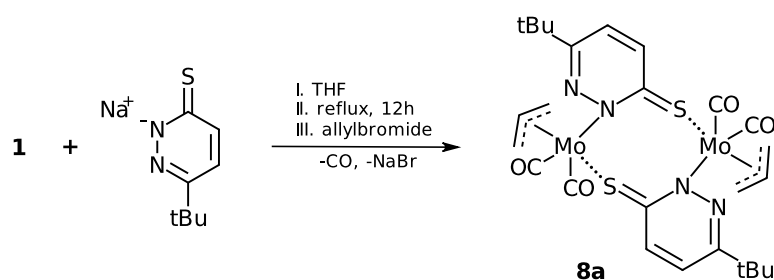
Scheme 2.7: Synthesis of **8a** from **6a**

---

[a]provided by Dipl.-Ing. Dr. Gernot Nuss

Characterisation of 8a The two Mo centers are coordinated in a distorted octahedral manner with both pyridazine moietes located at the same side of the molecule. The allyl ligands are in *trans* position to the sulfur atom of the pyridazine moiety forming the Mo-N bond with the respective Mo center. The distance of the central carbon (C1, 2.203 Å) to the Mo center is slightly shorter compared to the other two carbons (C11, 2.298 Å and C12, 2.343 Å). The C≡O bond lengths of 1.149, 1.156, 1.157 and 1.158 Å are only slightly elongated compared to bonding distance of 1.128 Å in free carbonmonoxide.[120] The two sulfur atoms act as bridges forming a four-membered Mo-S-Mo-S metallacycle. The metallacycle is a non-planar rhombus with two slightly different bond lengths (2.613 and 2.578 Å), angles of 80.6 and 94.1° and a dihedral of -24.1°. The distances and angles are within the expected ranges. Other isomers could not be isolated.
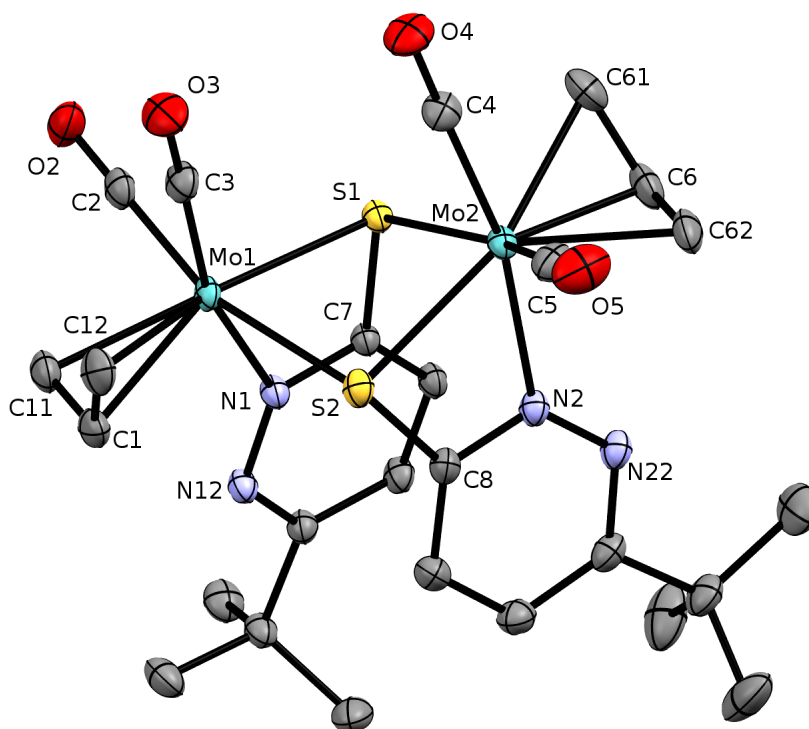
Figure 2.1: Crystal structure of **8a**

Dimeric Mo complexes featuring a similar sulfur bridging were published by Block *et al.*[121] and Cade *et al.*[122]. The complexes are shown in Figure 2.2, highlighting the common Mo-S-Mo-S cycle in red.

The structure reported by Block *et al.* (see Figure 2.2 I) exhibited three bridging atoms. The Mo1−Mo2 distance of 2.445(2) Å was significantly shorter than in **8a** and was drawn as an actual bond. The Mo-S distances of 2.447(5) (Mo1) 2.471(5) (Mo1), 2.467(5) (Mo2) and 2.465(4) (Mo2) were shorter as a consequence of the smaller ring. The angles of the ring were 100.0(2)° (S-Mo1-S) and 59.7(1)° (Mo-S-Mo), suggesting a more rhombic structure than in **8a**. A dihedral angle was not given in the supportive material.

Table 2.2: Selected bond length and angles of **8a**

	distance [Å]		angle [°]
Mo1-S1	2.578(4)	S1-Mo1-S2	80.6(1)
Mo1-S2	2.613(3)	Mo1-S1-Mo2	93.9(3)
Mo1-C1	2.203(1)	C3-Mo1-S1	101.1(1)
Mo1-C11	2.298(1)	C3-Mo1-N1	164.7(4)
Mo1-C12	2.343(1)	C1-Mo1-S2	90.4(1)
Mo1-C2	1.955(4)	Mo1-C2-O2	177.1(2)
Mo1-C3	1.984(2)		
Mo1-Mo2	3.792(5)		dihedral angle [°]
Mo1-N1	2.223(3)	S1-Mo1-S2-Mo2	-24.1(1)
C1-C11	1.416(3)		
C1-C12	1.408(2)		
C2-O2	1.158(1)		
C3-O3	1.149(2)		
N1-N12	1.346(1)		
S1-C7	1.757(4)		

The Mo1−S distances in Figure 2.2 II[122] were with 2.626(1) and 2.627(1)Å in the range of the observed bond lengths in **8a**. By contrast the Mo2−S distances were shorter (2.540(1) and 2.559(1)Å). The angles S-Mo1-S (79.28(4)°) and Mo1-S-Mo2 (97.30(4)°) were of comparable size. A dihedral angle of 15.82(4)° indicated a more planar Mo-S-Mo-S ring.
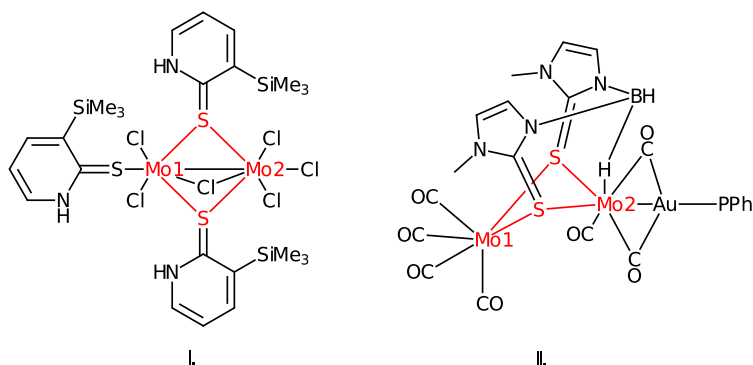
Figure 2.2: Complexes featuring a Mo-S-Mo-S motif

Synthesis of Li$^+$[PhBH$_3$]$^-$ (2)   The results presented above indicated that **4a** was sensitive to towards degradation. A possible explanation could be the relatively weak B-H bond in the scorpionate ligand. For this reason a phenyl substituted scorpionate ligand was envisioned, hoping to be less sensitive towards degradation.

Since boranes are known to form dimers with three center two electron (3c2e) bonds, substitution of the last remaining hydrogen in scorpionate ligands could prevent this form of stabilization. Consequently, ligand degradation, leading to complex **8a**, would become less likely, if the formation of of 3c2e bonds was the thermodynamic driving force. Additionally, a bulkier ligand could change the solubility, facilitating the isolation. Phenyl substituted scorpionates, featuring an phenyl moiety bound to the boron atom instead of hydrogen, are accessible from Li$^+$[PhBH$_3$]$^-$ (**2**).

Several modifications of the original procedure[123] have been published in literature. In this work the procedure was adapted from Reglinski and Spicer.[124] The reaction required an excess of $LiAlH_4$ to deprotonate $PhB(OH)_2$ and react with a certain amount of H_2O, depending on the quality of the hygroscopic $PhB(OH)_2$. 2,2'-biquinoline was used as indicator, showing a blue color in presence of unreacted $LiAlH_4$. The end of the reaction was indicated by a color change from blue to colorless.[123]

In order to find the right indicator concentration, a stock solution was added dropwise to the $LiAlH_4/Et_2O$ solution until a blue color of medium intensity was reached. At too low concentrations of 2,2'-biquinoline the end of the reaction was signalled to early. Residual $LiAlH_4$ reacted violently with DMSO-d6, indicating an incomplete turnover.; high concentrations led to a yellowish brownish color of the otherwise colorless solution and in further consequence product.

It was stated, that a solution of $PhB(OH)_2$ in Et_2O was added to $LiAlH_4$ in Et_2O. However, in our hands phenylboronic acid did not dissolve in Et_2O. A controlled addition of the formed suspension proved difficult. Hence $PhB(OH)_2$ was dissolved in THF and diluted with Et_2O, facilitating a controlled addition.

The formation of a greyish precipitate was observed. This reactive Al polymer ZITAT was separated using a Schlenk centrifuge. The solvent of the supernatant phase was removed in vacuo and **1b** was isolated in 84.9 % yield.
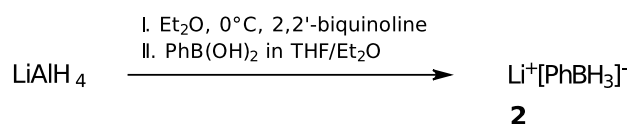
Scheme 2.8: Synthesis of **2**

Attempted synthesis of 5a   The formation of phenyl substituted scorpionate ligand **5a** could not be achieved under the same reaction conditions as H-substituted version **4a** (see Scheme 2.9).
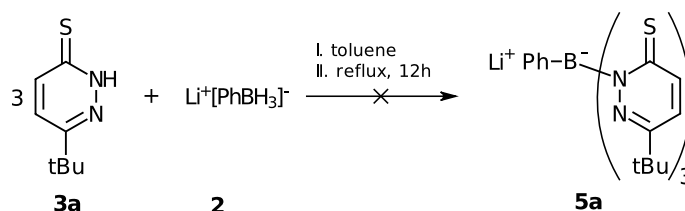
Scheme 2.9: Attempted synthesis of **5a**

Synthesis of 5e   The synthesis of the phenyl substituted ligand **5e**, featuring methimazole moieties, had been described in literature previously[124] and was modified by changing the correct stoichiometry of 3:1 methimazole to **2** to 4:1. (see Scheme 2.10). The excess of methimazole surpressed the formation of mono- and disubstituted intermediates. The yield was 56.6 % and ¹H-NMR spectroscopy showed the expected signal ratio of 3:1 (product to methiamzole). 80 % of the residual methimazole could be removed by washing three times with dry $CHCl_3$. The obtained mixture with 20 % of methimazole could directly be used for the complex synthesis.
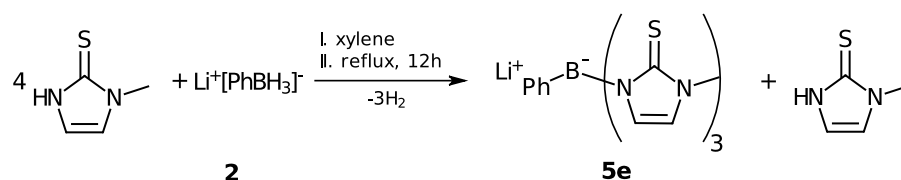
Scheme 2.10: Synthesis of **5e**

Synthesis of 7e   The reaction of **1** with **5e** (see Scheme 2.11) in dry THF yielded the yellow complex **7e** in 45.5 % yield (82 mg, based on Mo).
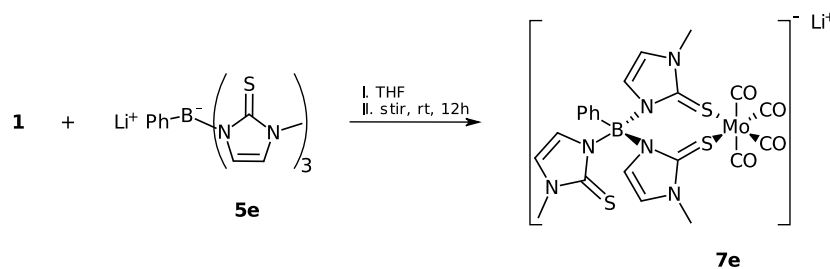
Scheme 2.11: Synthesis of **7e**

Synthesis of 8e   Complex **8e** was accessible from *in-situ* generated **1**, **5e** and NBu$_4$Cl in dry MeCN (see Scheme 2.12). Over a period of 72 h a slow, continuous color change to brown was being observed. Subsequent solvent removal *in vacuo* resulted in the formation of a brownish foam. Redissolving in THF led to the precipitation of **8e** as a yellow microcrystalline powder in 23.5 % yield (based on Mo).
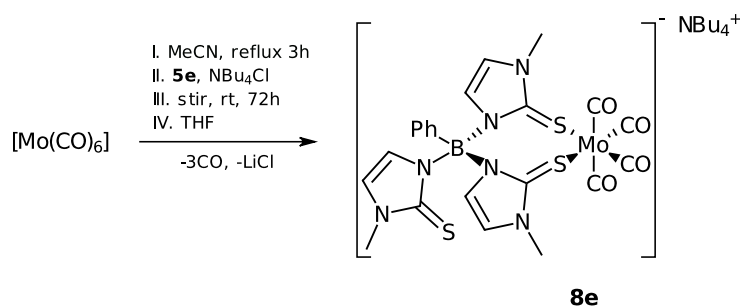
Scheme 2.12: Synthesis of **8e**

Characterisation of 7e and 8e   Since a degradation reaction was observed in DMSO-d6, NMR of **7e** and **8e** were recorded in THF-d8 and CD$_3$CN.

The ^{1}H NMR spectrum of **7e** showed four signals in the aromatic region. The five H atoms of the phenyl moiety were split into two signals integrating to two and three protons. There was only one set of signals for aromatic protons in the methimazole moieties, suggesting three equivalent methimazoles. Interestingly, no coupling could be observed. The signal of the methimazole's methyl groups was located under the THF solvent peak. An additional spectrum in CD$_3$CN showed two multiplets (6:3 protons) for the methyl groups. ^{13}C NMR analysis showed only a single signal for

carbonyl groups, other signals, especially those of quartenary carbon atoms, were obscured by the solvent peak or the signal to noise ratio due to solubility issues.

The aromatic region in the ^{1}H NMR spectrum of **8e** showed only three multiplet signals integrating to 5:3:3. A broad multiplet integrating to nine protons for the methimazole's methyl groups suggested a very flexible system. The carbon and hydrogen atoms of $[NBu_4]^+$ be assigned unequivocally in the ^{1}H and ^{13}C NMR spectra. By contrast to complex **7e** four CO signals were observed in the ^{13}C spectrum.

Unexpectedly, IR analysis showed four strong signals in the CO region, describing two symmetric (1890 and 1775 cm^{-1}) and to antisymmetric (1678 and 1634 cm^{-1}) modes. The symmetry of these modes was confirmed by DFT calculations (see Figure 2.3). This data suggested four carbonyl groups as shown in Scheme 2.11. Additionally, rapid decomposition under exposure to air was observed (see Figures 2.4 to 2.6). Within roughly 90 s the four CO signals lost most of their intensity, whereas a growing signal in the region of 3500-3000 cm^{-1} indicated the formation of a hydroxy species. The signals below 1500 cm^{-1} remained more or less unaffected.

(a) 1890 cm^{-1}

(b) 1775 cm^{-1}

(c) 1678 cm^{-1}

(d) 1634 cm^{-1}
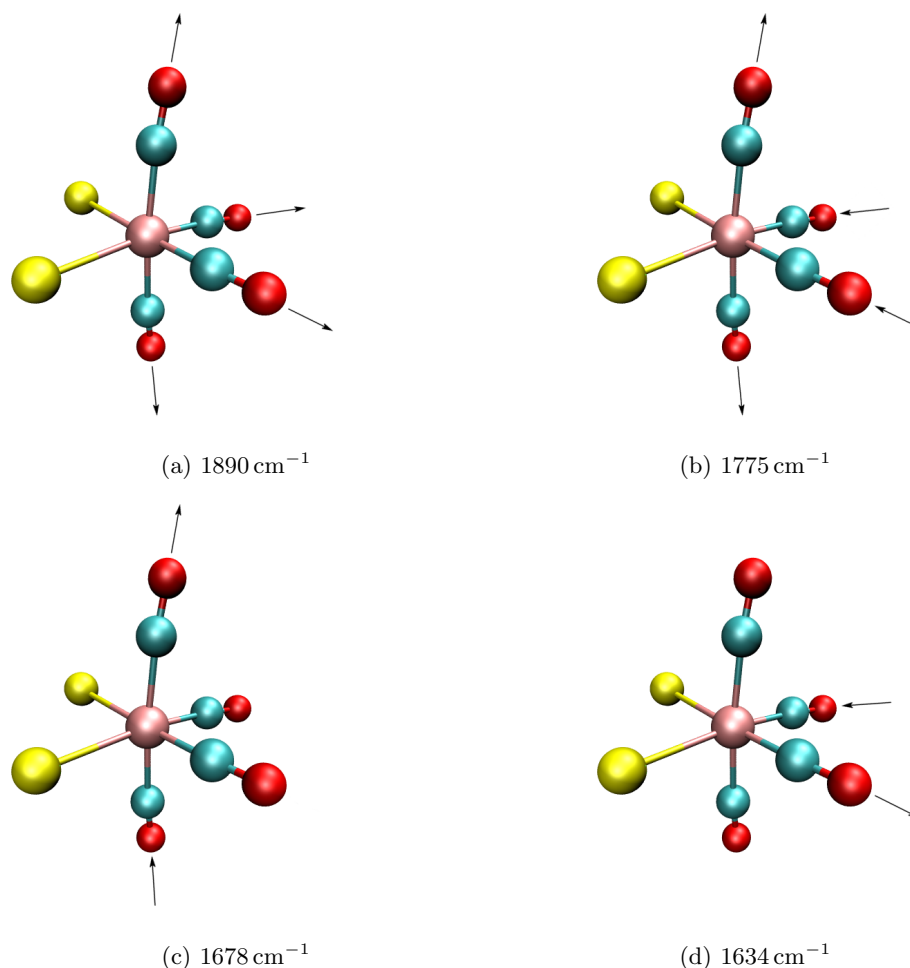
Figure 2.3: Carbonyl vibrations of **7e**
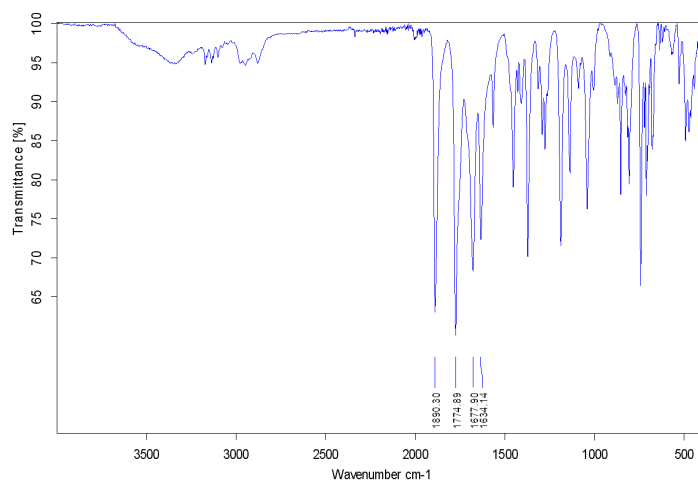
Figure 2.4: First IR spectrum of **7e** t= 0 s
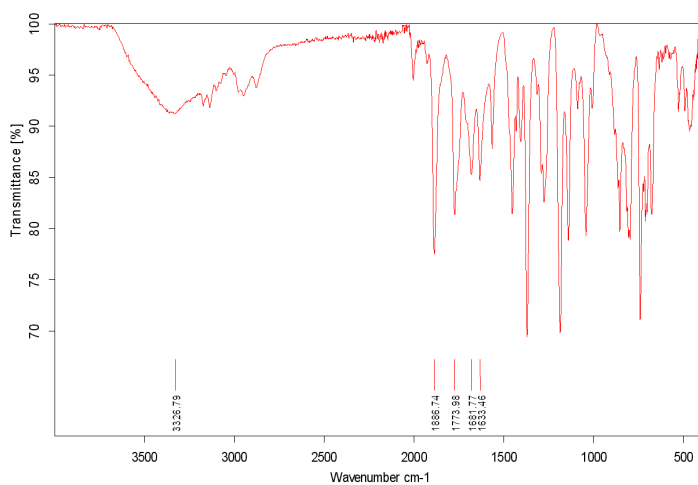
Figure 2.5: Second IR spectrum of **7e** t= 45 s
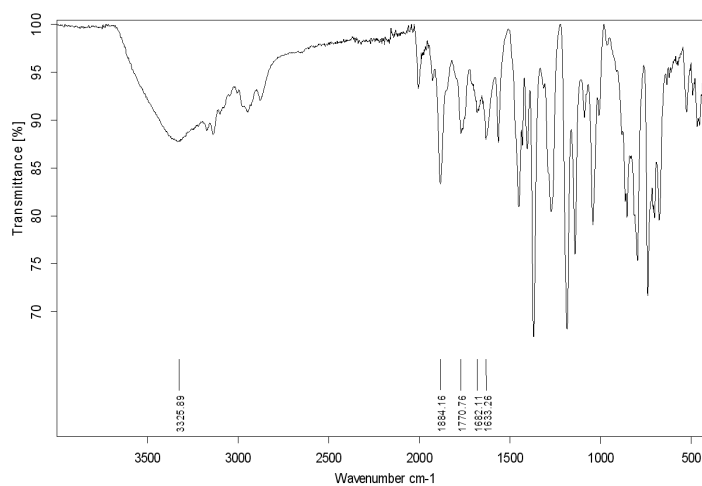
Figure 2.6: Third IR spectrum of **7e** t= 90 s

Single crystals suitable for X-ray analysis of **7e** were obtained by vapor diffusion of Et$_2$O in to a concentration **7e**/DMF solution; single crystals of **8e** by slow evaporation of the mother liquor (THF). The molecular views of **7e** and **8e** are shown in Figures 2.7 and 2.8. Selected bond lengths and angles are summarized in Table 2.3.
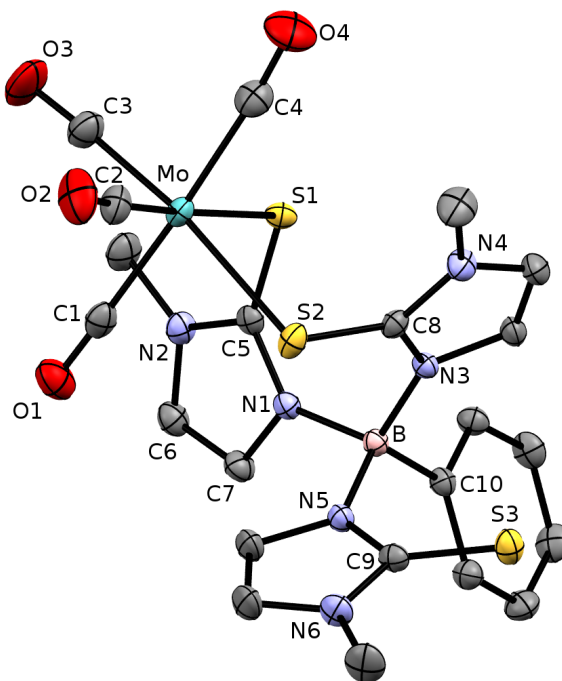
Figure 2.7: Crystal structure of **7e**. Hydrogen atoms, the Li$^+$ counterion and DMF solvent molecules have been omitted for clarity.
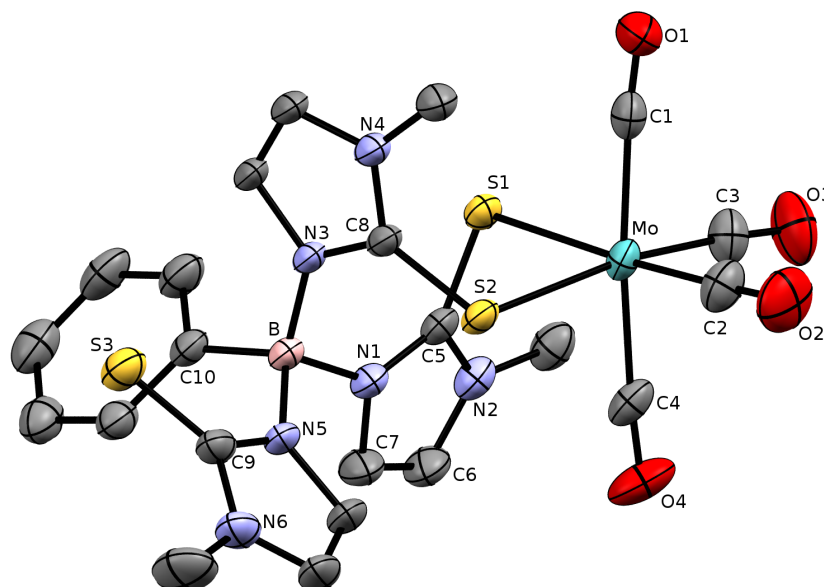
Figure 2.8: Crystal structure of **8e**. Hydrogen atoms, the [NBu$_4$]$^+$ counterion and THF solvent molecules have been omitted for clarity.

Table 2.3: Selected bond lengths and angles of **7e** and **8e**

Complex:	**7e** distance [Å]	**8e** distance [Å]		**7e** angle [°]	**8e** angle [°]
Mo-C1	2.035(3)	2.039(2)	Mo-C1-O1	175.3(1)	174.2(3)
Mo-C2	1.939(4)	1.953(2)	Mo-C2-O2	177.0(4)	177.4(1)
Mo-C3	1.944(4)	1.931(3)	C1-Mo-C4	176.4(1)	174.4(1)
Mo-C4	2.042(3)	2.042(2)	C1-Mo-S1	87.4(1)	86.6(3)
Mo-S1	2.601(4)	2.615(4)	C1-Mo-S2	98.5(1)	99.7(2)
Mo-S2	2.634(3)	2.640(5)	S1-Mo-S2	85.6(1)	84.6(2)
C1-O1	1.149(2)	1.147(2)	Mo-S1-C5	102.1(4)	100.0(5)
C2-O2	1.170(2)	1.163(2)	Mo-S2-C9	105.2(2)	104.3(4)
C3-O3	1.165(3)	1.168(4)	N1-B-N3	112.5(1)	111.4(5)
C4-O4	1.147(2)	1.140(3)	N1-B-N5	106.7(2)	107.1(4)
N1-C5	1.353(1)	1.358(1)	N1-B-C11	104.4(4)	102.9(5)
N2-C5	1.326(4)	1.360(1)	B-N1-C5	133.4(3)	131.8(3)
S1-C5	1.719(4)	1.717(1)			
S2-C9	1.721(1)	1.724(5)			
S3-C10	1.694(1)	1.698(4)			
B-N1	1.590(1)	1.588(4)			
B-N3	1.556(5)	1.550(3)			
B-N5	1.569(4)	1.567(4)			
B-C11	1.619(4)	1.624(4)			
C6-C7	1.305(3)	1.340(5)			

Both complexes exhibit κ^2-S,S' coordination of the scorpionate ligand. The crystal structures confirmed a fourth CO group located at the Mo central atom. This was unexpected, since $[Mo(CO)_3(MeCN)_3]$ was used as precursor. The Mo central atoms is coordinated in a slightly distorted octahedral manner. Exchanging the counterion had hardly any effect on the complex geometry, a comparison of the bonding distances and angles of **7e** and **8e** showed only small deviations. The complex were ordered, whereas the counterions and solvent molecules were disordered. Three possible positions for the Li^+ were detected.

The C=S distances of the coordinated sulfur atoms S1 and S2 are elongated by ca. 0.02 Å compared to the not coordinated S3 and differ only slightly from the C=S distances of the free ligand (1.697, 1.705 and 1.719 Å).[124] Owing the spacial demand of the phenyl moiety an elongation of the B-N1 bond is observed, an effect that has also been noted in the free ligand.[124] All bond lengths and angles are within the expected ranges. Mo complexes featuring a **cis**-coordination of two sulfur atoms and at least carbonyl groups were reported by Nemykin *et al.*[125] and Schwalbe *et al.*[56]. The complexes are shown in Figure 2.9.

The dithiolene complex reported by Nemykin *et al.* showed slightly shorter Mo−S bond distances of 2.525(2) and 2.520(1) Å. The Mo−C distances of axial carbonyl groups were in good agreement with those found in **7e** and **8e** (2.019(5) and 2.030(5) Å). The weaker trans effect of the sulfur atoms resulted in shorter equatorial Mo−C bonds of 1.945(6) and 1.964(6) Å. This was also observed in complexes **7e** and **8e**. The bite angle of 79.08(5) ° was a little lower.
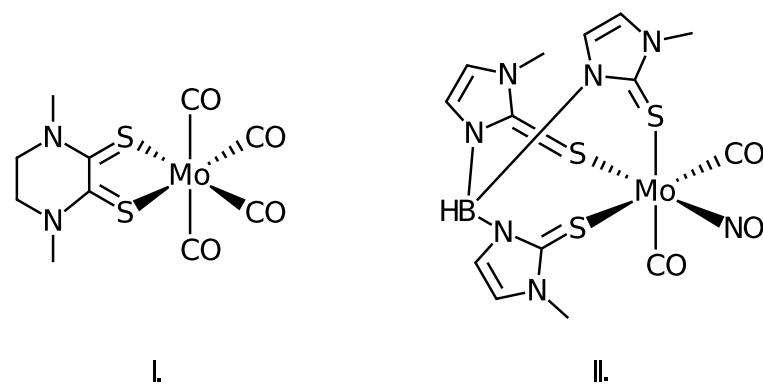
Figure 2.9: Complexes with structural similarity to **7e** and **8e**

The soft scorpionate complex shown in Figure 2.9II[56] exhibited slightly shorter Mo−S distances of Mo-S 2.5865(7) (*trans* to NO) 2.5594(6) and 2.5767(7) Å. The Mo−C bond lengths of 1.957(3) and 1.979(3) Å between the reported distances of **7e** and **8e**. The S-Mo-S angles between 89.29(2) and 90.56(2)° were slightly larger than found in **7e** and **8e**.

2.2 Results of Theoretical Investigations

The formation of the desired pyridazine based scorpionate complex **7a** could not be accomplished using established methods. Instead the dimeric molybdenum complex **8a**, featuring two pyridazine moieties, was obtained as a result of a ligand degradation reaction. Applying standard experimental techniques provided no further insight, hence computational methods were used to investigate the formation and possible degradation reactions of the complexes and ligands. The thermodynamical quantities were calculated with the *freeh* module as implemented in Turbomole according to the formulas 2.1 to 2.6.

The energy consists of the zero point energy and terms for the translatational, rotational and vibrational, with $\nu(i)$ being the frequency of the ith mode, as shown in equation 2.1.

$$energy = ZPE + 3RT + \sum_i \nu(i) \cdot \frac{1 + e^{\frac{\nu(i)}{kT}}}{2 * (1 - e^{\frac{-\nu(i)}{kT}})} \tag{2.1}$$

The enthalpy of formation $\Delta_f H$ is RT higher than the energy. The electronic energy E_{elec} has to be added to obtain the correct absolute potentials (see equation 2.2).

$$\Delta_f H = energy + RT + E_{elec} \tag{2.2}$$

The reaction enthalpies $\Delta_r H$ are obtained by summing over the formation enthalpies of the products $\Delta_f H_{prod}$ and subtract the sum of the formation enthalpies of the educts $\Delta_f H_{ed}$ (see equation 2.3).

$$\Delta_r H = \sum \Delta_f H_{prod} - \sum \Delta_f H_{ed} \tag{2.3}$$

The entropies are obtained according to equation 2.4 with *chem.pot.* being the chemical potential; the reaction entropies in analogy to the reaction enthalpies (see equation 2.3).

$$S = \frac{H - chem.pot.}{T} \tag{2.4}$$

An important thermodynamical quantitiy is the Gibbs free enthalpy ΔG (see equation 2.5). This thermodynamic potential describes the total amount of energy, that is being released or required for the reaction. Reactions with $\Delta G < 0$ are called exergonic and proceed voluntarily. Endergonic reaction with $\Delta G > 0$ are unfavored. ΔG contains no information about present barriers, hence the reaction rate is unknown, if only educts and products are considered.

$$\Delta G = \Delta H - T \Delta S \tag{2.5}$$

The equilibrium constant can be calculated from the Gibbs free energy (see equation 2.6) and shows whether the products or educts are favored in the state of equilibrium. Nevertheless formally unfavored reactions can still proceed with high yields, if the equilibrium is changed by the removal of an insoluble or gaseous product according to Le Chatelier's Principle.

$$K_i = e^{-\frac{\Delta G}{RT}} \tag{2.6}$$

2.2.1 Thermodynamics of the formation reactions

Tautomers For methimazole (mH) and pyridazine (n^{tBu}H) two forms similar to a keto-enol tautomerism can be assigned. The thiole and thione form are shown in Figure 2.10. The results of the thermodynamical investigation are summarized in Table 2.4. SH denotes the thiole form, NH the thione form. A "c"-prefix denotes, that the COSMO model had been applied.
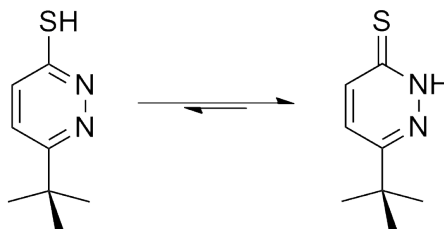
Figure 2.10: Tautomeric forms of Hn^{tBu}

The influence of THF as solvent was expressed by a preference of the thione form. The thione form was the prerequisite for the formation of a B−N bond in the ligand synthesis. Interestingly, the ΔG values for n^{tBu}H were less exergonic and hence the preference for the thione form less pronounced.

Table 2.4: Thermodynamical Data Tautomerism

equilibrium	ΔH [kJ/mol]	ΔS [kJ/mol·K]	$\Delta_r H$ [kJ/mol]	ΔG [kJ/mol]	K^{298}
mSH − mNH	8.32	-0.0142	-39.65 2	-35.41	$1.60 \cdot 10^6$
cmSH − cmNH	8.76	-0.00857	-53.83	-51.27	$9.62 \cdot 10^8$
n^{tBu}SH − n^{tBu}NH	10.68	-0.00296	-24.51	-23.63	$1.38 \cdot 10^4$
cn^{tBu}SH − cn^{tBu}NH	10.72	-0.00584	-33.71	-31.97	$4.00 \cdot 10^5$

Ligand formation The formation reactions of the ligands are shown in equations 2.7, 2.8 and 2.9. A series of four unsubstituted homo- and heteroscorpionates (Tn^{tBu}, Tmn^{tBu}_2, Tm_2n^{tBu} and Tm) and two phenyl substituted ligands ($PhTn^{tBu}$ and PhTm) are compared with each other. The ligands L_i are depicted in Figure 2.11. The influence of toluene was accounted for by applying the COSMO model with a dielectric constant of 2.38 for toluene.

$$BH_4^- + (3-n)\, n^{tBu}H + n\, mH \xrightarrow{\text{toluene}} HTn^{tBu}_{(3-n)}m_n + 3\,H_2 \qquad (2.7)$$

$$PhBH_3^- + 3\, n^{tBu}H \xrightarrow{\text{toluene}} PhTn^{tBu\,-} + 3\,H_2 \qquad (2.8)$$

$$PhBH_3^- + 3\, mH \xrightarrow{\text{toluene}} PhTm^- + 3\,H_2 \qquad (2.9)$$
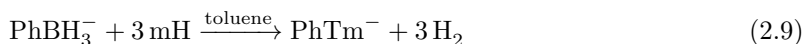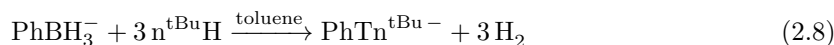
The results are summarized in Tables 2.5 and 2.6. The complete data sets are enlisted in the appendix. If not mentioned explicitly statements concern the results of both calculations with and without the COSMO model, hence the "c"-prefix will be omitted, if not necessary.
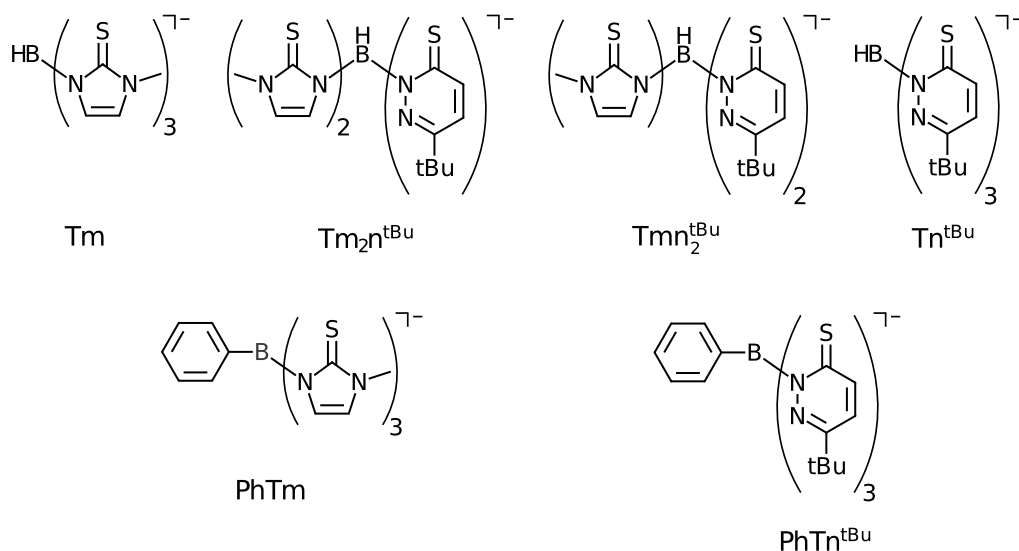
Figure 2.11: Methimazole and pyridazine based scorpionate ligands

Table 2.5: Thermodynamical Data Ligand Formation

L_i	$\Delta_r H$ [kJ/mol]	ΔS [kJ/mol·K]	ΔG [kJ/mol]	K^{298}
Tm	-321.06	-0.14936	-276.53	$2.807 \cdot 10^{48}$
$\text{Tm}_2\text{n}^{\text{tBu}}$	-326.94	-0.15974	-279.32	$8.652 \cdot 10^{48}$
$\text{Tmn}_2^{\text{tBu}}$	-331.08	-0.16617	-281.54	$2.118 \cdot 10^{49}$
Tn^{tBu}	-335.86	-0.15889	-288.49	$3.499 \cdot 10^{50}$
PhTm	-267.69	-0.17503	-215.50	$5.712 \cdot 10^{37}$
PhTn^{tBu}	-238.42	-0.23445	-168.52	$3.349 \cdot 10^{29}$

Table 2.6: Thermodynamical Data Ligand Formation (COSMO)

L_i	$\Delta_r H$ [kJ/mol]	ΔS [kJ/mol·K]	ΔG [kJ/mol]	K^{298}
cTm	-330.47	-0.15746	-283.52	$4.715 \cdot 10^{49}$
$\text{cTm}_2\text{n}^{\text{tBu}}$	-327.98	-0.15127	-282.88	$3.635 \cdot 10^{49}$
$\text{cTmn}_2^{\text{tBu}}$	-326.25	-0.15073	-281.31	$1.929 \cdot 10^{49}$
cTn^{tBu}	-329.72	-0.15039	-284.88	$8.165 \cdot 10^{49}$
cPhTm	-291.84	-0.18185	-237.62	$4.284 \cdot 10^{41}$
$\text{cPhTn}^{\text{tBu}}$	-252.99	-0.18636	-197.42	$3.883 \cdot 10^{34}$

Both datasets show, that the ligand formation is an exergonic reaction with the equilibrium (K^{298}) lying at far side of the products at rt. The formation of Tn^{tBu} is favored over the formation of Tm from a thermodynamical point of view. The formation of PhTm is considerably more exergonic than its pyridazine counterpart PhTn^{tBu}.

The shared electron number (SEN) of the starting materials and ligands are summarized in Tables 2.7, 2.8 and 2.9. A "*" in heteroscorpionates denotes an atom or bond in a pyridazine moiety.

Table 2.7: SEN Educts

compound	B-H	B-H/C [Å]	compound	N-H	C=S
BH_4^-	1.454	-	mH	1.254	1.596
$PhBH_3^-$	1.435	1.443	$n^{tBu}H$	1.281	1.607
cBH_4^-	1.458	-	cmH	1.279	1.569
$cPhBH_3^-$	1.437	1.446	$cn^{tBu}H$	1.254	1.558

Table 2.8: SEN Ligands

L_i	B-N1	B-N2	B-N3	C=S1	C=S2	C=S3	B-H/C
Tm	1.229	1.228	1.228	1.569	1.569	1.569	1.384
Tm_2n^{tBu}	1.188*	1.237	1.240	1.572	1.547	1.564*	1.383
Tmn_2^{tBu}	1.190*	1.197*	1.259	1.563*	1.553	1.553*	1.371
Tn^{tBu}	1.206	1.207	1.205	1.555	1.550	1.552	1.367
PhTm	1.166	1.191	1.255	1.579	1.569	1.585	1.376
$PhTn^{tBu}$	1.109	1.145	1.123	1.568	1.570	1.614	1.385

Table 2.9: SEN Ligands (COSMO)

L_i	B-N1	B-N2	B-N3	C=S1	C=S2	C=S3	B-H/C
cTm	1.231	1.228	1.229	1.526	1.525	1.524	1.398
cTm_2n^{tBu}	1.183*	1.239	1.247	1.526	1.522	1.525*	1.400
$cTmn_2^{tBu}$	1.189*	1.196*	1.263	1.527*	1.528	1.525*	1.392
cTn^{tBu}	1.204	1.203	1.205	1.524	1.523	1.522	1.393
cPhTm	1.192	1.189	1.233	1.545	1.530	1.547	1.385
$cPhTn^{tBu}$	1.110	1.078	1.107	1.525	1.538	1.566	1.389

A comparison showed, that the SEN for B−H or B−C, in case of phenyl substituted borates, was reduced in course of the reaction. Simulating a solvent cavity resulted in slightly higher SEN compared to purely gas phase calculations.

Both variants predicted a slightly higher SEN for a methimazole B−N bond than a pyridazine B−N bond. The SEN for pyridazine B−N bonds increased with decreasing number of methimazoles present in the ligand. The opposite trend is observed in case of methimazole.

The phenyl substituted ligands exhibited a considerably lower SEN for the respective B−N bonds. The SEN of the C=S bonds was found to decrease upon reaction with BH_4^- or $PhBH_3^-$. Nevertheless no clear trend can be observed in the series of ligands.

Table 2.10: Geometrical Data Starting Material

compound	B-H [Å]	B-C [Å]	compound	N-H [Å]	C=S [Å]
BH_4^-	1.252	-	mH	1.011	1.664
$PhBH_3^-$	1.249	1.619	$n^{tBu}H$	1.018	1.658
cBH_4^-	1.248	-	cmH	1.441	1.673
$cPhBH_3^-$	1.248	1.617	$cn^{tBu}H$	1.019	1.666

Table 2.11: Geometrical Data Ligands

L_i	B-N1 [Å]	B-N2 [Å]	B-N3 [Å]	C=S1 [Å]	C=S2 [Å]	C=S3 [Å]	B-H/C [Å]
Tm	1.558	1.558	1.559	1.680	1.679	1.679	1.211
Tm_2n^{tBu}	1.578*	1.552	1.551	1.680	1.687	1.672*	1.210
Tmn_2^{tBu}	1.567*	1.566*	1.537	1.668*	1.680	1.675*	1.197
Tn^{tBu}	1.560	1.561	1.561	1.677	1.676	1.676	1.210
PhTm	1.595	1.586	1.571	1.686	1.677	1.681	1.621
$PhTn^{tBu}$	1.607	1.569	1.613	1.666	1.679	1.668	1.617

Table 2.12: Geometrical Data Ligands (COSMO)

L_i	B-N1 [Å]	B-N2 [Å]	B-N3 [Å]	C=S1 [Å]	C=S2 [Å]	C=S3 [Å]	B-H/C [Å]
cTm	1.552	1.552	1.552	1.691	1.691	1.691	1.214
cTm_2n^{tBu}	1.576*	1.544	1.544	1.690	1.693	1.685*	1.213
$cTmn_2^{tBu}$	1.570*	1.567*	1.535	1.684*	1.690	1.689*	1.212
cTn^{tBu}	1.559	1.559	1.559	1.687	1.687	1.687	1.210
cPhTm	1.587	1.578	1.569	1.691	1.687	1.688	1.619
$cPhTn^{tBu}$	1.605	1.576	1.610	1.680	1.689	1.681	1.617

The trends found in the SEN were reproduced in the bond distances. The bond lengths of pyridazine $B-N$ decreases in absence of methimazole moieties.

The $B-N$ bond formation resulted in hardly any changes in the $B-C$ bond length. Unexpectedly, the remaining $B-H$ bond in unsubstituted borates was shortened by ca. 3 % even though the SEN was reduced.

The longest $B-N$ distances were observed in phenyl substituted ligands emphasizing the competition for electrons with the phenyl moiety.

Population analysis showed a relocation of the negative charge from the boron atom (charge: -0.746 $\rightarrow$ +0.56) to the methimazole and/or pyridazine moietes in course of the ligand formation. A significantly higher electron density was located at the methimazole bonding nitrogens. The total population at the bonding nitrogens remained constant, a slight increase could be observed at the sulfur atoms.

Table 2.13: Population Analysis Starting Material

compound	B	H	H/C	compound	N	S
BH_4^-	5.746	1.063	-	mH	7.519	16.284
$PhBH_3^-$	5.463	1.041	6.132	$n^{tBu}H$	7.307	16.186
cBH_4^-	5.749	1.063	-	cmH	7.514	16.349
$cPhBH_3^-$	5.463	1.049	6.154	$cn^{tBu}H$	7.299	16.251

Complex formation This section focusses on the formation of different (hypothetical) Mo scorpionate complexes. The starting material hexacarbonyl molybdenum(0) $[Mo(CO)_6]$ was refluxed in CH_3CN to yield the more reactive trisacetonitrile adduct $[Mo(CO)_3(CH_3CN)_3]$ **1** with the equilibrium constant K_1 (see equation 2.10).

Table 2.14: Population Analysis Ligands

L_i	B	N1	N2	N3	S1	S2	S3	H/C
Tm	4.446	7.524	7.523	7.523	16.344	16.345	16.344	0.992
$\text{Tm}_2\text{n}^{\text{tBu}}$	4.449	7.307*	7.524	7.515	16.343	16.371	16.235*	0.988
$\text{Tmn}_2^{\text{tBu}}$	4.454	7.289*	7.310*	7.522	16.231*	16.360	16.267*	0.979
Tn^{tBu}	4.461	7.297	7.296	7.295	16.255	16.255	16.254	0.971
PhTm	4.141	7.544	7.548	7.552	16.343	16.327	16.326	6.283
PhTn^{tBu}	4.085	7.336	7.366	7.330	16.194	16.251	16.170	6.290

Table 2.15: Population Analysis Ligands (COSMO)

L_i	B	N1	N2	N3	S1	S2	S3	H/C
cTm	4.434	7.522	7.522	7.522	16.434	16.433	16.434	1.020
$\text{cTm}_2\text{n}^{\text{tBu}}$	4.437	7.303*	7.525	7.519	16.432	16.438	16.341*	1.013
$\text{cTmn}_2^{\text{tBu}}$	4.441	7.291*	7.307*	7.522	16.338*	16.436	16.354*	1.007
cTn^{tBu}	4.446	7.297	7.297	7.297	16.348	16.348	16.348	0.999
cPhTm	4.140	7.543	7.545	7.547	16.416	16.414	16.405	6.273
$\text{cPhTn}^{\text{tBu}}$	4.081	7.333	7.356	7.330	16.309	16.334	16.285	6.295

$$[\text{Mo(CO)}_6] \xleftarrow{\text{CH}_3\text{CN}} [\text{Mo(CO)}_3(\text{CH}_3\text{CN})_3] + 3\,\text{CO} \tag{2.10}$$
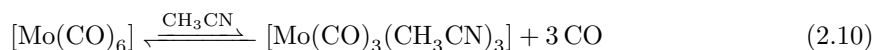
The Mo precursor **1** was reacted with the different ligands, denoted as L_i^-, to yield the respective Mo scorpionate complex. The equilibrium constant K_2 is the key quantity for this reaction.

$$[\text{Mo(CO)}_3(\text{CH}_3\text{CN})_3] + \text{L}_i^- \rightleftharpoons [\text{MoL}_i(\text{CO})_3]^- + 3\,\text{CH}_3\text{CN} \tag{2.11}$$
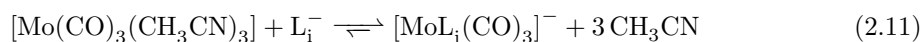
The overall reaction can be summarized as equation 2.12. The overall equilibrium constant of the formation reaction K_r is the product of K_1 and K_2.

$$[\text{Mo(CO)}_6] + \text{L}_i^- \rightleftharpoons [\text{MoL}_i(\text{CO})_3]^- + 3\,\text{CO} \tag{2.12}$$
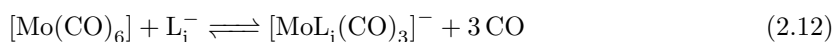
The thermodynamical data is summarized in Tables 2.16, 2.17 and 2.18. Since calculations without solvent contribution reproduce the same trends the respective tables are attached in the appendix. $[\text{Mo(CO)}_6]$ was found to be a relatively stable complex. Hence the formation of the reactive CH_3CN adduct was an endergonic reaction, that demanded activation energy in form of heat or radiation.

Table 2.16: Thermodynamical Data Precursor Formation (step 1)

	$\Delta_r H$ [kJ/mol]	ΔS [kJ/mol·K]	ΔG [kJ/mol]	K_1^{298}
no COSMO	169.81	0.01699	164.74	$1.370 \cdot 10^{-29}$
COSMO	161.93	-0.01086	165.17	$1.154 \cdot 10^{-29}$

The complexes of the type $[\text{L}_i\text{Mo(CO)}_3]$ will be denoted as $[L_i]$. The data shown in Table 2.17 predicted, that the reaction of 1 with Tm was favored over the reaction of 1 with Tn^{tBu} by a factor of roughly 10^6. This observation could not be extended to the phenyl substituted ligand.

Table 2.17: Thermodynamical Data Complex Formation (step2) (COSMO)

$[L_iMo(CO)_3]$	$\Delta_r H$ [kJ/mol]	ΔS [kJ/mol·K]	ΔG [kJ/mol]	K_2^{298}
c[Tm]	-5.99	0.23296	-75.45	$1.653 \cdot 10^{13}$
c[Tm$_2$n^{tBu}]	7.68	0.24030	-63.96	$1.607 \cdot 10^{11}$
c[Tmn$_2^{tBu}$]	24.75	0.24777	-49.12	$4.032 \cdot 10^{08}$
c[Tn^{tBu}]	40.45	0.26903	-39.77	$9.269 \cdot 10^{06}$
cPhTm	-23.26	0.23104	-92.15	$1.393 \cdot 10^{16}$
cPhTn^{tBu}	-23.81	0.26018	-101.38	$5.785 \cdot 10^{17}$

The coordination of the ligand demands a change in the conformation of the ligand. Figure 2.12 shows the stable structure of Tm and the necessary conformation for a κ^3-S,S',S" coordination of the ligand 2Tm.

(a) Tm
(b) 2Tm
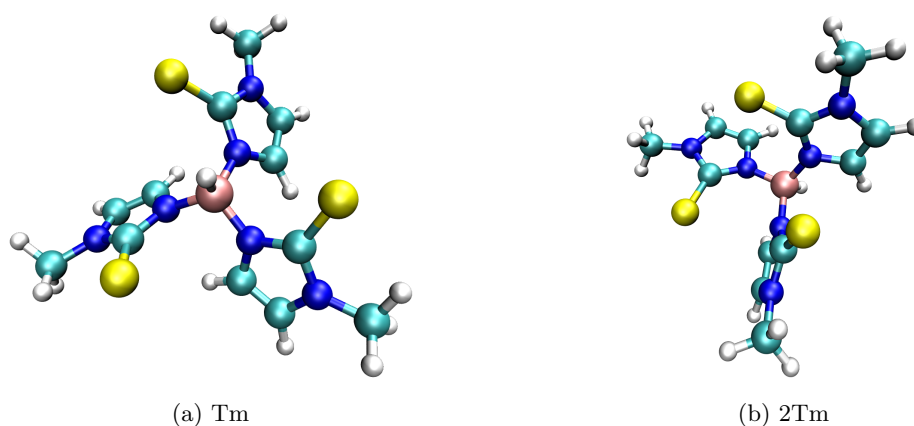
Figure 2.12: Conformers of Tm

The differences in energy (ΔE_{conf}) are enlisted in Table 2.18. The more pyridazine moieties the greater ΔE_{conf}. The more spacious phenyl moiety in PhTm and PhTn^{tBu} implicated a great reduction of ΔE_{conf}.

The overall reaction was endergonic for all ligand systems. The values for K_r^{298} were decreasing by a magnitude of 10^6 from Tm to Tn^{tBu}. Nevertheless the differences in ΔG and hence K_r^{298} were found to be tellingly small once the conformation suitable for coordination was reached. Relatively large values of K_r^{298} were found for the phenyl substituted ligands.

Analysis of the SEN in the complexes showed (see Tables 2.19 and 2.20), that the electron density in Mo−S bond of pyridazine scorpionate complexes were slightly higher than in their methimazole counterparts.

The coordination of CH_3CN increased the SEN for the Mo−C bonds of the remaining carbonyl ligands. The effect could also be observed in the scorpionate complexes.

A comparison to the uncoordinated ligands showed, that the SEN of the B−N bonds remained unaffected for the greater part. The SEN for the C=S bonds were reduced as a result of the coordination.

Table 2.18: Thermodynamical Data Complex Formation (total) (COSMO)

L_i	$\Delta_r H$ [kJ/mol]	ΔS [kJ/mol·K]	ΔG [kJ/mol]	K_r^{298}	ΔE_{conf} [kJ/mol]
cTm	155.94	0.22210	89.72	$1.906 \cdot 10^{-16}$	0.00
c2Tm	108.97	0.22595	41.60	$5.141 \cdot 10^{-08}$	47.45
cTm$_2$n^{tBu}	169.62	0.22944	101.21	$1.854 \cdot 10^{-18}$	0.00
c2Tm$_2$n^{tBu}	116.25	0.24833	42.21	$4.024 \cdot 10^{-08}$	53.57
cTmn$_2^{tBu}$	186.69	0.23691	116.05	$4.651 \cdot 10^{-21}$	0.00
c2Tmn$_2^{tBu}$	120.67	0.25048	45.99	$8.776 \cdot 10^{-09}$	66.59
cTn^{tBu}	202.38	0.25817	125.40	$1.069 \cdot 10^{-22}$	0.00
c2Tn^{tBu}	124.72	0.25839	47.68	$4.428 \cdot 10^{-09}$	79.28
cPhTm	138.67	0.22018	73.02	$1.607 \cdot 10^{-13}$	0.00
c2PhTm	121.39	0.22119	55.44	$1.937 \cdot 10^{-10}$	17.40
cPhTn^{tBu}	138.12	0.24932	63.79	$6.673 \cdot 10^{-12}$	0.00
c2PhTn^{tBu}	133.38	0.23876	62.19	$1.271 \cdot 10^{-11}$	5.17

Table 2.19: SEN Complexes 1 (COSMO)

$[L_i Mo(CO)_3]$	Mo-C1	Mo-C2	Mo-C3	Mo-S1	Mo-S2	Mo-S3
c[Tm]	0.974	0.969	0.965	0.228	0.231	0.228
c[Tm$_2$n^{tBu}]	0.957	0.972	0.954	0.236	0.233	0.237*
c[Tmn$_2^{tBu}$]	0.965	0.954	0.957	0.240*	0.241	0.243*
c[Tn^{tBu}]	0.956	0.956	0.954	0.250	0.249	0.251
c[PhTm]	0.957	0.962	0.963	0.233	0.240	0.225
c[PhTn^{tBu}]	0.971	0.956	0.958	0.259	0.244	0.251
c[Mo(CO)$_6$]	0.636	0.634	0.633			
c1	0.884	0.884	0.883			

Table 2.20: SEN Complexes 2 (COSMO)

$[L_i Mo(CO)_3]$	B-N1	B-N2	B-N3	C=S1	C=S2	C=S3	B-H/B-C
c[Tm]	1.240	1.237	1.240	1.476	1.476	1.473	1.338
c[Tm$_2$n^{tBu}]	1.170*	1.254	1.250	1.485	1.466	1.484*	1.347
c[Tmn$_2^{tBu}$]	1.181*	1.184*	1.263	1.486*	1.481	1.474*	1.339
c[Tn^{tBu}]	1.202	1.196	1.195	1.478	1.479	1.485	1.350
c[PhTm]	1.204	1.220	1.190	1.483	1.470	1.476	1.367
c[PhTn^{tBu}]	1.140	1.173	1.175	1.479	1.483	1.481	1.343

The effect of the coordination was expressed in a shortening of the Mo−CO bonds in accordance with increasing SEN. All values were found to be within expected ranges. The B−N bonds of pyridazine moieties in heteroscorpionate complexes were slightly elongated compared to homoscorpionate complex [Tn^{tBu}] as already observed in the free ligands.

The population analysis confirmed, that the coordination of the ligand resulted in a decrease of electron density in the ligand at all atoms. The coordinating sulfur atoms were affected significantly stronger than the other atoms.

The dipolmoments of the B_N bonds can be calculated according to equation 2.13. The charges

Table 2.21: Geometrical Data Complexes 1 (COSMO)

[L$_i$Mo(CO)$_3$]	Mo-C1 [Å]	Mo-C2 [Å]	Mo-C3 [Å]	Mo-S1 [Å]	Mo-S2 [Å]	Mo-S3 [Å]
c[Tm]	1.927	1.926	1.927	2.661	2.658	2.662
c[Tm$_2$n^{tBu}]	1.930	1.928	1.924	2.652	2.648	2.681*
c[Tmn$_2^{tBu}$]	1.928	1.933	1.928	2.665*	2.635	2.648*
c[Tn^{tBu}]	1.933	1.933	1.932	2.636	2.636	2.635
c[PhTm]	1.927	1.926	1.926	2.644	2.647	2.690
c[PhTn^{tBu}]	1.922	1.925	1.923	2.618	2.644	2.636
c[Mo(CO)$_6$]	2.057	2.057	2.057			
c**1**	1.955	1.955	1.955			

Table 2.22: Geometrical Data Complexes 2 (COSMO)

[L$_i$Mo(CO)$_3$]	B-N1 [Å]	B-N2 [Å]	B-N3 [Å]	C=S1 [Å]	C=S2 [Å]	C=S3 [Å]	B-H/C [Å]
c[Tm]	1.547	1.547	1.547	1.714	1.713	1.714	1.225
c[Tm$_2$n^{tBu}]	1.580*	1.540	1.538	1.711	1.713	1.713*	1.221
c[Tmn$_2^{tBu}$]	1.568*	1.572*	1.529	1.709*	1.708	1.711*	1.216
c[Tn^{tBu}]	1.557	1.560	1.560	1.708	1.709	1.707	1.211
c[PhTm]	1.564	1.559	1.574	1.712	1.716	1.715	1.644
c[PhTn^{tBu}]	1.579	1.588	1.569	1.71	1.707	1.706	1.649

are obtained by subtracting the population number from the respective element's charge number. In the case of Mo only 14 e$^-$ have to be considered since 28 are approximated by the effective core potential). A comparison of B−N1 bond Tm and Tn^{tBu} showed that the bond was more polarized in Tm (8.14 vs. 6.60 D).

$$\vec{\mu} = \frac{q \cdot \vec{l}}{3.33 \cdot 10^{-33}} \ [D] \tag{2.13}$$

Table 2.23: Population Analysis Complexes (COSMO)

[L$_i$Mo(CO)$_3$]	Mo	B	N1	N2	N3	S1	S2	S3	H/C
c[Tm]	14.699	4.421	7.515	7.516	7.516	16.257	16.255	16.257	1.051
c[Tm$_2$n^{tBu}]	14.698	4.420	7.291*	7.525	7.514	16.248	16.247	16.209*	1.040
c[Tmn$_2^{tBu}$]	14.717	4.419	7.283*	7.300*	7.523	16.190*	16.232	16.180*	1.027
c[Tn^{tBu}]	14.742	4.419	7.304	7.296	7.295	16.164	16.168	16.157	1.014
c[PhTm]	14.691	4.169	7.536	7.539	7.532	16.251	16.247	16.259	6.275
c[PhTn^{tBu}]	14.726	4.116	7.336	7.325	7.340	16.148	16.150	16.156	6.263
c[Mo(CO)$_6$]	15.176								
c**1**	14.502								

2.2.2 Thermodynamical Investigation of the 1st dissociation reaction

The two possible ways for the first dissociation are shown in equations 2.14 and 2.15. X denotes the hydrogen or phenyl moiety, R the respective methimazole and/or pyridazine moieties. Structures featuring a THF molecule will be denoted with a "t" prefix, charges -, 0 or +.

In the first case the negative charge remained at residual boron compound, in the second case the charge was located at the dissociated methimazole or pyridazine moiety. The results are summarized in Tables 2.24 and 2.25.

$$XBR_3^- \longrightarrow XBR_2^- + R \qquad (2.14)$$

$$XBR_3^- \longrightarrow XBR_2 + R^- \qquad (2.15)$$

A comparison of the Gibbs free enthalpies and the equilibrium constants showed, that a dissociation of the second case (see equation 2.15) was significantly more likely than the first case, with the charge remaining at the boron compound.

In heteroscorpionates the dissociation of a methimazole moiety was favored over the pyridazines, indicating that the negative charge was better stabilized by pyridazines. In the case of the homoscorpionates the Tm ligand was less prone to dissociation.

Table 2.24: Thermodynamical Data Dissociation 1.R1

educt	product	ΔH [kJ/mol]	ΔS [kJ/mol·K]	$\Delta_r H$ [kJ/mol]	ΔG [kJ/mol]	K^{298}
Tm	Dm-	-11.93	0.19158	396.43	339.31	$3.56 \cdot 10^{-60}$
Tm_2n^{tBu}	Dmn^{tBu}-	-14.02	0.20628	288.97	227.47	$1.40 \cdot 10^{-40}$
Tm_2n^{tBu}	Dm-	-13.01	0.20162	452.75	392.64	$1.62 \cdot 10^{-69}$
Tmn_2^{tBu}	Dn^{tBu}-	-13.40	0.17752	276.36	223.43	$7.15 \cdot 10^{-40}$
Tmn_2^{tBu}	Dmn^{tBu}-	-14.86	0.21237	354.06	290.75	$1.15 \cdot 10^{-50}$
Tn^{tBu}	Dn^{tBu}-	-14.64	0.16990	336.66	286.01	$7.78 \cdot 10^{-51}$

In the second case the equilibrium constant of Tm was smaller by a factor of 10^6 than that of Tn^{tBu}. Boranes tend to form diboranes with two three-center-two-electron (3c2e) bonds. Relaxation of an appropriate input geometry resulted in structure dBm0 with a B−B distance of 3.584 Å with no obvious 3c2e bonds. The formation of the obtained dimer consisting of two Dm0 units was found to be thermodynamically unfavored.

A closer look at the obtained structures showed the formation of B−S bonds (see Figure 2.13a). Fan et al.[126] investigated the dissociation of B_2H_6 in DMS and reported, that the solvent significantly lowered the activation barriers. Hence the first dissociation was investigated with a THF molecule to stabilize the reaction product (see Figure 2.13b).

A negative charge at the boron atom prevented a stable THF adduct. Hence no stabilizing effect was observed (see Table 2.26). The equilibrium constants were reduced by a factor of 10^{-10}-10^{-14}. The neutral dissociation products were found to form stable THF adducts. This resulted in significantly less positive ΔG values for both the substituted and unsubstituted ligands. Noticable was, that the dissociation of Tm was more favorable than of Tn^{tBu} by ca. 10 kJ/mol. The B−O bond distance was 1.559 Å in both structures. However, in the heteroscorpionate ligands the dissociation

Table 2.25: Thermodynamical Data Dissociation 1.R2

educt	product	ΔH [kJ/mol]	ΔS [kJ/mol·K]	$\Delta_r H$ [kJ/mol]	ΔG [kJ/mol]	K^{298}
Tm	Dm0	-8.00	0.17955	235.26	181.73	$1.447 \cdot 10^{-32}$
$\text{Tm}_2\text{n}^{\text{tBu}}$	$\text{Dmn}^{\text{tBu}}0$	-7.96	0.17851	194.80	141.58	$1.569 \cdot 10^{-25}$
$\text{Tm}_2\text{n}^{\text{tBu}}$	Dm0	-8.08	0.19073	216.79	159.93	$9.566 \cdot 10^{-29}$
$\text{Tmn}_2^{\text{tBu}}$	$\text{Dn}^{\text{tBu}}0$	-8.08	0.17814	213.98	160.87	$6.543 \cdot 10^{-29}$
$\text{Tmn}_2^{\text{tBu}}$	$\text{Dmn}^{\text{tBu}}0$	-7.80	0.18574	177.48	122.10	$4.051 \cdot 10^{-22}$
Tn^{tBu}	$\text{Dn}^{\text{tBu}}0$	-8.32	0.17166	199.49	148.31	$1.036 \cdot 10^{-26}$
Tm	dDm0	5.30	-0.16630	-28.15	21.44	$1.756 \cdot 10^{-4}$

(a) $\text{Dn}^{\text{tBu}}0$ (b) $\text{tDn}^{\text{tBu}}0$
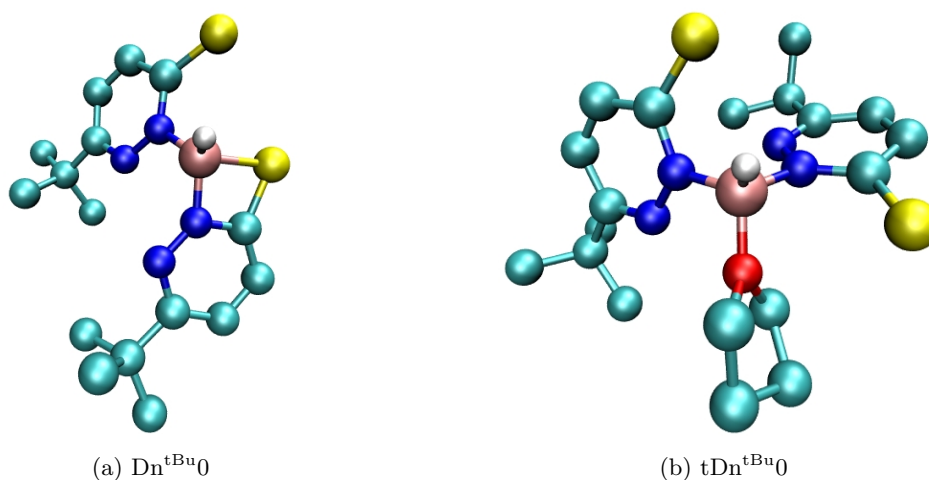
Figure 2.13: Dissociation products with and without THF

of pyridazine showed ΔG values 30-40 kJ/mol smaller than the values in case of a methimazole dissociation, resulting in greater equilibrium constants by the order of 10^5-10^6.

The results for a dissociation with the charge remaining using the COSMO option are enlisted in the appendix, since results only differed slightly from the values given in Table 2.26.

The solvent's influence was significantly more important in dissociations of the second type. The values for ΔG were lowered to +100 kJ/mol and lower. The B−O distance was reduced to 1.549 Å (ctTm) and 1.527 (ctTn$^{\text{tBu}}$). In contrast to the results discussed above, the dissociation reaction of Tn$^{\text{tBu}}$ was marginally preferred over the dissociation of Tm.

The stability of PhTm was in the same range as the unsubstituted ligands; PhTn$^{\text{tBu}}$ was identified the least stable system.

Table 2.26: Thermodynamical Data Dissociation 1.R1 (THF)

educt	product	ΔH [kJ/mol]	ΔS [kJ/mol·K]	$\Delta_r H$ [kJ/mol]	ΔG [kJ/mol]	K^{298}
Tm	tDm-	-7.02	-0.01012	412.89	415.91	$1.35 \cdot 10^{-73}$
Tm$_2$n^{tBu}	tDmn^{tBu}-	-5.42	0.00269	286.92	286.12	$7.43 \cdot 10^{-51}$
Tm$_2$n^{tBu}	tDm-	-8.10	-0.00008	469.21	469.24	$6.15 \cdot 10^{-83}$
Tmn$_2^{tBu}$	tDn^{tBu}-	-7.23	0.00547	292.53	290.90	$1.08 \cdot 10^{-51}$
Tmn$_2^{tBu}$	tDmn^{tBu}-	-6.26	0.00878	344.39	341.77	$1.32 \cdot 10^{-60}$
Tn^{tBu}	tDn^{tBu}-	-8.47	-0.00215	352.84	353.48	$1.18 \cdot 10^{-62}$
PhTm	tPhDm-	-7.78	-0.00465	372.23	373.62	$3.48 \cdot 10^{-66}$
PhTn^{tBu}	tPhDn^{tBu}-	-5.71	0.01109	300.59	297.28	$8.24 \cdot 10^{-53}$

Table 2.27: Thermodynamical Data Dissociation 1.R2 (THF)

educt	product	ΔH [kJ/mol]	ΔS [kJ/mol·K]	$\Delta_r H$ [kJ/mol]	ΔG [kJ/mol]	K^{298}
Tm	tDm0	1.39	-0.00832	142.69	145.17	$3.68 \cdot 10^{-26}$
Tm$_2$n^{tBu}	tDmn^{tBu}0	1.98	-0.01884	152.50	158.12	$1.98 \cdot 10^{-28}$
Tm$_2$n^{tBu}	tDm0	1.31	0.00286	124.22	123.37	$2.43 \cdot 10^{-22}$
Tmn$_2^{tBu}$	tDn^{tBu}0	1.26	0.01332	170.77	166.80	$5.97 \cdot 10^{-30}$
Tmn$_2^{tBu}$	tDmn^{tBu}0	2.14	-0.01161	135.18	138.64	$5.12 \cdot 10^{-25}$
Tn^{tBu}	tDn^{tBu}0	1.02	0.00684	156.29	154.25	$9.44 \cdot 10^{-28}$
PhTm	tPhDm0	0.43	0.00174	214.12	213.60	$3.77 \cdot 10^{-38}$
PhTn^{tBu}	tPhDn^{tBu}0	2.04	0.00203	68.64	68.03	$1.20 \cdot 10^{-12}$

Table 2.28: Thermodynamical Data Dissociation 1.R2 (COSMO/THF)

educt	product	ΔH [kJ/mol]	ΔS [kJ/mol·K]	$\Delta_r H$ [kJ/mol]	ΔG [kJ/mol]	K^{298}
cTm	cdDm0	-13.32	0.21283	159.41	95.95	$1.54 \cdot 10^{-17}$
cTm	ctDm0	1.00	-0.00978	96.86	99.78	$3.30 \cdot 10^{-18}$
cTm$_2$n^{tBu}	ctDmn^{tBu}0	0.73	-0.01036	99.74	102.83	$9.65 \cdot 10^{-19}$
cTm$_2$n^{tBu}	ctDm0	1.96	-0.01474	78.99	83.38	$2.46 \cdot 10^{-15}$
cTmn$_2^{tBu}$	ctDn^{tBu}0	0.96	-0.00342	101.17	102.19	$1.25 \cdot 10^{-18}$
cTmn$_2^{tBu}$	ctDmn^{tBu}0	1.30	-0.00967	87.14	90.03	$1.69 \cdot 10^{-16}$
cTn^{tBu}	ctDn^{tBu}0	1.70	-0.00253	91.89	92.64	$5.88 \cdot 10^{-17}$
cPhTm	ctPhDm0	-11.99	-0.00041	90.07	90.19	$1.58 \cdot 10^{-16}$
cPhTn^{tBu}	ctPhDn^{tBu}0	2.53	0.00722	57.52	55.37	$1.99 \cdot 10^{-10}$

2.2.3 Thermodynamical Investigation of the 2nd dissociation reaction

In order to compare the results of the first dissociation to similar systems, the dissociation of a second pyridazine or methimazole moiety was considered, starting from the obtained dissociation products.

Since the first dissociation, without a THF molecule present, resulted in the formation of a doubtful B−S bond, the second dissociation was unreasonable.

A neutral compound could dissociate in three different ways, as shown in equations 2.16-2.18. In the first type a negative charge remained at the boron compound and the cleaved moiety was positively charged. The second type described a homolytic and the third a heterolytic bond dissociation with the negative charge located at the free methimazole or pyridazine moiety.

$$tXBR_2 + THF \longrightarrow t_2XBR^- + R^+ \tag{2.16}$$

$$tXBR_2 + THF \longrightarrow t_2XBR + R \tag{2.17}$$

$$tXBR_2 + THF \longrightarrow t_2XBR^+ + R^- \tag{2.18}$$
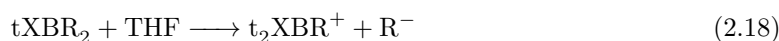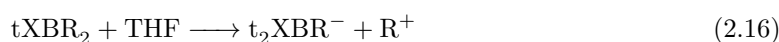
Additionally, a second dissociation of the less probable negatively species was investigated. The two types of dissociations considered, are shown in equations 2.19 and 2.20.

All calculations were performed in presence of a second THF molecule. Only in the case of tBm0 and tBm- local minimum could not be found.

$$tXBR_2^- + THF \longrightarrow t_2XBR^- + R \tag{2.19}$$

$$tXBR_2^- + THF \longrightarrow t_2XBR + R^- \tag{2.20}$$
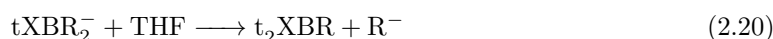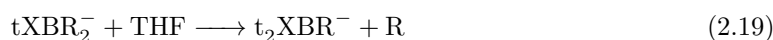
The results enlisted in Table 2.29 suggested, that a second bond dissociation was less likely than the first one. Unexpectedly, a homolytic bond cleavage was preferred over the heterolytic dissociations. The ΔG values were $>300\,\text{kJ/mol}$, except for the dissociation of PhDm ($209\,\text{kJ/mol}$).

A reaction similar to the first dissociation showed, that a negative charge greatly enhanced tendency towards dissociation. Dissociation reactions with the negative charge remaining at the boron compound feature ΔG values $>1000\,\text{kJ/mol}$, making this reaction highly unfavorable.

A hypothetical dissociation, starting from a negatively charged residual ligand, confirmed, that the negative charge would be located at the cleaved pyridazine or methiamzole moiety. The equilibrium constants were found to be significantly higher by several orders of magnitudes, than a second dissociation of a neutral compound, emphasizing the relevance of the negative charge. Remarkably, the dissociation of PhDm- was found to be more favorable, than the dissociation of PhDn$^{\text{tBu}}$.

Table 2.29: Thermodynamical Data Dissociation 2.R1 (THF)

educt	product	ΔH [kJ/mol]	ΔS [kJ/mol·K]	$\Delta_r H$ [kJ/mol]	ΔG [kJ/mol]	K^{298}
tDm0	tBm0	-13.40	0.19176	414.18	357.00	$2.83 \cdot 10^{-63}$
tBmn^{tBu}0	tBm0	-15.07	0.21232	460.68	397.38	$2.39 \cdot 10^{-70}$
tBmn^{tBu}0	t$_2$Bn^{tBu}0	-7.27	0.01505	328.75	324.26	$1.54 \cdot 10^{-57}$
tDn^{tBu}0	t$_2$Bn^{tBu}0	-7.39	-0.01102	367.95	371.23	$9.11 \cdot 10^{-66}$
tPhDm0	t$_2$PhBm0	-6.36	0.04414	222.57	209.41	$2.04 \cdot 10^{-37}$
tPhDn^{tBu}0	t$_2$PhBn^{tBu}0	-6.68	0.02154	387.37	380.95	$1.81 \cdot 10^{-67}$
tDm0	t$_2$Bm+	-2.37	0.00060	520.28	520.10	$7.53 \cdot 10^{-92}$
tDmn^{tBu}0	t$_2$Bm+	-3.04	0.02230	492.00	485.35	$9.25 \cdot 10^{-86}$
tDmn^{tBu}0	t$_2$Bn^{tBu}+	-2.45	0.01695	525.23	520.18	$7.30 \cdot 10^{-92}$
tDn^{tBu}0	t$_2$Bn^{tBu}+	-1.57	-0.00798	489.64	492.02	$6.27 \cdot 10^{-87}$
tPhDm0	t$_2$PhBm+	-2.38	0.00159	431.52	431.05	$3.01 \cdot 10^{-76}$
tPhDn^{tBu}0	t$_2$PhBn^{tBu}+	-1.31	0.00252	497.87	497.12	$8.01 \cdot 10^{-88}$
tDm0	tBm-	-21.20	0.19962	1240.12	1180.60	$1.43 \cdot 10^{-207}$
tDmn^{tBu}0	tBm-	-26.19	0.22328	1332.38	1265.81	$1.69 \cdot 10^{-222}$
tDmn^{tBu}0	t$_2$Bn^{tBu}-	-14.58	0.06315	1042.81	1023.98	$3.95 \cdot 10^{-180}$
tDn^{tBu}0	t$_2$Bn^{tBu}-	-18.02	0.04018	1127.77	1115.79	$3.24 \cdot 10^{-196}$
tPhDm0	tPhBm-	-20.13	0.20058	1076.28	1016.47	$8.16 \cdot 10^{-179}$
tPhDn^{tBu}0	tPhBn^{tBu}-	-21.29	0.20298	1132.76	1072.24	$1.38 \cdot 10^{-188}$

Table 2.30: Thermodynamical Data Dissociation 2.R2 (THF)

educt	product	ΔH [kJ/mol]	ΔS [kJ/mol·K]	$\Delta_r H$ [kJ/mol]	ΔG [kJ/mol]	K^{298}
tDm-	tBm0	-4.99	0.19356	143.97	86.26	$7.70 \cdot 10^{-16}$
tDmn^{tBu}-	tBm0	-6.67	0.19193	251.47	194.25	$9.27 \cdot 10^{-35}$
tDmn^{tBu}-	t$_2$Bn^{tBu}0	0.13	-0.00648	194.33	196.26	$4.12 \cdot 10^{-35}$
tDn^{tBu}-	t$_2$Bn^{tBu}0	2.10	-0.00203	171.40	172.00	$7.32 \cdot 10^{-31}$
tPhDm-	t$_2$PhBm0	1.85	0.05053	64.46	49.40	$2.22 \cdot 10^{-9}$
tPhDn^{tBu}-	t$_2$PhBn^{tBu}0	1.07	0.01248	155.42	151.70	$2.65 \cdot 10^{-27}$
tDm-	tBm-	-10.09	0.19686	396.27	337.57	$7.18 \cdot 10^{-60}$
tDmn^{tBu}-	tBm-	-12.77	0.19409	578.56	520.69	$5.94 \cdot 10^{-92}$
tDmn^{tBu}-	t$_2$Bn^{tBu}-	-4.48	0.03706	334.75	323.70	$1.94 \cdot 10^{-57}$
tDn^{tBu}-	t$_2$Bn^{tBu}-	-3.51	0.04037	386.61	374.57	$2.37 \cdot 10^{-66}$
tPhDm-	tPhBm-	-9.22	0.20241	344.53	284.18	$1.63 \cdot 10^{-50}$
tPhDn^{tBu}-	tPhBn^{tBu}-	-8.52	0.18512	356.19	301.00	$1.84 \cdot 10^{-53}$

Using the COSMO model provided results, which did not coincide with the trends, obtained from the calculations without solvent interactions. The equilibrium constants for a homolytic $B-N$ bond cleavage remained in the order of 10^{-50} and smaller. By contrast, the ΔG values for a heterolytic bond dissociation, resulting in a positively charged residual boron compound and negatively charged methimazole or pyridazine moiety, were reduced by several $100\,\text{kJ/mol}$, associated with equilibrium constants in the order of 10^{-30}.

The ΔG values for Dm0 and Dn$^{\text{tBu}}$0 differed only by $4\,\text{kJ/mol}$, suggesting a similar bondstrength. A dissociation of pyridazine in a mixed Dmn$^{\text{tBu}}$0 species was found to be preferred over a methimazole cleavage by ca. $35\,\text{kJ/mol}$.

Both variants agreed on a disfavored heterolytic cleavage, in the case of the negative charge remaining at boron compound, with equilibrium constants in the order of 10^{-120} smaller.

Table 2.31: Thermodynamical Data Dissociation 2.R1 (COSMO/THF)

educt	product	ΔH [kJ/mol]	ΔS [kJ/mol·K]	$\Delta_r H$ [kJ/mol]	ΔG [kJ/mol]	K^{298}
ctDm0	ct$_2$Bm0	-5.91	0.00296	454.24	453.35	$3.73 \cdot 10^{-80}$
ctDmn$^{\text{tBu}}$0	ct$_2$Bm0	-5.07	-0.00032	505.29	505.39	$2.85 \cdot 10^{-89}$
ctDmn$^{\text{tBu}}$0	ct$_2$Bn$^{\text{tBu}}$0	-2.83	-0.01134	305.38	308.76	$8.02 \cdot 10^{-55}$
ctDn$^{\text{tBu}}$0	ct$_2$Bn$^{\text{tBu}}$0	-2.88	-0.01649	363.16	368.07	$3.26 \cdot 10^{-65}$
ctPhDm0	ct$_2$PhBm0	9.25	0.03118	310.50	301.21	$1.69 \cdot 10^{-53}$
ctPhDn$^{\text{tBu}}$0	ct$_2$PhBn$^{\text{tBu}}$0	-2.06	-0.01120	308.46	311.80	$2.35 \cdot 10^{-55}$
ctDm0	ct$_2$Bm+	0.28	0.00125	191.59	191.21	$3.16 \cdot 10^{-34}$
ctDmn$^{\text{tBu}}$0	ct$_2$Bm+	1.51	-0.00313	170.83	171.77	$8.05 \cdot 10^{-31}$
ctDmn$^{\text{tBu}}$0	ct$_2$Bn$^{\text{tBu}}$+	1.06	-0.00522	205.81	207.37	$4.66 \cdot 10^{-37}$
ctDn$^{\text{tBu}}$0	ct$_2$Bn$^{\text{tBu}}$+	1.40	-0.01147	191.78	195.20	$6.31 \cdot 10^{-35}$
ctPhDm0	ct$_2$PhBm+	13.55	-0.00461	177.61	178.99	$4.38 \cdot 10^{-32}$
ctPhDn$^{\text{tBu}}$0	ct$_2$PhBn$^{\text{tBu}}$+	2.66	-0.00354	143.73	144.79	$4.30 \cdot 10^{-26}$
ctDm0	ct$_2$Bm-	-11.20	0.04233	807.70	795.08	$5.02 \cdot 10^{-140}$
ctDmn$^{\text{tBu}}$0	ct$_2$Bm-	-14.69	0.05069	923.94	908.82	$5.92 \cdot 10^{-160}$
ctDmn$^{\text{tBu}}$0	ct$_2$Bn$^{\text{tBu}}$-	-9.61	0.02369	700.58	693.52	$3.12 \cdot 10^{-122}$
ctDn$^{\text{tBu}}$0	ct$_2$Bn$^{\text{tBu}}$-	-13.99	0.03018	823.54	814.54	$1.95 \cdot 10^{-143}$
ctPhDm0	ct$_2$PhBm-	-3.59	0.20163	759.94	699.83	$2.45 \cdot 10^{-123}$
ctPhDn$^{\text{tBu}}$0	ct$_2$PhBn$^{\text{tBu}}$-	-16.65	0.19381	756.05	698.26	$4.60 \cdot 10^{-123}$

2.2.4 The B−N bond dissociation

A stepwise elongation of the B−N bond allows a more detailed view on the dissociation process. A rather simple potential to describe dissociations without relaxations is the Morse potential (see equation 2.21). The dissociation energy D_e is obtained by extrapolation.

$$V(x) = D_e \cdot (1 - e^{-a(x-x_0)})^2 \tag{2.21}$$

An interesting aspect is the consideration of the negative first derivative of the potential, the force F (see equation 2.22). The curve progression of the force as a function of the bond length often provides a clearer picture of the actual bond strength than the potential energy curve.

$$F(x) = -\frac{dV(x)}{dx} = -2aD_e \cdot (e^{-a(x-x_0)} - e^{-2a(x-x_0)}) \tag{2.22}$$

The force constant k describes the flexibility of the bond and is obtained by calculating the curvature of the potential at the equilibrium distance x_0 (see equation 2.23). Large force constants are tantamount to rigid bonds and are associated with large forces.

$$k = \frac{d^2V(x_0)}{dx^2} = 2a^2 D_e \tag{2.23}$$

Since a Morse potential is not able to describe a dissociation with relaxation processes, a polynomial fit will be applied in these cases. Fits of higher orders allow a more precise description of the energy curve in range around the equilibrium distance. The disadvantage lies in the oscillations created at larger distances. A seventh order fit has been chosen, steering the middle course between short and long range accuracy (see equation 2.24).

$$V(x) = a_1 \cdot (x-x_0) + a_2 \cdot (x-x_0)^2 + a_3 \cdot (x-x_0)^3 + a_4 \cdot (x-x_0)^4 + a_5 \cdot (x-x_0)^5 + a_6 \cdot (x-x_0)^6 + a_7 \cdot (x-x_0)^7 \tag{2.24}$$

The force progression and force constant are calculated in the same manner as with the Morse potential, utilizing the first and second derivative of the polynomial fit (see equations 2.25 and 2.26).

$$F(x) = -\frac{dV(x)}{dx} = -(a_1 + 2a_2 \cdot (x - x_0) + 3a_3 \cdot (x - x_0)^2 + 4a_4 \cdot (x - x_0)^3 + 5a_5 \cdot (x - x_0)^4 +$$
$$6a_6 \cdot (x - x_0)^5 + 7a_7 \cdot (x - x_0)^6) \tag{2.25}$$

$$k = \frac{d^2V(x_0)}{dx^2} = 2a_2 \tag{2.26}$$

The potential energy curves of the dissociation of different ligands are shown in Figures 2.14 and 2.15. Table 2.32 summarize the key parameters of the Morse potentials and fits. A ”*” denotes a Morse potential fit up to a B−N distance of 2.4 Å (ctTm) or 2.7 Å, in order to extrapolate to a hypothetical dissociation energy in case of relaxation processes.
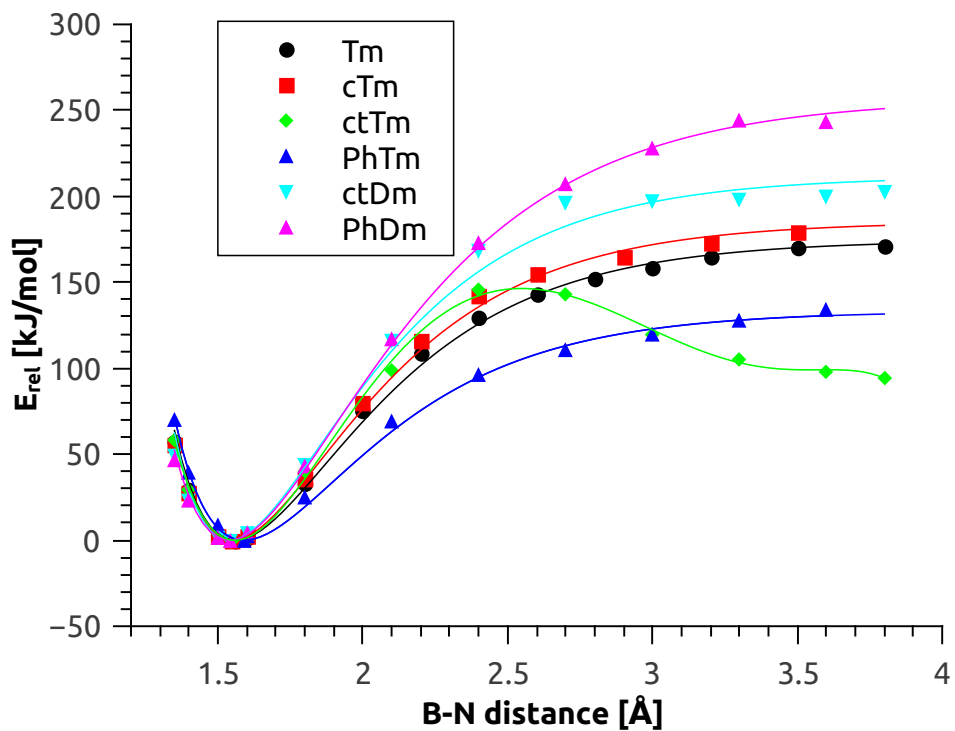
Figure 2.14: Dissociation of methimazole based scorpionates
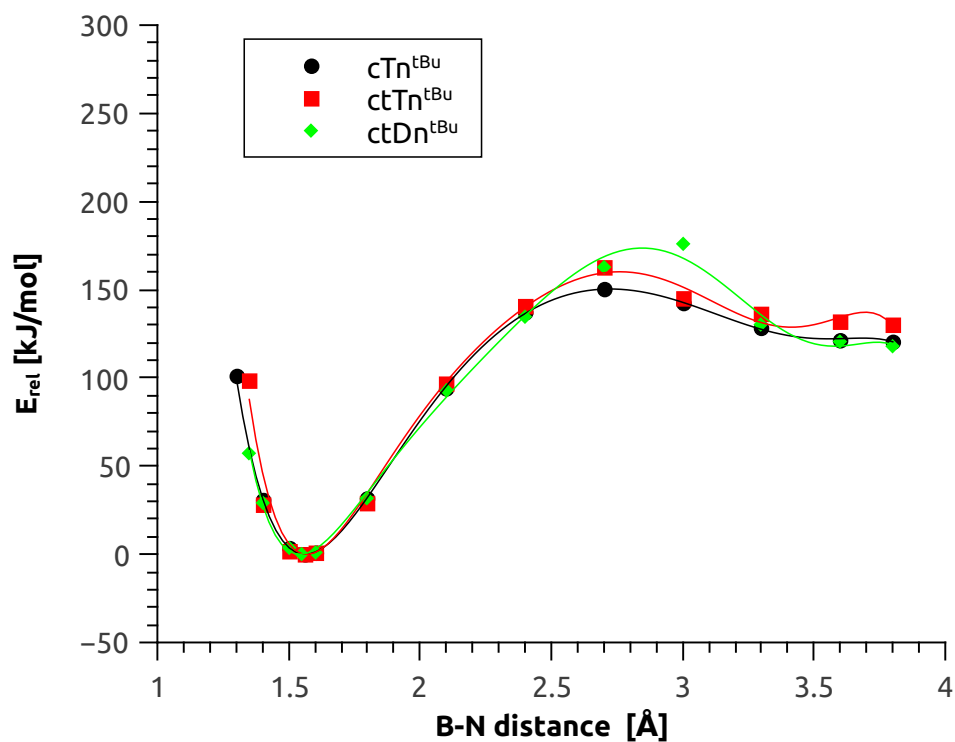
Figure 2.15: Dissociation of pyridazine based scorpionates

The curve progression for Tm, cTm and ctTm were found to be similar in the area around the equilibrium bond length. cTm showed slightly higher energies than Tm, but the graphs ran parallel to each other. The dissociation of ctTm showed a barrier with a maximum of 150 kJ/mol at 2.5 Å, followed by a decrease in energy, caused by the stabilization of the dissociation fragment by THF. The phenyl substituted ligand PhTm was characterized by a less pronounced rise of the slope in course of the elongation than the other ligands. The second dissociation step (ctDm and PhDm) resulted in a steeper slope. This was in accordance with thermodynamical results, suggesting an easier first dissociation.

The B$-$N dissociations of the three pyridazine based ligands exhibited relaxation processes. In case of ctTn^{tBu} a THF adduct was formed. In cTn^{tBu} and ctDn^{tBu} the sulfur atom stabilized the electron deficient boron atom. The maximum barrier heights were ca. 150, 160 and 175 kJ/mol at 2.7-2.8 Å.

The obtained dissociation energies for Tm and Tn^{tBu} ligands were in the range of 180-190 kJ/mol. PhTm showed a significantly lower dissociation energy.

The force constants were within the expected ranges of 200-400 N/m. ctTn^{tBu} featured the strongest curvature with a $k = 383$ N/m, suggesting more rigid bond than methimazole based ligands. Force constants (k_{fit}, calculated from the polynomial fit, were slightly larger than the values obtained from a Morse potential fit (2-5 %).

Table 2.32: Dissociation parameters

compound	x_0 [Å]	E_{diss} [kJ/mol]	a [Å^{-1}]	k [N/m]	k_{fit} [N/m]
Tm	1.56	174.54	2.251	294	-
cTm	1.55	185.23	2.281	320	-
ctTm*	1.56	208.26	2.139	316	324
cTn^{tBu}*	1.56	189.38	2.128	285	301
ctTn^{tBu}*	1.56	180.79	2.527	383	391
PhTm	1.59	133.24	2.291	232	-
ctDm	1.54	211.52	2.283	366	-
ctDn^{tBu}*	1.55	192.21	2.170	300	314
tPhDm	1.54	257.17	1.956	327	-

The force curves are in Figures 2.16 and 2.17. The forces calculated from the energy potentials are restoring forces, that acting against displacement from the equilibrium distance. Positive forces describe a force in +x, negative forces a force in -x direction.

Intersection of the functions around 1.55 Å with the zero line marked the equilibrium bond length, intersections in the range of 2.6-2.8 Å the barrier maxima. The forces converged to zero with increasing B$-$N distance. Deviations were caused by the oscillations of the polynomial fit.

As already indicated by the energy curve, k and D_e the forces for a dissociation of PhTm were lower, whereas the slope in case of compression was steeper than for the other ligands. The force progressions showed minima between 1.7-1.8 Å. The force function of ctTm was characterized by a steeper slope between 2.2-2.5 Å than Tm and cTm, associated with a faster decrease of the restoring force.

Interestingly, the ctDn^{tBu} had less distinct minimum than ctTn^{tBu} and cTn^{tBu}, but a flatter slope.
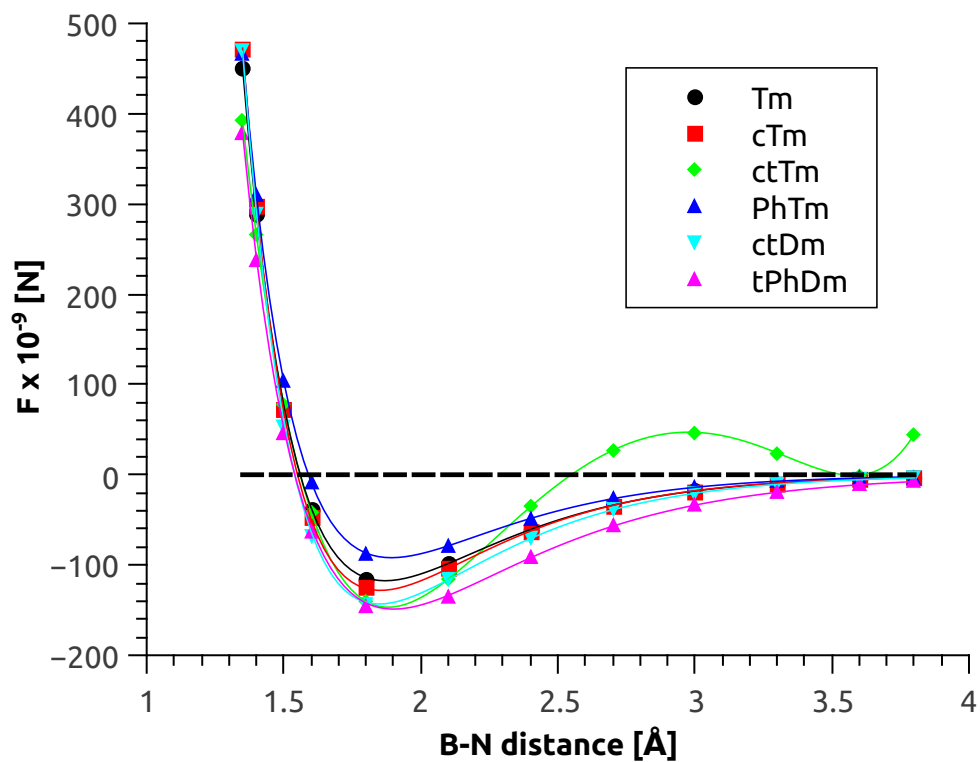
Figure 2.16: Forces of the B−N bond dissociation I
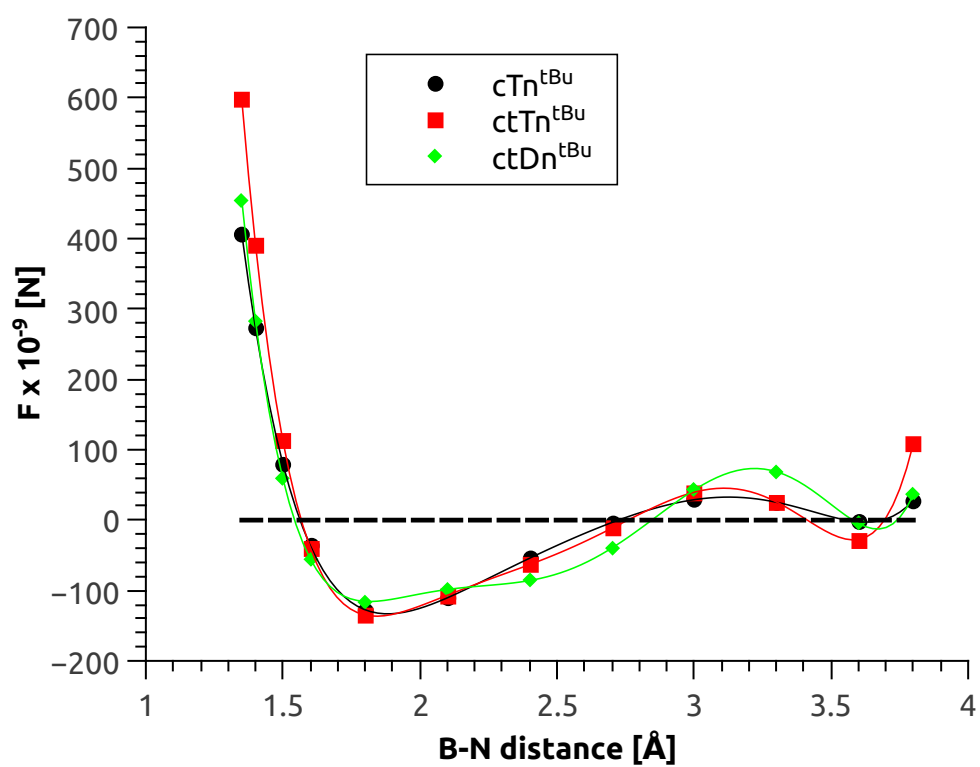
Figure 2.17: Forces of the B−N bond dissociation II

Chapter 3

Discussion

3.1 Synthesis

Generally, the results of the ligand synthesis reproduced to the yields reported in literature. Nevertheless the synthesis of *tert*-butylpyridazine-3-one precursor **2a** in a larger scale demanded an optimized procedure to increase the overall yield. The concentration of glyoxlic acid was increased from 55 % to ca. 77 % by partially removing the water content. In comparison to the original procedure only a single phase instead of two was obtained after the first reflux step. The drastic increase in yield might be traced back to the better miscibilty in presence of a reduced water content. Chemical drying agents were not applied to further reduce the water content. The reduction of water in the system in combination with different work up procedure were effective steps, increasing the yield by a factor of 3-4 (17 vs. 61 %).

The formation of the **4a** scorpionate ligand exhibits a broad range of yields. No conversion was observed when using dry toluene. Hence the reaction seems to sensitive towards the H_2O content in the solvent. Preliminary results indicate a dependency on the quality of the reactants and their concentration in the reaction solution.

The formation of a low valent pyridazine based Mo-scorpionate complex could not be achieved using established methods. The reaction was tested in different solvents (THF, MeCN, MeOH) but ligand degradation could not be avoided. The addition of allyl bromide was necessary to isolate the dimeric complex **8a**, albeit in poor yields. Isolation proved somewhat complicated, due to the similar solubilities of **8a** and the degradation products of the scorpionate ligand. This result showed, that pyridazine based scorpionate Mo complexes were under the applied reaction conditions.

The reaction of different pyridazines with NaH results in clean products with high yields. The use of the sodium salt **5a** provided an alternative synthetic pathway for **8a** with slightly better yields. Only a single isomer could be isolated upon controlled evaporation. Nevertheless the formation of other isomers could not be excluded by NMR analysis of the reaction solution.

Since RR'B−H species have a tendency to form three center two electron bonds, the use of substituted borates might offer a way to make a B-N bond dissociation thermodynamically less favorable (see Figure 3.1).

The precursor for phenyl substituted scorpionate ligands was $LiPhBH_3$ **2**. Several modifications of the original procedure [123] were published in literature. The applied procedure was adapted from
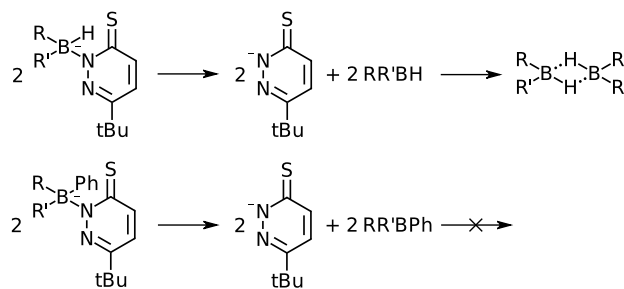
Figure 3.1: Formation of three center two electron bonds

Spicer and Reglinski[124] using 2,2'-biquinoline as an indicator. In absence of LiAlH$_4$ the solution's color changed from deep blue to colorless. Since phenylboronic acid is hardly soluble in Et$_2$O a mixture of dry THF/Et$_2$O was used, facilitating a controlled addition to the LiAlH$_4$/Et$_2$O solution.

The formation of the phenyl substituted pydrazine based scorpionate ligand **5a** could not be achieved using the same synthetical pathway as with the H-substituted counterparts. The reaction conditions were not changed due to time issues.

This observation might be traced back the sterical demand of the substituents in 6-position of the pyridazine moiety, but neither the reactions with less demanding Me- nor the H-substituted pyridazines showed any conversion in preliminary tests.

A different possible explanation is, that the formation of **4a** demanded a certain water content in the reaction. Lithium phenylborohydride **2** prohibited the use of technical grade solvents, since it was more sensitive towards degradation. If the formation of **5a** is catalyzed by a certain concentration H$_2$O in solution, a change to higher boiling solvents might provide a way to access this type of ligand overcoming the thermodynamical barrier.

The results of complex formation and degradation reaction of the ligand from a thermodynamical point of view will be discussed in the section below.

The phenyl substituted methimazole version of the scorpionate ligand had already been established in literature. Nevertheless no complex with Mo has been reported so far. The original procedure, published by Santos *et al.*, was modified by Reglinski and Spicer[124] by using the higher boiling xylene instead of toluene to promote a full conversion and surpress the formation of the mono- and bisubstituted intermediates. The overall yield was only 37 %.

In this project the ratio of methimazole to **2** was changed from 3:1 to 4:1 to shift the equilibrium towards the desired scorpionate complex. Roughly 80 % of the residual methiamzole were removed by washing three times with CHCl$_3$ and the product was found sufficiently pure for further use.

The reaction of [Mo(CO)$_6$] or the MeCN adduct **1** in dry MeCN or THF did not yield the expected threefold coordinated scorpionate complex but rather the twofold coordinated complex **7e** with four carbonyl groups. The possibility of the mono- or bisubstituted [Mo(CO)$_5$(MeCN)] and [Mo(CO)$_4$(MeCN)$_2$] acting as CO donors was ruled out by X-ray analysis of crystals obtained by vapor diffusion of pentane into a saturated MeCN solution of **1** and subsequently a reaction using only the obtained crystalline material also resulting in the formation **7e**.

Cation exchange with NBu$_4$Cl facilitated crystallisation and the yellow complex **8e** was obtained. The yields were calculated based on a 1:1 ratio (Mo precursor to ligand) with the metal precursor being the limiting factor. Finding the optimal ratio will give valuable insight into the CO transfer

reaction since the mechanism and formed by-products have yet to be determined.

An approach e.g. using $[\text{Mo(CO)}_4(2,2'\text{bipy})_2]$ [127–129] or $[\text{Mo(CO)}_4(\text{en})]$ [129] as $[\text{Mo(CO)}_4]$ fragment precursor may result in a cleaner reaction and higher yields, since a CO transfer is no necessary to reach [**3e**] or [**4e**]. This remains yet to be tested.

Both complexes were air- and/or moisture sensitive. A rapid degradation accompanied by a decreasing signals in the CO region and an increasing signal in the range of the OH-region was observed using IR spectroscopy. Complexes **7e** and **8e** are the first structural examples of formally Mo^0 complexes with soft scorpionate ligands, since a crystallographical description of the $\text{Na[TmMo(CO)}_3]$ has yet to be achieved.

Higher oxidation states might be accessible by controlled substitution of the obviously labile CO groups. This task is a promising one, since the Mo^{VI} complex featuring a Tm ligand was found to be active in OAT [115], suggesting similar reactivity for its PhTm counterpart.

3.2 Theoretical Investigation

3.2.1 Ligand formation

The ligand formation in toluene was exergonic for all ligands. The main driving force of the reaction was the continuous removal of H_2 from the system. Tn^{tBu} showed the most negative ΔG values. This trend has to be treated with caution since small errors in the computation of the thermodynamical potentials result in large deviations of K^{298} due to its exponential dependency. In addition consideration of the solvation using the COSMO model levelled the K^{298} values to the same order of magnitude. PhTn^{tBu} was the least favored reaction. A possible explanation could be the increased sterical strain in presence of the more spacious phenyl moiety.

The SEN of the B−N bonds suggested slightly weaker pyridazine B−N bonds compared to their methimazole counterparts. This effect was enhanced in heteroscorpionate ligands (2-6 %).

This effect was also observed in the B−N bond lengths in the same magnitude.

In course of the reaction the greatest change of the population was observed at the boron atoms $(5.7 \rightarrow 4.4)$. The population at the sulfur and binding nitrogen atoms of the pyridazine and methimazole moieties remained almost constant.

The results obtained from the investigation of the formation reactions provided the first, but only weak hints for an explanation of the ligand degradation in case of the Tn^{tBu} ligand.

3.2.2 Complex formation

The formation of precursor **1** was found to be a thermodynamically unfavoured reaction. The reaction demanded activation energy in form of heat. The driving force was the constant shift of the equilibrium by elimination of gaseous CO.

The reactivity of **1** was reflected in an immediate reaction. This experimental observation could be underpinned with a negative value for ΔG and equilibrium constant in the order of 10^6-10^{17}.

The difference in the conformation energy was found to increase with the number of pyridazine moieties. This could be explained by the increased sterical demand. Hence a conformation, in which the spacious *tert* butyl groups were located as far as possible from each other, was preferred. A more spacial substituent such as a phenyl group and resulted in a significant reduction

of ΔE_{conf}.

The comparably large values of K_r^{298} in the case of phenyl substituted ligands in their most stable conformation were not a sign of greater reactivity but rather of a relatively high energy caused by the sterical strain of four bulky moieties bonded to the boron atom.

If ligand degradation and complex formation are competitive reactions, the greater barrier for the Tn^{tBu} ligand to reach the right conformation might be a possible explanation for its liability towards degradation.

No evidence for a B$-$N bond activation as a result of the coordination could be found based on the analysis of the SEN, population and geometrical data. As expected the C=S bonds in the complexes were found to be weaker than in the uncoordinated ligand.

3.2.3 1st Dissociation reaction

Generally, there were two possible ways for the dissociation to happen. The first case, in which the negative charge remained at the residual ligand, was significantly less preferred to a dissociation, in which charge was located at cleaved methimazole or pyridazine moiety. The dissociation without further modifications showed, that B$-$S bonds were formed to one of the remaining methimazole or pyridazine moieties. Hence the dissociation products were calculated with a THF molecule located in close distance to the boron atom, simulating a more realistic environment.

The facilitated dissociation in case of the THF adducts could be explained by a stabilisation of the neutral product. Relaxation of a similar input geometry with a THF molecule in close proximity to the boron atom with a negative charge did not form a stable adduct, since the electrons remaining p-orbital of the boron atom forbid donor-acceptor interactions with the oxygen's lone pairs.

The significantly facilitated dissociation of the n^{tBu} moiety in heteroscorpionates was the result of the reduced SENs, going hand in hand with elongated bonds in presence of methimazole moieties. The consideration of a THF cavity clearly influenced the stability of the dissociation product. The ΔG values were reduced by up to $70\,\text{kJ/mol}$. No clear tendency could be found in the results for the homoscorpionate ligands. The formation of a dimeric species was ruled out on basis of the obtained data.

While the thermodynamical quantities of PhTm were in the order of the unsubstituted scorpionate ligands, PhTn^{tBu} was less stable in terms of ΔG.

3.2.4 2nd Dissociation reaction

A comparison of the first and second dissociation step showed, that a negative charge significantly facilitated the dissociation. Without consideration of solvent effects the ΔG values of the heterolytic cleavage, with the electrons located at the pyridazine or methimazole moiety, increased by a factor of 3-4.

Unexpectedly, a homolytic bond dissociation, forming in two radical species, was suggested to be the most probable way of dissociation. A degradation with the negative charge remaining at the boron atom could be ruled out by ΔG values of $>1000\,\text{kJ/mol}$.

When starting from a negatively charged first dissociation product, a second dissociation proceeded in a way, that the charge would reside at the formed pyridazine or methimazole moiety. No clear trend could be found in this type of reaction. This could be traced back to a number of local

minima, associated with numerous different energies, describing different relative positions of the respective compound and the THF molecule. Even slight differences of several kJ/mol would have a great impact on the value of equilibrium constant due to the exponential dependency on the energy.

Consideration of THF as solvent suggested a dissociation in the same manner as the first, a heterolytic bond breaking with the negative charge being located at cleaved pyridazine or methimazole. A possible explanation was, that a solvent with a dipolmoment, such as THF, would stabilize charged dissociation products better then neutral species.

The obtained values for ΔG of ctDm0 and ctDn^{tBu}0 were in a close range, differing by only 4 kJ/mol. Compound Dmn^{tBu}0, featuring both a methimazole and a pyridazine moiety, reproduced the result, found throughout all calculations. In heterotype ligands the B$-$N bonds of pyridazines were weaker than in compound featuring solely pyridazines.

3.2.5   The B-N bond dissociation

A stepwise dissociation allowed a more detailed examination of the dissociation processes. The presence of a THF molecule in proximity to the boron atom, resulted in the formation of a stable adduct at a B$-$N distance 2.5 Å. This stabilisation greated a barrier of ca. 150 kJ/mol. The dissociation energy D_e of "unstabilized" Tm and cTm was in the range of 180 kJ/mol, emphasizing the influence of solvent molecules.

The same effect could be observed in ctTn^{tBu}. One of the main differences was the formation of B$-$S bonds in cTn^{tBu} and ctDn^{tBu}, causing a stabilisation of dissociation products. ctTn^{tBu} featured the highest force constant (383 N/m). The difference to cTn^{tBu} (285 N/m) was significantly higher than between cTm (320 N/m) and ctTm (316 N/m). This could be a result of less stable local minima caused by the presence of THF, prior to the formation of the THF adduct.

The sterical demand of the phenyl moiety in PhTm was expressed in the lowest E_{diss} of 133 kJ/mol and force constant of 232 N/m. The second dissociation of the neutral compounds featured higher force constants and E_{diss}. This was in agreement with the thermodynamic trends, predicting a facilitated degradation in negatively charged and sterically more strained compounds.

The obtained data shows no distinct proof for a significant difference in the nature of the B$-$N bonds of pyridazine and methimazole based ligands. Analysis of geometrical data, the populations, SENs and thermodynamical data indicates a slightly weaker B$-$N bond in the Tn^{tBu} ligand compared to Tm. From a thermodynamical point of view, the B$-$N bonds in all ligands are not prone to degradation. This result does not account for possible consecutive reactions leading to thermodynamic sinks.

An interesting observation was the formation of B$-$S bonds in the ligands in course of the dissociations. In mixed ligands the B$-$S interactions were always caused by a pyridazine's sulfur. The angle between substituents in six membered rings is lower than in five membered rings, facilitating B$-$S interactions. The strain of the B-N-C-S cycle could facilitate a B$-$N bond cleavage. An mechanistically interesting intermediate might be the thiol forms of methimazole and pyridazine. The aromatization of the pyridazine moiety in combination with the more favorable angle in the six membered rings resulted in a less exergonic ΔG value (-32 vs. -51 kJ/mol) and hence greater importance of the thiol form.

The immediate dissociation of Tn^{tBu} in presence of the Mo precursor **1** suggests a Mo mediated process. The discussed marginal difference in the B$-$N stabilities might be crucial for the dissociation of Tn^{tBu} and the formation of stable scorpionate Mo complexes with Tm. The isolated dimeric complex **8a** might act as a thermodynamic sink, promoting the degradation. The synthesis of the heteroscorpionate ligands Tm_2n^{tBu}, Tmn_2^{tBu} and the phenyl substituted $PhTn^{tBu}$ and their reaction with the Mo precursor could provide valuable insight into this reaction.

Chapter 4

Experimental

4.1 General

All starting materials, if not mentioned otherwise, were purchased from commercial sources and used without further purification, except for absolute solvents, which were dried with a Pure-Solv MD-4-EN solvent purification system (Innovative Technology, Inc). Experiments demanding inert conditions were carried out under Ar or N_2 atmosphere using standard Schlenk and glovebox techniques.

NMR spectra were recorded with a Bruker Avance III (300 MHz) instrument, mass spectra with an Agilent 5973 MSD-Direct Probe using EI ionization technique. A Bruker Alpha Platinum ATR spectrometer was used to obtain IR spectra. X-Ray structures were determined by Prof. Ferdinand Belaj using a Bruker-Axs Smart Apex 2 CCD diffractometer. All measurements were performed using graphite-monochromatized Mo K_α radiation at 100K. The structures were solved by direct methods (SHELXS-97)[130] and refined by full-matrix least-squares techniques against F2 (SHELXL-97)[130].

The compounds pyridazine-3-thione (**1c**) and 6-*p*-tolyl-pyridazine-3-thione (**1d**) were provided by Dr. Gernot Nuss; $[Mo_2Br_4(CO)_7]$ was provided by Lydia Peschel, MSc.

The precursors $[Mo(CO)_3(MeCN)_3]$[123] **1**, $[MoCl_4(thf)_2]$[131] and $[MoCl_3(thf)_3]$[131] were synthesized according to published procedures.

4.2 Ligands

2-Hydroxy-5,5-dimethyl-4-oxopentanoic acid (1a) The literature procedure[116] was modified by partially removing H_2O of a glyoxylic acid solution in H_2O (55 %) to obtain a concentration of approx. 77 % (2 g, 27 mmol, 1 equiv). 3,3-Dimethylbutanone (3.24 g, 32 mmol, 1.2 equiv) was added and the biphasic solution stirred under reflux for 20 h.

NH_4OH (33 %) was added to the obtained orange solution until pH=8 was reached. Residual 3,3-dimethylbutanone was removed by extracting the solution with Et_2O/H_2O. The obtained solution containing **1a** was directly used for the synthesis of **2a**.

6-*tert*-Butylpyridazine-3-one (2a)   1.38 mL of $N_2H_4 \cdot H_2O$ (80 %, 22 mmol, 0.8 equiv) were added to the obtained solution of **1a** and stirred under reflux for 3 h. The aqueous solution was extracted three times with CH_2Cl_2. The collected organic phases were joined, dried with Na_2SO_4 and 2.037 g of **2a** (60.8 %) were obtained upon solvent removal.

^{1}H NMR (300 MHz, DMSO-d6) δ 12.72 (s, 1H), 7.62 (d, J = 9.9 Hz, 1H), 6.83 (d, J = 9.9 Hz, 1H), 1.21 (s, 9H).

4,5-Dihydro-6-methylpyridazine-3-one (1b)   The reaction was performed according to published methods[118] and the product isolated in 92 % yield.

^{1}H NMR (300 MHz, DMSO-d6) δ 10.38 (s, 1H), 2.35 - 2.45 (m, 2H), 2.21 - 2.30 (m. 2H), 1.92 (s, 3H).

6-Methylpyridazine-3-one (2b)   The reaction was performed according to published methods[118] and the product isolated in 76.6 % yield.

^{1}H NMR (300 MHz, DMSO-d6) δ 12.72 (s, 1H), 7.30 (d, J = 9.7 Hz, 1H), 6.79 (d, J = 9.7 Hz, 1H), 2.21 (s, 3H).

6-*tert*-Butylpyridazine-3-thione (3a) and 6-methylpyridazine-3-thione (3b)   The reaction was performed according to published methods[117] and the product isolated in 48.7 % (**3a**) and 53.2 % **3b** yield.

3a: ^{1}H NMR (300 MHz, DMSO-d6) δ 14.52 (s, 1H), 7.57 (dd, J = 9.4, 2.1 Hz, 1H), 7.49 (d, J = 9.4 Hz, 1H), 1.22 (s, 9H).

3b: ^{1}H NMR (300 MHz, DMSO-d6) δ 14.53 (s, 1H), 7.53 (d, J = 9.1 Hz, 1H), 7.20 (d, J = 9.1 Hz, 1H), 2.30 (s, 3H).

Sodium hydrotris(6-*tert*-butylpyridazine-3-thionyl)borate (4a)   Sodium borohydride (0.112 g, 2.96 mmol 1 equiv) and **3a** (1.5 g, 8.88 mmol, 3 equiv) were suspended in technical grade toluene and stirred under reflux for 20 h. After cooling to rt the solvent was removed and the precipitate washed with hot cyclohexane twice. The product was isolated in 86 % yield (1.365 g).

^{1}H NMR (300 MHz, DMSO-d6) δ 7.39 (d, J = 9.1 Hz, 3H), 7.02 (d, J = 9.1 Hz, 3H), 0.93 (s, 27H).

All experiments following, were conducted under inert conditions.

General procedure for the preparation of the the following sodium salts: 6a, 6b, 6b2, 6c and 6d   **3a** (1.648 g, 9.8 mmol, 1 equiv) were stirred with NaH (approx. 55 %, 0.255 g, 10.8 mmol, 1.1 equiv) in 15 mL dry toluene under reflux. The end of the reaction was indicated with aid of a bubbler. Upon cooling the solution to rt, the product precipitated and was isolated by removing the solvent in 98,5 % yield.

6a: ^{1}H NMR (300 MHz, DMSO-d6) δ 7.11 (d, J = 9.0 Hz, 1H), 6.91 (d, J = 9.0 Hz, 1H), 1.24 (s, 9H).

6b: ^{1}H NMR (300 MHz, DMSO-d6) δ 6.76 (d, J = 9.1 Hz, 1H), 6.06 (d, J = 9.1 Hz, 1H), 2.21 (s, 3H).

6b2: ^{1}H NMR (300 MHz, DMSO-d6) δ 7.00 (d, J = 8.7 Hz, 1H), 6.60 (d, J = 8.7 Hz, 1H), 2.26 (s, 3H).

6c: ^{1}H NMR (300 MHz, DMSO-d6) δ 8.25 (dd, J = 4.4, 1.7 Hz, 1H), 7.09 (dd, J = 8.7, 1.7 Hz, 1H), 6.71 (dd, J = 8.7, 4.4 Hz, 1H).

6d: ^{1}H NMR (300 MHz, DMSO-d6) δ 7.75 (d, J = 8.0 Hz, 2H), 7.63 (d, J = 9.5 Hz, 1H), 7.21 (d, J = 8.0 Hz, 2H), 6.48 (d, J = 9.5 Hz, 1H), 2.31 (s, 3H).

Lithium phenylborohydride (2) The procedure was modified from from the method published by Reglinski and Spicer [124]. 20 mL 1M LiAlH$_4$ in Et$_2$O (20 mmol, 1 equiv) was diluted with 20 mL Et$_2$O in a centrifuge Schlenk flask. A concentrated indicator solution of 2,2'-biquinoline in 1M LiAlH$_4$ in Et$_2$O was added dropwise until a medium intense blue color was achieved. Phenylboronic acid (2.439 g., 0.02 mmol, 1 equiv) was dissolved in 10 mL THF and diluted 10 mL Et$_2$O. The phenylboronic acid solution was slowly added until the reaction solution was colorless. The solution and greyish precipitate was centrifuged (15 min, 2000 rpm) and the supernatant organic phase separated via cannula filtration. The residual was resuspended in 15 mL Et$_2$O, centrifuged and the combined organic phases were dried in vacuo. **2**·1.75 THF was isolated as white powder in 84.9 % yield (3.82 g).

^{1}H NMR (300 MHz, DMSO-d6) δ 7.13 (bs, 2H), 6.82 (t, J = 7.3 Hz, 2H), 6.65 (t, J = 7.3 Hz, 1H), 1.28 (-BH$_3$, m, 3H).

Lithium trismethimazolylphenylborate (5e) The procedure was modified from the method published by Reglinski and Spicer [124] by suspending **2** (2.453, 10.94 mmol, 1 equiv) and with an excess of methimazole (5 g, 43.79 mmol, 4 equiv) in 35 mL dry xylene. The mixture was stirred under reflux for 16 h and **5e** isolated as white powder with 1 equiv of methimazole (2.684 g, 56.5 %). Three washing steps with CHCl$_3$ removed ~80 % of the remaining methimazole and the product was sufficiently pure for further use.

^{1}H NMR (300 MHz, DMSO-d6) δ 7.23 - 7.08 (m, 5H), 6.97 - 6.91 (m, 3H), 6.75 - 6.65 (m, 3H), 3.35 (s, 9H).

4.3 Complexes

Bis(6-tert-butylpyridazine-3-thiolato-N,S)-bis(η^3-allyl)-tetracarbonyl-di-molybdenum(II) 8a from 4a [Mo(CO)$_3$(MeCN)$_3$] **1** (499 mg, 1.65 mmol, 1 equiv) was stirred under reflux with the scorpionate ligand **4a** (692 mg, 2.47 mmol, 1.5 equiv) in THF for 12 h. Allylbromide (199 mg, 1.65 mmol, 1 equiv) was added and the solution stirred under reflux for another 2 h. The mother liquor was separated from the precipitated NaBr via cannula filtration and the solvent slowly removed *in vacuo* upon which **8a** could be isolated as an orange powder in 5.9 % yield (70 mg.) Crystals suitable for X-ray analysis were obtained by vapor diffusion of Et$_2$O into a saturated THF solution of **8a** at -25°C.

^{1}H NMR (300 MHz, DMSO-d6) δ 7.43 (d, J = 9.0 Hz, 1H), 7.07 (d, J = 9.0 Hz, 1H), 3.96 (tt, J = 10.0, 6.5 Hz, 1H), 3.50 - 4.42 (m, 2H), 3.20 - 3.11 (m, 2H), 1.28 (s, 9H).

Bis(6-tert-butylpyridazine-3-thiolato-N,S)-bis(η^3-allyl)-tetracarbonyl-di-molybde-num(II) 8a from 6a $[Mo(CO)_6]$ (100 mg, 0.38 mmol, 1 equiv) was stirred under reflux in ace-tonitrile 16 h. The solvent was removed *in vacuo*. Obtained **1** was stirred with the sodium salt **6a** (72 mg, 0.38 mmol, 1 equiv) in THF for 12 h. Allylbromide (46 mg, 0.38 mmol, 1 equiv) was added and the solution stirred under reflux for another 2 h. The mother liquor was separated from the precipitated NaBr via cannula filtration and the solvent slowly removed *in vacuo* upon which **8a** could be isolated as an orange powder in 16.0% yield (22 mg). ^{1}H NMR signals matched the signals from **8a**.

Lithium tetracarbonyl-(tris(3-methyl-2-thioxo-2,3-dihydro-1H-imidazol-1-yl)(phenyl) borato-S,S')molybdenum(0) 7e A solution of **5e** (122 mg, 0.28 mmol, 1 equiv) in 10 ml THF was added to a solution of crystalline **1**·MeCN (95 mg, 0.28 mmol, 1 equiv) in 5 ml THF and stirred for 12 h at rt under inert conditions. The dark brown solution was filtered and the obtained yellow **7e** washed twice with 5 mL THF and 5 mL pentane. Residual solvent was removed *in vacuo* (82 mg, % based on Mo). Crystals suitable for X-ray analysis were obtained by vapor diffusion of Et$_2$O into a saturated DMF solution of **7e** at -25°C.

^{1}H NMR (300 MHz, THF-d8) δ 7.69 (d, J = 7.2 Hz, 2H, CH (Ph)), 7.28 - 7.14 (m, 3H, CH (Ph)), 6.74 (s, 3H, CH (mt)), 6.65 (s, 3H, CH (mt)) 3.58 (s, 9H, CH$_3$ (mt)).

^{13}C NMR (300 MHz, acetonitrile-d3) δ 224.07 (CO), 135.07 (CH, Ph), 127.30 (CH, Ph), 126.14 (CH, Ph), 115.97 (CH, mt), 35.27 (CH$_3$, mt), 34.72 (CH$_3$, mt).

IR (cm^{-1}): CO-region 1890, 1775, 1678, 1634.

Tetra(n-butyl)ammonium tetracarbonyl-(tris(3-methyl-2-thioxo-2,3-di-hydro-1H-imid-azol-1-yl)(phenyl)borato-S,S')molybdenum(0) 8e $[Mo(CO)_3(MeCN)_3]$ **1** was generated *in situ* in 10 mL MeCN from $[Mo(CO)_6]$ (250 mg, 0.95 mmol, 1 equiv). **4e** (411 mg, 0.95 mmol, 1 equiv) and dry NBu$_4$Cl (263 mg, 0.95 mmol, 1 equiv) were added and the initially deep yellow solution changed its color to brown stirred for 3 d at rt. MeCN was removed *in vacuo* and the dark brown foam dissolved in 8 mL THF. The mother liquor was removed by cannula filtration and the yellow powder washed four times with 1 mL of THF each and with 5 mL of pentane (195 mg, 23.5 % based on Mo). Crystals suitable for X-ray analysis were obtained by controlled evaporation of the mother liquor at rt.

^{1}H NMR (300 MHz, acetonitrile-d3) δ 7.38 - 6.97 (m, 5H (Ph)), 6.90 - 6.46 (m, 6H, CH (mt)), 3.74 - 3.34 (m, 9H, CH$_3$ (mt)), 3.15 - 2.99 (m, 8H, CH$_2$ (NBu$_4$)), 1.69 - 1.49 (m, 8H, CH$_2$ (NBu$_4$)), 1.47 - 1.23 (m, 8H, CH$_2$ (NBu$_4$)), 0.96 (t, J = 7.3 Hz, 12H, CH$_3$ (NBu$_4$)).

^{13}C NMR (300 MHz, acetonitrile-d3) δ 227.61 (CO), 224.05 (CO), 210.59 (CO), 209.18 (CO), 166.32 (C$_q$, mt), 135.02 (CH, Ph), 127.26 (CH, Ph), 125.62 (CH, Ph), 115.83 (CH, mt), 59.24 (CH$_2$, [NBu$_4$]$^+$), 35.10 (CH$_3$, mt), 34.75 (CH$_3$, mt), 24.24 (CH$_2$, [NBu$_4$]$^+$), 20.26 (CH$_2$, [NBu$_4$]$^+$), 13.78 (CH$_3$, [NBu$_4$]$^+$).

Chapter 5

Theoretical Methodology

All structures were drawn with Avogadro and pre-optimized with the implemented unrestricted force field (UFF) method.[132]

DFT calculations were performed using the pbe0 functional[133] as implemented in the TURBO-MOLE program.[134–136] Geometry optimizations were calculated on double-ζ level, using the def2-SVP basis set[137] and the corresponding ecp-28-mwb-SVP basis set[138] and ecp-28-mwb effective core potential[139] for the Mo central atom. Analytical vibrational analysis[140] was performed to confirm an energetic minimum structure.

Single point or full optimization calculations were performed on the SVP-optimized geometries using the triple ζ-basis set def2-TZVP[141] and the accordant ecp-28-mwb-TZVP basis set[138] and ecp-28-mwb effective core potential for the Mo central atom.

Dispersion correction was integrated by Grimme's DFT-D3 model.[142] Additionally the compounds were analyzed using natural population analysis (NPA)[143] and shared electron numbers (SEN)[144] of selected bonds.

Solvent effects were accounted for using the COSMO model[145] with the dielectric constant $\epsilon = 7.52$[146] for THF and 2.38 for toluene[147]. Default values were used for the atomic radii, except for B ($r = 2.141\,\text{Å}$)[148] and Mo ($r = 2.574\,\text{Å}$)[148].[a] Vibrational analysis of COSMO calculations were performed using the numerical module NumForce with the *-central* option (central differences) and if necessary *-frznuclei* to exclude frozen coordinates from the force constant matrix.

Thermodynamical data was calculated with the **freeh** modul using the default values ($T = 298.15k$). 0.9512 was applied as scaling factors for the IR frequencies.

Potential energy and force curves were fitted using QTIplot.

---

[a] values multiplied by 1.2 as proposed on `http://www.nwchem-sw.org/index.php/COSMO_Solvation_Model`

Bibliography

[1] Wiberg, A. F.; Hollemann, N. *Lehrbuch der anorganischen Chemie*, 102nd ed.; Walter de Gruyter: Berlin, 2007; pp 1582–1606.

[2] Chappell, W. R.; Meglen, R. R.; Moure-Eraso, R.; Solomons, C. C.; Tsongas, T. A.; Walravens, P. A.; Winston, P. W. *Human health effects of molybdenum in drinking water*; Technical Report, 1979; pp 1–113.

[3] Prasad, P. M.; Mankhand, T. R.; Prasad, A. J. K. *NML Tech. J.* **1997**, *39*, 39–58.

[4] Shields, J. A. *Applications of Molybdenum Metal and its Alloys*, 2nd ed.; International Molybdenum Association (IMOA): London, 2013; pp 1–44.

[5] Gupta, C. K. *Extractive Metallurgy of Molybdenum*; CRC Press, 1992; p 404.

[6] Heijerick, D. G.; Regoli, L.; Carey, S. *Sci. Total Environ.* **2012**, *435-436*, 179–187.

[7] Anke, M.; Holzinger, S.; Seifert, M.; Müller, R.; Schäfer, U. *Acta Alimentaria* **2010**, *39*, 1–11.

[8] "Panel on Micronutrients; Subcommittees on Upper Reference Levels of Nutrients and of Interpretation and Use of Dietary Reference Intakes and the Standing Committee on the Scientific Evaluation of Dietary Reference Intakes", *Dietary Reference Intakes for Vitamin A, Vitamin K, Arsenic, Boron, Chromium, Copper, Iodine, Iron, Manganese, Molybdenum, Nickel, Silicon, Vanadium, and Zinc*; The National Academies Press, 2001.

[9] Turnlund, J. R.; Friberg, L. T. Chapter 34 - Molybdenum. In *Handbook on the Toxicology of Metals (Third Edition)*; Nordberg, G. F., Fowler, B. A., Nordberg, M., Friberg, L. T., Eds., Third Edit ed.; Academic Press: Burlington, 2007; pp 731–741.

[10] Vyskocil, A.; Viau, C. *J. Appl. Toxicol.* **1999**, *19*, 185–92.

[11] Enemark, J. H.; Cooney, J. J. A.; Wang, J.-J.; Holm, R. H. *Chem. Rev.* **2004**, *104*, 1175–1200.

[12] Burgess, B. K.; Lowe, D. J. *Chem. Rev.* **1996**, *96*, 2983–3012.

[13] Howard, J. B.; Rees, D. C. *Chem. Rev.* **1996**, *96*, 2965–2982.

[14] Hoffman, B. M.; Lukoyanov, D.; Dean, D. R.; Seefeldt, L. C. *Acc. Chem. Res.* **2013**, *46*, 587–95.

[15] Spatzal, T.; Aksoyoglu, M.; Zhang, L.; Andrade, S. L. A.; Schleicher, E.; Weber, S.; Rees, D. C.; Einsle, O. *Science* **2011**, *334*, 940.

[16] Lancaster, K. M.; Roemelt, M.; Ettenhuber, P.; Hu, Y.; Ribbe, M. W.; Neese, F.; DeBeer, S. *Science* **2011**, *334*, 974–976.

[17] Hille, R. *Chem. Rev.* **1996**, *96*, 2757–2816.

[18] Mendel, R. R.; Bittner, F. *Biochim. Biophys. Acta* **2006**, *1763*, 621–35.

[19] Kappler, U.; Friedrich, C. G.; Trüper, H. G.; Dahl, C. *Arch. Microbiol.*

[20] Gonzalez, P. J.; Rivas, M. G.; Mota, C. S.; Brondino, C. D.; Moura, I.; Moura, J. J. *Coord. Chem. Rev.* **2013**, *257*, 315–331.

[21] Mtei, R. P.; Lyashenko, G.; Stein, B.; Rubie, N.; Hille, R.; Kirk, M. L. *J. Am. Chem. Soc.* **2011**, *133*, 9762–9774.

[22] McAlpine, A. S.; McEwan, A. G.; Bailey, S. *J. Mol. Biol.* **1998**, *275*, 613–623.

[23] Murray, K. N.; Watson, J. . G.; Chaykin, S. *J. Biol. Chem.* **1966**, *241*, 4798–4801.

[24] Hille, R.; Sprecher, H. *J. Biol. Chem.* **1987**, *262*, 10914–10917.

[25] Ricard, L.; Estienne, J.; Karagiannidis, P.; Toledano, P.; Fischer, J.; A., M.; Weiss, R. *Coord. Chem. Rev.* **1974**, *3*, 277.

[26] Berg, J. M.; Hodgson, K. O. *Inorg. Chem.* **1980**, *19*, 2180–2181.

[27] Holm, R. H. *Coord. Chem. Rev.* **1990**, *100*, 183–221.

[28] Thapper, A.; Donahue, J. P.; Musgrave, K. B.; Willer, M. W.; Nordlander, E.; Hedman, B.; Hodgson, K. O.; Holm, R. H. *Inorg. Chem.* **1999**, *38*, 4104–4114.

[29] Mader, M. L.; Carducci, M. D.; Enemark, J. H. *Inorg. Chem.* **2000**, *39*, 525–531.

[30] Lim, B. S.; Willer, M. W.; Miao, M.; Holm, R. H. *J. Am. Chem. Soc.* **2001**, *123*, 8343–8349.

[31] Das, S. K.; Chaudhury, P. K.; Biswas, D.; Sarkar, S. *J. Am. Chem. Soc.* **1994**, *116*, 9061–9070.

[32] Schindelin, H.; Kisker, C.; Hilton, J.; Rajagopalan, K. V.; Rees, D. C. *Science* **1996**, *272*, 1615–1621.

[33] Schrauzer, G. N.; Mayweg, V. P.; Heinrich, W. *J. Am. Chem. Soc.* **1966**, *88*, 5174–5179.

[34] Lim, B. S.; Holm, R. H. *J. Am. Chem. Soc.* **2001**, *123*, 1920–1930.

[35] Donahue, J. P.; Goldsmith, C. R.; Nadiminti, U.; Holm, R. H. *J. Am. Chem. Soc.* **1998**, *120*, 12869–12881.

[36] Hauser, S.; Cokoja, M.; Kühn, F. E. *Catal. Sci. Technol.* **2013**, *3*, 552–561.

[37] Schachner, J. A.; Traar, P.; Sala, C.; Melcher, M.; Harum, B. N.; Sax, A. F.; Volpe, M.; Belaj, F.; Mösch-Zanetti, N. C. *Inorg. Chem.* **2012**, *51*, 7642–7649.

[38] Sugimoto, H.; Tatemoto, S.; Toyota, K.; Ashikari, K.; Kubo, M.; Ogura, T.; Itoh, S. *Chem. Commun.* **2013**, *49*, 4358–4360.

[39] Berg, J. M.; Holm, R. H. *J. Am. Chem. Soc.* **1985**, *107*, 917–925.

[40] Schulzke, C. *Eur. J. Inorg. Chem.* **2011**, 1189–1199.

[41] Curtis, M. D.; Shiu, K.-B.; Butler, W. M. *Organometallics* **1983**, *2*, 1475–1477.

[42] Curtis, M. D.; Shiu, K.-B.; Butler, W. M. *J. Am. Chem. Soc.* **1986**, *108*, 1550–1561.

[43] Pettinari, C. In *Introduction*; Imperial College Press, 2008; Chapter 1, pp 1–67.

[44] Trofimenko, S. *Polyhedron* **2004**, *23*, 197–203.

[45] Calabrese, J. C.; Trofimenko, S.; Thompson, J. S. *J. Chem. Soc., Chem. Commun.* **1986**, 1122–1123.

[46] Trofimenko, S.; Calabrese, J. C.; Thompson, J. S. *Inorg. Chem.* **1987**, *26*, 1507–1514.

[47] Reger, D. L.; Foley, E. A.; Smith, M. D. *Inorg. Chem.* **2010**, *49*, 234–242.

[48] Trofimenko, S. *J. Am. Chem. Soc.* **1967**, *89*, 3170–3177.

[49] Sorrell, T. N.; Allen, W. E.; White, P. S. *Inorg. Chem.* **1995**, *34*, 952–960.

[50] Pullen, E. E.; Rabinovich, D. *Inorg. Chem.* **2000**, *39*, 1561–1567.

[51] Richburg, L. M.; Farouq, J. A.; Incarvito, C. D.; Rheingold, A. L.; Rabinovich, D. *Polyhedron* **2000**, *19*, 1815–1820.

[52] Gwengo, C.; Silva, R. M.; Smith, M. D.; Lindeman, S. V.; Gardinier, J. R. *Inorg. Chim. Acta* **2009**, *362*, 4127–4136.

[53] Trofimenko, S. *Scorpionates: The Coordination Chemistry of Polypyrazolylborate Ligands*; Imperial College Press: London, 1999; pp 1–282.

[54] Garner, M.; Lehmann, M.-A.; Reglinski, J.; Spicer, M. D. *Organometallics* **2001**, *20*, 5233–5236.

[55] Alvarez, H. M.; Tran, T. B.; Richter, M. A.; Alyounes, D. M.; Rabinovich, D.; Tanski, J. M.; Krawiec, M. *Inorg. Chem.* **2003**, *42*, 2149–56.

[56] Schwalbe, M.; Andrikopoulos, P. C.; Armstrong, D. R.; Reglinski, J.; Spicer, M. D. *Eur. J. Inorg. Chem.* **2007**, *2007*, 1351–1360.

[57] Kitajima, N.; Koda, T.; Hashimoto, S.; Kitagawa, T.; Moro-oka, Y. *J. Am. Chem. Soc.* **1991**, *113*, 5664–5671.

[58] Amoroso, A. J.; Thompson, A. M. C.; Jeffery, J. C.; Jones, P. L.; McCleverty, J. A.; Ward, M. D. *J. Chem. Soc., Chem. Commun.* **1994**, 2751–2752.

[59] Trofimenko, S. *J. Am. Chem. Soc.* **1967**, *89*, 6288–6294.

[60] Trofimenko, S. *Chem. Rev.* **1972**, *72*, 497–509.

[61] Tsoureas, N.; Bevis, T.; Butts, C. P.; Hamilton, A.; Owen, G. R. *Organometallics* **2009**, *28*, 5222–5232.

[62] Calabrese, J. C.; Domaille, P. J.; Thompson, J. S.; Trofimenko, S. *Inorg. Chem.* **1990**, *29*, 4429–4437.

[63] Ball, R. G.; Ghosh, C. K.; Hoyano, J. K.; McMaster, A. D.; Graham, W. A. G. *J. Chem. Soc., Chem. Commun.* **1989**, *69*, 341–342.

[64] Dias, H. V. R.; Lu, H.-L. *Inorg. Chem.* **2000**, *39*, 2246–2248.

[65] Spicer, M. D.; Reglinski, J. *Eur. J. Inorg. Chem.* **2009**, 1553–1574.

[66] Kisala, J.; Bialonska, A.; Ciunik, Z.; Kurek, S.; Wolowiec, S. *Polyhedron* **2006**, *25*, 3222–3230.

[67] Kosky, C. A.; Ganis, P.; Avitabile, G. *Acta Crystallogr. Sect. B* **1971**, *27*, 1859.

[68] Trofimenko, S. *J. Am. Chem. Soc.* **1970**, *92*, 5118–5126.

[69] Trofimenko, S. *Acc. Chem. Res.* **1971**, *4*, 17–22.

[70] Cramer, S. P.; Liu, C.-L.; Mortenson, L. E.; Spence, J. T.; Liu, S.-M.; Yamamoto, I.; Ljungdahl, L. G. *J. Inorg. Biochem* **1985**, *23*, 119.

[71] Eagle, A. A.; Tiekink, E. R. T.; Young, C. G. *J. Chem. Soc., Chem. Commun.* **1991**, 1746–1748.

[72] Eagle, A. A.; Harben, S. M.; Tiekink, E. R. T.; Young, C. G. *J. Am. Chem. Soc.* **1994**, *116*, 9749–9750.

[73] Eagle, A. A.; Tiekink, E. R. T.; Young, C. G. *Inorg. Chem.* **1997**, *36*, 6315–6322.

[74] Sheldon, R. A.; Kochi, J. K. *Metal-Catalysed Oxidation of Organic Compounds*; Academic: New York, 1981.

[75] Sheldon, R. A.; van Santen, R. A. *Catalytic Oxidation: Principles and Applications*; World Scientific: Singapore, 1995.

[76] Young, C. G.; Thomas, S.; Gable, R. W. *Inorg. Chem.* **1998**, *37*, 1299–1306.

[77] Thomas, S.; Young, C. G. *Inorg. Synth.* **2002**, *33*, 218–227.

[78] Thomas, S.; Tiekink, E. R. T.; Young, C. G. *Inorg. Chem.* **2006**, *45*, 352–361.

[79] Klein, E. L.; Astashkin, A. V.; Raitsimring, A. M.; Enemark, J. H. *Coord. Chem. Rev.* **2013**, *257*, 110–118.

[80] Stiefel, E. I.; Coucouvanis, D.; Newton, W. E. Molybdenum Enzymes, Cofactors, and Model Systems. In *ACS Symposium Series 535*; American Chemical Society: Washington DC, 1993; pp 1–387.

[81] Roberts, S. A.; Young, C. G.; Cleland Jr., W. E.; Ortega, R. B.; Enemark, J. H. *Inorg. Chem.* **1988**, *27*, 3044–3051.

[82] Xiao, Z.; Young, C. G.; Enemark, J. H.; Wedd, A. G. *J. Am. Chem. Soc.* **1992**, *114*, 9194–9195.

[83] Sengar, R. S.; Nemykin, V. N.; Basu, P. *J. Inorg. Biochem.* **2008**, *102*, 748–56.

[84] Smith, P. D.; Slizys, D. A.; George, G. N.; Young, C. G. *J. Am. Chem. Soc.* **2000**, *122*, 2946–2947.

[85] Reger, D. L.; Grattan, T. C.; Brown, K. J.; Little, C. A.; Lamba, J. J. S.; Rheingold, A. L.; Sommer, R. *J. Organomet. Chem.* **2000**, *120*, year.

[86] Kläui, W.; Berghahn, M.; Rheinwald, G.; Lang, H. *Angew. Chem., Int. Ed.* **2000**, *39*, 2464.

[87] Hammes, B. S.; Carrano, M. W.; Carrano, C. J. *J. Chem. Soc., Dalton Trans.* **2001**, 1448.

[88] Jensen, L. M.; Abrahams, B. F.; Young, C. G. *J. Coord. Chem.* **2013**, *66*, 1252–1263.

[89] Ge, P.; Haggerty, B. S.; Rheingold, A. L.; Riordan, C. G. *J. Am. Chem. Soc.* **1994**, *116*, 8406–8407.

[90] Garner, M.; Reglinski, J.; Cassidy, I.; Spicer, M. D.; Kennedy, A. R. *Chem. Commun.* **1996**, 1975–1976.

[91] Dodds, C. A.; Kennedy, A. R.; Reglinski, J.; Spicer, M. D. *Inorg. Chem.* **2004**, *43*, 394–5.

[92] Maria, L.; Paulo, A.; Santos, I. C.; Santos, I.; Kurz, P.; Spingler, B.; Alberto, R. *J. Am. Chem. Soc.* **2006**, *128*, 14590–14598.

[93] Kimblin, C.; Hascall, T.; Parkin, G. *Inorg. Chem.* **1997**, *36*, 5680–5681.

[94] Kimblin, C.; Bridgewater, B. M.; Churchill, D. G.; Parkin, G. *Chem. Commun. (London)* **1999**, 2301–2302.

[95] Bailey, P. J.; Dawson, A.; McCormack, C.; Moggach, S. A.; Oswald, I. D. H.; Parsons, S.; Rankin, D. W. H.; Turner, A. *Inorg. Chem.* **2005**, *44*, 8884–8898.

[96] Tesmer, M.; Shu, M.; Vahrenkamp, H. *Inorg. Chem.* **2001**, *40*, 4022–4029.

[97] Garcia, R.; Paulo, A.; Domingos, A.; Santos, I. *Dalton Trans.* **2003**, 2757–2760.

[98] Ojo, J. F.; Slavin, P. A.; Reglinski, J.; Garner, M.; Spicer, M. D.; Kennedy, A. R.; Teat, S. J. *Inorg. Chim. Acta* **2001**, *313*, 15–20.

[99] Bailey, P. J.; Lanfranchi, M.; Marchio, L.; Parsons, S. *Inorg. Chem.* **2001**, *40*, 5030–5035.

[100] Silva, R. M.; Gwengo, C.; Lindeman, S. V.; Smith, M. D.; Gardinier, J. R. *Inorg. Chem.* **2006**, *45*, 10998–11007.

[101] Wang, Y.-L.; Cao, R.; Bi, W.-H. *Polyhedron* **2005**, *24*, 585–591.

[102] Dyson, G.; Hamilton, A.; Mitchell, B.; Owen, G. R. *Dalton Trans.* **2009**, 6120–6126.

[103] Owen, G. R.; Gould, H. P.; Charmant, J. P. H.; Hamilton, A.; Saithong, S. *Dalton Trans.* **2010**, *39*, 392–400.

[104] Nuss, G.; Saischek, G.; Harum, B. N.; Volpe, M.; Gatterer, K.; Belaj, F.; Mösch-Zanetti, N. C. *Inorg. Chem.* **2011**, *50*, 1991–2001.

[105] Crossley, I. R.; Hill, A. F.; Humphrey, E. R.; Smith, M. K.; Tshabang, N.; Willis, A. C. *Chem. Commun.* **2004**, 1878–1879.

[106] Nuss, G.; Saischek, G.; Harum, B. N.; Volpe, M.; Belaj, F.; Mösch-Zanetti, N. C. *Inorg. Chem.* **2011**, *50*, 12632–12640.

[107] Hill, A. F.; Owen, G. R.; White, A. J. P.; Williams, D. J. *Angew. Chem., Int. Ed.* **1999**, *38*, 2759–2761.

[108] Owen, G. R.; Gould, P. H.; Hamilton, A.; Tsoureas, N. *Dalton Trans.* **2010**, *39*, 49–52.

[109] Landry, V. K.; Melnick, J. G.; Buccella, D.; Pang, K.; Ulichny, J. C.; Parkin, G. *Inorg. Chem.* **2006**, *45*, 2588–2597.

[110] Foreman, M. R. S.-J.; Hill, A. F.; Tshabang, N.; White, A. J. P.; Williams, D. J. *Organometallics* **2003**, *22*, 5593–5596.

[111] Foreman, M. R. S.-J.; Hill, A. F.; White, A. J. P.; Williams, D. J. *Organometallics* **2003**, *22*, 3831–3840.

[112] Hill, A. F.; Tshabang, N.; Willis, A. C. *Eur. J. Inorg. Chem.* **2007**, 3781–3785.

[113] Abernethy, R. J.; Foreman, M. R. S.-J.; Hill, A. F.; Tshabang, N.; Willis, A. C.; Young, R. D. *Organometallics* **2008**, *27*, 4455–4463.

[114] Tran, B. L.; Carrano, C. J. *Inorg. Chem.* **2007**, *46*, 5429–5438.

[115] Wallace, D.; Gibson, L. T.; Reglinski, J.; Spicer, M. D. *Inorg. Chem.* **2007**, *46*, 3804–3806.

[116] Coates, W. J.; McKillop, A. *Synthesis* **1993**, 334–342.

[117] Arakawa, K.; Miysaka, T.; Satoh, K. *Chem. Pharm. Bull.* **1977**, *25*, 299–306.

[118] Overend, W. G.; Wiggins, L. F. *J. Chem. Soc.* **1947**, 239–244.

[119] Werner, H.; Deckelmann, K.; Schönenberger, U. *Helv. Chim. Acta* **1970**, *53*, 2002–2009.

[120] NIST Computational Chemistry Comparison and Benchmark Database, *Listing of experimental data for CO (Carbon monoxide)*, 2014. `http://cccbdb.nist.gov/exp2.asp?casno=630080#NISTdiatomic`.

[121] Block, E.; Gernon, M.; Kang, H.; Ofori-Okai, G.; Zubieta, J. *Inorg. Chem.* **1991**, 1736–1747.

[122] Cade, I. A.; Hill, A. F.; Tshabang, N.; Smith, M. K. *Organometallics* **2009**, *28*, 1143–1147.

[123] Singaram, B.; Cole, T. E.; Brown, H. C. *Organometallics* **1984**, *3*, 774–777.

[124] Dodds, C. A.; Garner, M.; Reglinski, J.; Spicer, M. D. *Inorg. Chem.* **2006**, *45*, 2733–2741.

[125] Nemykin, V. N.; Olsen, J. G.; Perera, E.; Basu, P. *Inorg. Chem.* **2006**, *45*, 3557–3568.

[126] Fan, Y.-B.; Ding, Z.-B.; Wang, Q.-R.; Tao, F.-G. *Chem. Phys. Let.* **2000**, *328*, 39–44.

[127] Manuta, D. M.; Lees, A. J. *Inorg. Chem. Commun.* **1983**, *22*, 572–573.

[128] Mukerjee, S. L.; Nolan, S. P.; Hoff, C. D.; de la Vega, R. L. *Inorg. Chem.* **1988**, *27*, 81–85.

[129] VanAtta, S. L.; Duclos, B. A.; Green, D. B. *Organometallics* **2000**, *19*, 2397–2399.

[130] Sheldrick, G. M. *Acta Cryst. A64* **2008**, 112–122.

[131] Stoffelbach, F.; Saurenz, D.; Poli, R. *Eur. J. Inorg. Chem.* **2001**, 2699–2703.

[132] Hanwell, M. D.; Curtis, D. E.; Lonie, D. C.; Vandermeersch, T.; Zurek, E.; Hutchison, G. R. *J. Cheminform.* **2012**, *4*, 17.

[133] Adamo, C.; Barone, V.; Adamo, C. *J. Chem. Phys.* **1999**, *110*, 6158–6170.

[134] *TURBOMOLE V6.3 2011, a development of University of Karlsruhe and Forschungszentrum Karlsruhe GmbH, 1989-2007, TURBOMOLE GmbH, since 2007; available from* `http://www.turbomole.com`.

[135] Ahlrichs, R.; Bar, M.; Marco, H.; Horn, H.; Ktjlmel, C. *Chem. Phys. Let.* **1989**, *162*, 165–169.

[136] Eichkorn, K.; Weigend, F.; Treutler, O.; Ahlrichs, R. *Theor. Chem. Acc.* **1997**, *97*, 119.

[137] Schäfer, A.; Horn, H.; Ahlrichs, R. *J. Chem. Phys.* **1992**, *97*, 2571.

[138] Weigend, F.; Ahlrichs, R. *Phys. Chem. Chem. Phys.* **2005**, *7*, 3297–3305.

[139] Andrae, D.; Häußermann, U.; Dolg, M.; Stoll, H.; Preuß, H. *Theor. Chem. Acc.* **1990**, *77*, 123–141.

[140] Treutler, O.; Ahlrichs, R. *J. Chem. Phys.* **1995**, *102*, 346.

[141] Weigend, F.; Häser, M.; Patzelt, H.; Ahlrichs, R. *Chem. Phys. Lett.* **1998**, *294*, 143–152.

[142] Grimme, S.; Antony, J.; Ehrlich, S.; Krieg, H. *J. Chem. Phys.* **2010**, *132*, 154104.

[143] Reed, A. E.; Weinstock, R. B.; Weinhold, F. *J. Chem. Phys.* **1985**, *83*, 735–746.

[144] Ehrhardt, C.; Ahlrichs, R. *Theor. Chim. Acta* **1985**, *68*, 231–245.

[145] Klamt, A.; Schüürmann, G. *J. Chem. Soc. Perkin Trans. 2* **1993**, 799–805.

[146] Sigma-Aldrich Co., LLC., *Tetrahydrofuran*, 13.04.2014. `http://www.sigmaaldrich.com/chemistry/solvents/tetrahydrofuran-center.html`.

[147] Sigma-Aldrich Co., LLC., *Toluene*, 08.06.2014. `http://www.sigmaaldrich.com/chemistry/solvents/toluene-center.html`.

[148] Batsanov, S. S. *Inorg. Mater.* **2001**, *37*, 871–885.

List of Figures

List of Schemes

List of Tables

Appendix

Table 5.1: Results Ligand Formation 1

compound	E_{elec} [H]	E_{elec}^{SP} [H]	energy [kJ/mol]	ΔH [kJ/mol]	ΔS [kJ/mol·K]
BH_4^-	-27.17945	-27.21552	91.25	93.73	0.21077
$PhBH_3^-$	-257.82721	-258.09992	313.14	315.62	0.34393
H_2	-1.16376	-1.16807	31.16	33.64	0.13669
mH	-662.98616	-663.40646	274.54	277.02	0.34554
$n^{tBu}H$	-818.70665	-819.29047	511.62	514.10	0.44142

Table 5.2: Results Ligand Formation 2

product	E_{elec} [H]	E_{elec}^{SP} [H]	energy [kJ/mol]	ΔH [kJ/mol]	ΔS [kJ/mol·K]
Tm	-0.10868	-0.10323	-35.72	-35.72	-0.14936
Tm_2n^{tBu}	-0.11037	-0.10175	-37.17	-37.17	-0.15974
Tmn_2^{tBu}	-0.11130	-0.10062	-38.86	-38.86	-0.16617
Tn^{tBu}	-0.11263	-0.10072	-40.15	-40.15	-0.15889
PhTm	-0.08698	-0.07888	-39.33	-39.33	-0.17503
$PhTn^{tBu}$	-0.07360	-0.05763	-45.18	-45.18	-0.23445

Table 5.3: Results Ligand Formation 3

product	E_{elec} [kJ/mol]	E_{elec}^{SP} [H]	$\Delta_r H$ [kJ/mol]	ΔG [kJ/mol]	K^{298}
Tm	-285.34	-271.03	-306.75	-262.22	$8.726 \cdot 10^{45}$
Tm_2n^{tBu}	-289.77	-267.14	-304.31	-256.69	$9.381 \cdot 10^{44}$
Tmn_2^{tBu}	-292.22	-264.17	-303.03	-253.49	$2.581 \cdot 10^{44}$
Tn^{tBu}	-295.71	-264.43	-304.58	-257.21	$1.159 \cdot 10^{45}$
PhTm	-228.36	-207.09	-246.42	-194.24	$1.073 \cdot 10^{34}$
$PhTn^{tBu}$	-193.24	-151.30	-196.48	-126.58	$1.504 \cdot 10^{22}$

Table 5.4: Results Ligand Formation 4 (COSMO)

compound	E_{elec} [H]	E_{elec}^{SP} [H]	energy [kJ/mol]	ΔH [kJ/mol]	ΔS [kJ/mol·K]
cBH_4^-	-27.23655	-27.27237	92.25	94.73	0.21063
$cPhBH_3^-$	-257.87414	-258.14710	315.07	317.55	0.32715
cH_2	-1.16395	-1.16825	31.29	33.77	0.13669
cmH	-662.99419	-663.41540	275.30	277.78	0.33867
cpyH	-818.71287	-819.29765	513.38	515.86	0.42332

Table 5.5: Results Ligand Formation 5 (COSMO)

product	E_{elec} [H]	E_{elec}^{SP} [H]	energy [kJ/mol]	ΔH [kJ/mol]	ΔS [kJ/mol·K]
cTm	-0.11247	-0.10864	-35.17	-35.17	-0.15746
cTm_2n^{tBu}	-0.11050	-0.10415	-37.85	-37.85	-0.15127
$cTmn_2^{tBu}$	-0.10897	-0.10181	-40.14	-40.14	-0.15073
cTn^{tBu}	-0.10936	-0.10067	-42.60	-42.60	-0.15039
CPhTm	-0.09589	-0.08910	-40.07	-40.07	-0.18185
$cPhTn^{tBu}$	-0.07751	-0.06355	-49.48	-49.48	-0.18636

Table 5.6: Results Ligand Formation 6 (COSMO)

product	E_{elec} [kJ/mol]	E_{elec}^{SP} [H]	$\Delta_r H$ [kJ/mol]	ΔG [kJ/mol]	K^{298}
cTm	-295.30	-285.23	-320.40	-273.46	$8.128 \cdot 10^{47}$
cTm_2n^{tBu}	-290.13	-273.43	-311.28	-266.18	$4.323 \cdot 10^{46}$
$cTmn_2^{tBu}$	-286.11	-267.31	-307.45	-262.51	$9.816 \cdot 10^{45}$
cTn^{tBu}	-287.12	-264.32	-306.92	-262.08	$8.265 \cdot 10^{45}$
CPhTm	-251.77	-233.93	-274.00	-219.78	$3.202 \cdot 10^{38}$
$cPhTn^{tBu}$	-203.51	-166.86	-216.34	-160.77	$1.472 \cdot 10^{28}$

Table 5.7: Results Complex Formation 1

compound	E_{elec} [H]	E_{elec}^{SP} [H]	E_{elec}^{TZVP} [H]	ΔE [kJ/mol]	ΔE_{conf} [kJ/mol]
[Mo(CO)$_6$]	-747.06307	-747.85544	-747.85580	0.95	-
CO	-113.09608	-113.23092	-113.23098	0.14	-
[**1**]	-805.18618	-806.02265	-	-	-
CH$_3$CN	-132.49268	-132.64175	-	-	-
2Tm	-2012.74078	-2014.01848	-2014.01998	3.93	40.48
2Tm$_2$n^{tBu}	-2168.46014	-2169.89868	-2169.90063	5.12	46.60
2Tmn$_2^{tBu}$	-2324.17750	-2325.77714	-2325.77969	6.68	58.20
2Tn^{tBu}	-2479.89485	-2481.65606	-2481.65892	7.51	71.82
Tm	-2012.75533	-2014.03390	-2014.03537	3.86	0.00
Tm$_2$n^{tBu}	-2168.47751	-2169.91643	-2169.91863	5.76	0.00
Tmn$_2^{tBu}$	-2324.19893	-2325.79931	-	-	0.00
Tn^{tBu}	-2479.92075	-2481.68342	-	-	0.00
CTm	-2420.47567	-2422.13947	-2422.14153	5.41	-
CTm$_2$n^{tBu}	-2576.18589	-2578.01210	-2578.01563	9.26	-
CTmn$_2^{tBu}$	-2731.89717	-2733.88804	-2733.89113	8.10	-
CTn^{tBu}	-2887.61227	-2889.76686	-		-
2PhTm	-2243.37631	-2244.88860	-2244.89074	5.61	14.03
2PhTn^{tBu}	-2710.52961	-2712.52575	-	-	-2.70
PhTm	-2243.38139	-2244.89395	-	-	0.00
PhTn^{tBu}	-2710.52948	-2712.52473	-	-	0.00
CPhTm	-2651.10342	-2653.00282	-	-	-
CPhTn^{tBu}	-3118.24265	-3120.63013	-	-	-

Table 5.8: Results Complex Formation 2

compound	energy [kJ/mol]	ΔH [kJ/mol]	ΔS [kJ/mol·K]
$[\text{Mo(CO)}_6]$	165.65	168.13	0.52232
CO	19.13	21.61	0.19777
[**1**]	475.63	478.11	0.70428
CH_3CN	122.98	125.46	0.25276
2Tm	785.73	788.21	0.69917
$2\text{Tm}_2\text{n}^{\text{tBu}}$	1021.01	1023.49	0.78520
$2\text{Tmn}_2^{\text{tBu}}$	1256.30	1258.78	0.87656
2Tn^{tBu}	1492.19	1494.67	0.95872
Tm	785.67	788.15	0.68796
$\text{Tm}_2\text{n}^{\text{tBu}}$	1021.30	1023.78	0.77346
$\text{Tmn}_2^{\text{tBu}}$	1256.69	1259.17	0.86291
Tn^{tBu}	1492.48	1494.96	0.96607
CTm	879.98	882.46	0.81558
$\text{CTm}_2\text{n}^{\text{tBu}}$	1115.19	1117.67	0.92559
$\text{CTmn}_2^{\text{tBu}}$	1349.07	1351.55	1.05405
CTn^{tBu}	1583.44	1585.92	1.12827
2PhTm	1004.41	1006.89	0.78417
$2\text{PhTn}^{\text{tBu}}$	1709.12	1711.60	1.04547
PhTm	1003.95	1006.43	0.79545
PhTn^{tBu}	1709.34	1711.82	1.02367
CPhTm	1098.40	1100.88	0.90957
$\text{CPhTn}^{\text{tBu}}$	1800.70	1803.18	1.21536

Table 5.9: Results Complex Formation Step 1a

	E_{elec} [H]	E_{elec}^{SP} [H]	energy [kJ/mol]	ΔH [kJ/mol]	ΔS [kJ/mol·K]
no COSMO	0.06668	0.06527	-1.57	-1.57	0.01699
COSMO	0.06235	0.06217	-1.30	-1.30	-0.01086

Table 5.10: Results Complex Formation Step 1b

	E_{elec} [kJ/mol]	E_{elec}^{SP} [H]	$\Delta_r H$ [kJ/mol]	ΔG [kJ/mol]	K^{298}
no COSMO	175.07	171.38	169.81	164.74	$1.370 \cdot 10^{-29}$
COSMO	163.71	163.23	161.93	165.17	$1.154 \cdot 10^{-29}$

Table 5.11: Results Complex Formation Step 2a

L_i	E_{elec} [H]	E_{elec}^{SP} [H]	energy [kJ/mol]	ΔH [kJ/mol]	ΔS [kJ/mol·K]
Tm	-0.01221	-0.00818	-12.38	-7.42	0.18162
2Tm	-0.02676	-0.02360	-12.44	-7.48	0.17041
Tm$_2$n$^{\text{tBu}}$	-0.00025	0.00173	-12.80	-7.84	0.20613
2Tm$_2$n$^{\text{tBu}}$	-0.01762	-0.01602	-12.51	-7.55	0.19439
Tmn$_2^{\text{tBu}}$	0.00989	0.00866	-14.31	-9.35	0.24514
2Tmn$_2^{\text{tBu}}$	-0.01154	-0.01351	-13.92	-8.96	0.23149
Tn$^{\text{tBu}}$	0.01662	0.01395	-15.73	-10.77	0.21620
2Tn$^{\text{tBu}}$	-0.00929	-0.01340	-15.44	-10.48	0.22355
PhTm	-0.01390	-0.01147	-12.24	-7.28	0.16812
2PhTm	-0.01897	-0.01682	-12.70	-7.74	0.17940
PhTn$^{\text{tBu}}$	-0.00503	-0.00801	-15.33	-10.37	0.24569
2PhTn$^{\text{tBu}}$	-0.00490	-0.00698	-15.11	-10.15	0.22389

Table 5.12: Results Complex Formation Step 2b

L_i	E_{elec} [kJ/mol]	E_{elec}^{SP} [H]	$\Delta_r H$ [kJ/mol]	ΔG [kJ/mol]	K^{298}
Tm	-32.05	-21.47	-28.90	-83.05	3.549·10^{14}
2Tm	-70.25	-61.95	-69.44	-120.24	1.167·10^{21}
Tm$_2$n$^{\text{tBu}}$	-0.66	4.53	-3.31	-64.77	2.227·10^{11}
2Tm$_2$n$^{\text{tBu}}$	-46.26	-42.07	-49.63	-107.58	7.059·10^{18}
Tmn$_2^{\text{tBu}}$	25.97	22.74	13.39	-59.70	2.884·10^{10}
2Tmn$_2^{\text{tBu}}$	-30.29	-35.46	-44.42	-113.44	7.506·10^{19}
Tn$^{\text{tBu}}$	43.63	36.63	25.86	-38.60	5.793·10^{06}
2Tn$^{\text{tBu}}$	-24.38	-35.19	-45.67	-112.33	4.784·10^{19}
PhTm	-36.49	-30.13	-37.41	-87.53	2.168·10^{15}
2PhTm	-49.81	-44.16	-51.90	-105.39	2.912·10^{18}
PhTn$^{\text{tBu}}$	-13.21	-21.02	-31.39	-104.64	2.156·10^{18}
2PhTn$^{\text{tBu}}$	-12.87	-18.32	-28.48	-95.23	4.832·10^{16}

Table 5.13: Results Complex Formation Step 2a (COSMO)

L_i	E_{elec} [H]	E_{elec}^{SP} [H]	energy [kJ/mol]	ΔH [kJ/mol]	ΔS [kJ/mol·K]
cTm	-0.00459	0.00108	-13.77	-8.81	0.23296
c2Tm	-0.02173	-0.01700	-13.29	-8.33	0.23681
cTm$_2$n$^{\text{tBu}}$	0.00356	0.00651	-14.37	-9.41	0.24030
c2Tm$_2$n$^{\text{tBu}}$	-0.01600	-0.01389	-14.17	-9.21	0.25919
cTmn$_2^{\text{tBu}}$	0.01156	0.01324	-14.97	-10.01	0.24777
c2Tmn$_2^{\text{tBu}}$	-0.01196	-0.01212	-14.40	-9.44	0.26134
cTn$^{\text{tBu}}$	0.01929	0.01967	-16.15	-11.19	0.26903
c2Tn$^{\text{tBu}}$	-0.00853	-0.01053	-14.53	-9.57	0.26925
cPhTm	-0.01003	-0.00571	-13.22	-8.26	0.23104
c2PhTm	-0.01615	-0.01234	-13.10	-8.14	0.23205
cPhTn$^{\text{tBu}}$	-0.01321	-0.00541	-14.56	-9.60	0.26018
c2PhTn$^{\text{tBu}}$	-0.01621	-0.00738	-14.14	-9.18	0.24962

Table 5.14: Results Complex Formation Step 2b (COSMO)

L_i	E_{elec} [kJ/mol]	E_{elec}^{SP} [H]	$\Delta_r H$ [kJ/mol]	ΔG [kJ/mol]	K^{298}
cTm	-12.06	2.82	-5.99	-75.45	$1.653 \cdot 10^{13}$
c2Tm	-57.05	-44.63	-52.96	-123.57	$4.457 \cdot 10^{21}$
cTm$_2$n^{tBu}	9.34	17.10	7.68	-63.96	$1.607 \cdot 10^{11}$
c2Tm$_2$n^{tBu}	-42.01	-36.47	-45.68	-122.96	$3.489 \cdot 10^{21}$
cTmn$_2^{tBu}$	30.36	34.77	24.75	-49.12	$4.032 \cdot 10^{08}$
c2Tmn$_2^{tBu}$	-31.41	-31.82	-41.27	-119.18	$7.608 \cdot 10^{20}$
cTn^{tBu}	50.64	51.64	40.45	-39.77	$9.269 \cdot 10^{06}$
c2Tn^{tBu}	-22.41	-27.64	-37.21	-117.49	$3.839 \cdot 10^{20}$
cPhTm	-26.34	-15.00	-23.26	-92.15	$1.393 \cdot 10^{16}$
c2PhTm	-42.40	-32.40	-40.55	-109.73	$1.679 \cdot 10^{19}$
cPhTn^{tBu}	-34.69	-14.21	-23.81	-101.38	$5.785 \cdot 10^{17}$
c2PhTn^{tBu}	-42.56	-19.37	-28.55	-102.98	$1.102 \cdot 10^{18}$

Table 5.15: Results Complex Formation (total) 1

L_i	E_{elec} [H]	E_{elec}^{SP} [H]	energy [kJ/mol]	ΔH [kJ/mol]	ΔS [kJ/mol·K]
Tm	0.05447	0.05709	-13.95	-8.99	0.19861
2Tm	0.03992	0.04168	-14.01	-9.05	0.18740
Tm$_2$n^{tBu}	0.06643	0.06700	-14.37	-9.41	0.22312
2Tm$_2$n^{tBu}	0.04906	0.04925	-14.08	-9.12	0.21138
Tmn$_2^{tBu}$	0.07657	0.07393	-15.88	-10.92	0.26213
2Tmn$_2^{tBu}$	0.05514	0.05177	-15.49	-10.53	0.24848
Tn^{tBu}	0.05447	0.05709	-13.95	-8.99	0.19861
2Tn^{tBu}	0.05739	0.05187	-17.01	-12.05	0.24054
PhTm	0.05278	0.05380	-13.81	-8.85	0.18511
2PhTm	0.04771	0.04846	-14.27	-9.31	0.19639
PhTn^{tBu}	0.06165	0.05727	-16.90	-11.94	0.26268
2PhTn^{tBu}	0.06178	0.05830	-16.68	-11.72	0.24088

Table 5.16: Results Complex Formation (total) 2

L_i	E_{elec} [kJ/mol]	E_{elec}^{SP} [H]	$\Delta_r H$ [kJ/mol]	ΔG [kJ/mol]	K^{298}
Tm	143.02	149.90	140.91	81.69	$4.863 \cdot 10^{-15}$
2Tm	104.82	109.42	100.37	44.50	$1.599 \cdot 10^{-08}$
Tm$_2$n^{tBu}	174.41	175.91	166.50	99.97	$3.052 \cdot 10^{-18}$
2Tm$_2$n^{tBu}	128.81	129.30	120.18	57.16	$9.674 \cdot 10^{-11}$
Tmn$_2^{tBu}$	201.04	194.12	183.19	105.04	$3.953 \cdot 10^{-19}$
2Tmn$_2^{tBu}$	144.78	135.92	125.38	51.30	$1.029 \cdot 10^{-09}$
Tn^{tBu}	143.02	149.90	140.91	81.69	$4.863 \cdot 10^{-15}$
2Tn^{tBu}	150.69	136.18	124.13	52.42	$6.557 \cdot 10^{-10}$
PhTm	138.58	141.25	132.40	77.21	$2.971 \cdot 10^{-14}$
2PhTm	125.26	127.22	117.91	59.35	$3.991 \cdot 10^{-11}$
PhTn^{tBu}	161.86	150.36	138.42	60.10	$2.955 \cdot 10^{-11}$
2PhTn^{tBu}	162.20	153.05	141.33	69.51	$6.622 \cdot 10^{-13}$

Table 5.17: Results Complex Formation (total) 3 (COSMO)

L_i	E_{elec} [H]	E_{elec}^{SP} [H]	energy [kJ/mol]	ΔH [kJ/mol]	ΔS [kJ/mol·K]
cTm	0.05776	0.06325	-15.07	-10.11	0.22210
c2Tm	0.04062	0.04517	-14.59	-9.63	0.22595
cTm$_2$n^{tBu}	0.06591	0.06868	-15.67	-10.71	0.22944
c2Tm$_2$n^{tBu}	0.04635	0.04828	-15.47	-10.51	0.24833
cTmn$_2^{tBu}$	0.07392	0.07541	-16.27	-11.31	0.23691
c2Tmn$_2^{tBu}$	0.05039	0.05005	-15.70	-10.74	0.25048
cTn^{tBu}	0.08164	0.08184	-17.45	-12.49	0.25817
c2Tn^{tBu}	0.05382	0.05164	-15.83	-10.87	0.25839
cPhTm	0.05232	0.05646	-14.52	-9.56	0.22018
c2PhTm	0.04621	0.04983	-14.40	-9.44	0.22119
cPhTn^{tBu}	0.04914	0.05676	-15.86	-10.90	0.24932
c2PhTn^{tBu}	0.04614	0.05479	-15.44	-10.48	0.23876

Table 5.18: Results Complex Formation (total) 4 (COSMO)

L_i	E_{elec} [kJ/mol]	E_{elec}^{SP} [H]	$\Delta_r H$ [kJ/mol]	ΔG [kJ/mol]	K^{298}
cTm	151.65	166.06	155.94	89.72	$1.906 \cdot 10^{-16}$
c2Tm	106.66	118.60	108.97	41.60	$5.141 \cdot 10^{-08}$
cTm$_2$n^{tBu}	173.05	180.33	169.62	101.21	$1.854 \cdot 10^{-18}$
c2Tm$_2$n^{tBu}	121.70	126.76	116.25	42.21	$4.024 \cdot 10^{-08}$
cTmn$_2^{tBu}$	194.07	198.00	186.69	116.05	$4.651 \cdot 10^{-21}$
c2Tmn$_2^{tBu}$	132.30	131.41	120.67	45.99	$8.776 \cdot 10^{-09}$
cTn^{tBu}	214.35	214.87	202.38	125.40	$1.069 \cdot 10^{-22}$
c2Tn^{tBu}	141.30	135.59	124.72	47.68	$4.428 \cdot 10^{-09}$
cPhTm	137.37	148.23	138.67	73.02	$1.607 \cdot 10^{-13}$
c2PhTm	121.31	130.83	121.39	55.44	$1.937 \cdot 10^{-10}$
cPhTn^{tBu}	129.02	149.02	138.12	63.79	$6.673 \cdot 10^{-12}$
c2PhTn^{tBu}	121.15	143.86	133.38	62.19	$1.271 \cdot 10^{-11}$

Table 5.19: SEN Ligands

L_i	B-N1	B-N2	B-N3	C=S1	C=S2	C=S3	B-H/C
Tm	1.229	1.228	1.228	1.569	1.569	1.569	1.384
2Tm	1.256	1.261	1.260	1.565	1.562	1.558	1.380
Tm$_2$n^{tBu}	1.188*	1.237	1.240	1.572	1.547	1.564*	1.383
2Tm$_2$n^{tBu}	1.188*	1.272	1.254	1.574	1.548	1.540*	1.371
Tmn$_2^{tBu}$	1.190*	1.197*	1.259	1.563*	1.553	1.553*	1.371
2Tmn$_2^{tBu}$	1.190*	1.198*	1.275	1.544*	1.552	1.542*	1.384
Tn^{tBu}	1.206	1.207	1.205	1.555	1.550	1.552	1.367
2Tn^{tBu}	1.207	1.203	1.205	1.545	1.546	1.548	1.391
PhTm	1.166	1.191	1.255	1.579	1.569	1.585	1.376
2PhTm	1.172	1.197	1.174	1.543	1.592	1.556	1.374
PhTn^{tBu}	1.109	1.145	1.123	1.568	1.570	1.614	1.385
2PhTn^{tBu}	1.214	1.162	1.170	1.581	1.565	1.553	1.360

Table 5.20: Population Analysis Ligands

L_i	B	N1	N2	N3	S1	S2	S3	H/C
Tm	4.446	7.524	7.523	7.523	16.344	16.345	16.344	0.992
2Tm	4.411	7.531	7.532	7.531	16.348	16.352	16.352	1.074
Tm_2n^{tBu}	4.449	7.307*	7.524	7.515	16.343	16.371	16.235*	0.988
$2Tm_2n^{tBu}$	4.416	7.308*	7.542	7.522	16.337	16.369	16.264*	1.057
Tmn_2^{tBu}	4.454	7.289*	7.310*	7.522	16.231*	16.360	16.267*	0.979
$2Tmn_2^{tBu}$	4.421	7.303*	7.318*	7.532	16.249*	16.363	16.272*	1.038
Tn^{tBu}	4.461	7.297	7.296	7.295	16.255	16.255	16.254	0.971
$2Tn^{tBu}$	4.425	7.311	7.310	7.310	16.264	16.262	16.260	1.020
PhTm	4.141	7.544	7.548	7.552	16.343	16.327	16.326	6.283
2PhTm	4.156	7.537	7.540	7.566	16.383	16.314	16.346	6.264
$PhTn^{tBu}$	4.085	7.336	7.366	7.330	16.194	16.251	16.170	6.290
$2PhTn^{tBu}$	4.113	7.347	7.337	7.338	16.196	16.216	16.262	6.257

Table 5.21: Geometrical Data Ligands

L_i	B-N1 [Å]	B-N2 [Å]	B-N3 [Å]	C=S1 [Å]	C=S2 [Å]	C=S3 [Å]	B-H/C [Å]
Tm	1.558	1.558	1.559	1.680	1.679	1.679	1.211
Tm_2n^{tBu}	1.578*	1.552	1.551	1.680	1.687	1.672*	1.210
Tmn_2^{tBu}	1.567*	1.566*	1.537	1.668*	1.680	1.675*	1.197
Tn^{tBu}	1.560	1.561	1.561	1.677	1.676	1.676	1.210
PhTm	1.595	1.586	1.571	1.686	1.677	1.681	1.621
$PhTn^{tBu}$	1.607	1.569	1.613	1.666	1.679	1.668	1.617

Table 5.22: SEN Ligands (COSMO)

L_i	B-N1	B-N2	B-N3	C=S1	C=S2	C=S3	B-H/C
cTm	1.231	1.228	1.229	1.526	1.525	1.524	1.398
c2Tm	1.256	1.257	1.260	1.526	1.526	1.522	1.379
cTm_2n^{tBu}	1.183	1.239	1.247	1.526	1.522	1.525	1.400
$c2Tm_2n^{tBu}$	1.183	1.268	1.255	1.536	1.522	1.505	1.376
$cTmn_2^{tBu}$	1.189	1.196	1.263	1.527	1.528	1.525	1.392
$c2Tmn_2^{tBu}$	1.197	1.194	1.276	1.505	1.527	1.513	1.376
cTn^{tBu}	1.204	1.203	1.205	1.524	1.523	1.522	1.393
$c2Tn^{tBu}$	1.209	1.206	1.207	1.516	1.516	1.520	1.380
cPhTm	1.192	1.189	1.233	1.545	1.530	1.547	1.385
c2PhTm	1.182	1.208	1.163	1.521	1.547	1.520	1.391
$cPhTn^{tBu}$	1.110	1.078	1.107	1.525	1.538	1.566	1.389
$c2PhTn^{tBu}$	1.199	1.133	1.174	1.542	1.531	1.525	1.377

Table 5.23: Population Analysis Ligands (COSMO)

L_i	B	N1	N2	N3	S1	S2	S3	H/C
cTm	4.434	7.522	7.522	7.522	16.434	16.433	16.434	1.020
c2Tm	4.412	7.528	7.526	7.526	16.430	16.431	16.430	1.071
cTm$_2$n^{tBu}	4.437	7.303	7.525	7.519	16.432	16.438	16.341	1.013
c2Tm$_2$n^{tBu}	4.413	7.305	7.538	7.522	16.420	16.430	16.354	1.060
cTmn$_2^{tBu}$	4.441	7.291	7.307	7.522	16.338	16.436	16.354	1.007
c2Tmn$_2^{tBu}$	4.413	7.304	7.313	7.531	16.348	16.425	16.342	1.047
cTn^{tBu}	4.446	7.297	7.297	7.297	16.348	16.348	16.348	0.999
c2Tn^{tBu}	4.415	7.313	7.312	7.312	16.339	16.338	16.336	1.033
cPhTm	4.140	7.543	7.545	7.547	16.416	16.414	16.405	6.273
c2PhTm	4.155	7.534	7.536	7.558	16.443	16.406	16.425	6.276
cPhTn^{tBu}	4.081	7.333	7.356	7.330	16.309	16.334	16.285	6.295
c2PhTn^{tBu}	4.110	7.341	7.330	7.337	16.304	16.298	16.344	6.265

Table 5.24: Geometrical Data Ligands (COSMO)

L_i	B-N1 [Å]	B-N2 [Å]	B-N3 [Å]	C=S1 [Å]	C=S2 [Å]	C=S3 [Å]	B-H/B [Å]
cTm	1.552	1.552	1.552	1.691	1.691	1.691	1.214
cTm$_2$n^{tBu}	1.576*	1.544	1.544	1.690	1.693	1.685*	1.213
cTmn$_2^{tBu}$	1.570*	1.567*	1.535	1.684*	1.690	1.689*	1.212
cTn^{tBu}	1.559	1.559	1.559	1.687	1.687	1.687	1.210
cPhTm	1.587	1.578	1.569	1.691	1.687	1.688	1.619
cPhTn^{tBu}	1.605	1.576	1.610	1.680	1.689	1.681	1.617

Table 5.25: SEN Complexes 1

$[L_i\text{Mo(CO)}_3]$	Mo-C1	Mo-C2	Mo-C3	Mo-S1	Mo-S2	Mo-S3
[Tm]	0.985	0.977	0.973	0.216	0.219	0.215
[Tm$_2$n^{tBu}]	0.964	0.949	0.925	0.228	0.223	0.240
[Tmn$_2^{tBu}$]	0.953	0.948	0.961	0.248	0.236	0.242
[Tn^{tBu}]	0.938	0.936	0.935	0.264	0.263	0.264
[PhTm]	0.968	0.973	0.976	0.219	0.226	0.212
[PhTn^{tBu}]	0.939	0.921	0.935	0.279	0.263	0.263
[Mo(CO)$_6$]	0.635	0.633	0.632			
[**1**]	0.844	0.843	0.842			

Table 5.26: SEN Complexes 2

$[L_i\text{Mo(CO)}_3]$	B-N1	B-N2	B-N3	C=S1	C=S2	C=S3	B-H/C
[Tm]	1.234	1.231	1.234	1.510	1.509	1.507	1.317
[Tm$_2$n^{tBu}]	1.182	1.244	1.234	1.509	1.495	1.541	1.315
[Tmn$_2^{tBu}$]	1.187	1.189	1.257	1.518	1.517	1.510	1.331
[Tn^{tBu}]	1.204	1.205	1.207	1.511	1.513	1.513	1.342
[PhTm]	1.200	1.212	1.193	1.515	1.504	1.511	1.365
[PhTn^{tBu}]	1.137	1.187	1.175	1.511	1.512	1.509	1.337

Table 5.27: Population Analysis Complexes

$[L_i\mathrm{Mo(CO)_3}]$	Mo	B	N1	N2	N3	S1	S2	S3	H/C
[Tm]	14.721	4.418	7.526	7.526	7.526	16.217	16.216	16.218	1.059
[Tm$_2$n$^{\mathrm{tBu}}$]	14.726	4.421	7.317	7.532	7.518	16.210	16.219	16.159	1.042
[Tmn$_2^{\mathrm{tBu}}$]	14.761	4.422	7.293	7.314	7.528	16.095	16.193	16.102	1.027
[Tn$^{\mathrm{tBu}}$]	14.799	4.426	7.312	7.312	7.312	16.070	16.071	16.071	1.010
[PhTm]	14.716	4.169	7.548	7.549	7.542	16.213	16.209	16.216	6.257
[PhTn$^{\mathrm{tBu}}$]	14.796	4.125	7.348	7.339	7.351	16.053	16.055	16.066	6.248
[Mo(CO)$_6$]	15.185								
[**1**]	14.549								

Table 5.28: Geometrical Data Complexes 1

$[L_i\mathrm{Mo(CO)_3}]$	Mo-C1 [Å]	Mo-C2 [Å]	Mo-C3 [Å]	Mo-S1 [Å]	Mo-S2 [Å]	Mo-S3 [Å]
[Tm]	1.929	1.929	1.930	2.685	2.683	2.686
[Tm$_2$n$^{\mathrm{tBu}}$]	1.937	1.933	1.931	2.673	2.669	2.703*
[Tmn$_2^{\mathrm{tBu}}$]	1.941	1.942	1.931	2.648*	2.648	2.646*
[Tn$^{\mathrm{tBu}}$]	1.946	1.946	1.946	2.614	2.615	2.614
[PhTm]	1.930	1.929	1.929	2.686	2.668	2.714
[PhTn$^{\mathrm{tBu}}$]	1.948	1.948	1.945	2.594	2.620	2.621
[Mo(CO)$_6$]	2.058	2.059	2.058			
[**1**]	1.974	1.974	1.974			

Table 5.29: Geometrical Data Complexes 2

$[L_i\mathrm{Mo(CO)_3}]$	B-N1 [Å]	B-N2 [Å]	B-N3 [Å]	C=S1 [Å]	C=S2 [Å]	C=S3 [Å]	B-H/B-C [Å]
[Tm]	1.547	1.546	1.547	1.705	1.705	1.705	1.230
[Tm$_2$n$^{\mathrm{tBu}}$]	1.575*	1.543	1.547	1.705	1.708	1.703*	1.223
[Tmn$_2^{\mathrm{tBu}}$]	1.565*	1.531	1.568	1.696*	1.701	1.700*	1.219
[Tn$^{\mathrm{tBu}}$]	1.556	1.556	1.556	1.695	1.695	1.695	1.216
[PhTm]	1.561	1.571	1.557	1.704	1.707	1.706	1.648
[PhTn$^{\mathrm{tBu}}$]	1.573	1.579	1.565	1.696	1.695	1.694	1.654

Table 5.30: SEN Complexes 1 (COSMO)

$[L_i\mathrm{Mo(CO)_3}]$	Mo-C1	Mo-C2	Mo-C3	Mo-S1	Mo-S2	Mo-S3
c[Tm]	0.974	0.969	0.965	0.228	0.231	0.228
c[Tm$_2$n$^{\mathrm{tBu}}$]	0.957	0.972	0.954	0.236	0.233	0.237
c[Tmn$_2^{\mathrm{tBu}}$]	0.965	0.954	0.957	0.240	0.241	0.243
c[Tn$^{\mathrm{tBu}}$]	0.956	0.956	0.954	0.250	0.249	0.251
c[PhTm]	0.957	0.962	0.963	0.233	0.240	0.225
c[PhTn$^{\mathrm{tBu}}$]	0.971	0.956	0.958	0.259	0.244	0.251
c[Mo(CO)$_6$]	0.636	0.634	0.633			
c[**1**]	0.884	0.884	0.883			

Table 5.31: SEN Complexes 2 (COSMO)

$[L_i\text{Mo(CO)}_3]$	B-N1	B-N2	B-N3	C=S1	C=S2	C=S3	B-H/C
c[Tm]	1.240	1.237	1.240	1.476	1.476	1.473	1.338
c[Tm$_2$n$^{\text{tBu}}$]	1.170	1.254	1.250	1.485	1.466	1.484	1.347
c[Tmn$_2^{\text{tBu}}$]	1.181	1.184	1.263	1.486	1.481	1.474	1.339
c[Tn$^{\text{tBu}}$]	1.202	1.196	1.195	1.478	1.479	1.485	1.350
c[PhTm]	1.204	1.220	1.190	1.483	1.470	1.476	1.367
c[PhTn$^{\text{tBu}}$]	1.140	1.173	1.175	1.479	1.483	1.481	1.343

Table 5.32: Population Analysis Complexes (COSMO)

$[L_i\text{Mo(CO)}_3]$	Mo	B	N1	N2	N3	S1	S2	S3	H/C
c[Tm]	14.699	4.421	7.515	7.516	7.516	16.257	16.255	16.257	1.051
c[Tm$_2$n$^{\text{tBu}}$]	14.698	4.420	7.291	7.525	7.514	16.248	16.247	16.209	1.040
c[Tmn$_2^{\text{tBu}}$]	14.717	4.419	7.283	7.300	7.523	16.190	16.232	16.180	1.027
c[Tn$^{\text{tBu}}$]	14.742	4.419	7.304	7.296	7.295	16.164	16.168	16.157	1.014
c[PhTm]	14.691	4.169	7.536	7.539	7.532	16.251	16.247	16.259	6.275
c[PhTn$^{\text{tBu}}$]	14.726	4.116	7.336	7.325	7.340	16.148	16.150	16.156	6.263
c[Mo(CO)$_6$]	15.176								
c[**1**]	14.502								

Table 5.33: Geometrical Data Complexes 1 (COSMO)

$[L_i\text{Mo(CO)}_3]$	Mo-C1 [Å]	Mo-C2 [Å]	Mo-C3 [Å]	Mo-S1 [Å]	Mo-S2 [Å]	Mo-S3 [Å]
c[Tm]	1.927	1.926	1.927	2.661	2.658	2.662
c[Tm$_2$n$^{\text{tBu}}$]	1.930	1.928	1.924	2.652	2.648	2.681*
c[Tmn$_2^{\text{tBu}}$]	1.928	1.933	1.928	2.665*	2.635	2.648*
c[Tn$^{\text{tBu}}$]	1.933	1.933	1.932	2.636	2.636	2.635
c[PhTm]	1.927	1.926	1.926	2.644	2.647	2.690
c[PhTn$^{\text{tBu}}$]	1.922	1.925	1.923	2.618	2.644	2.636
c[Mo(CO)$_6$]	2.057	2.057	2.057			
c[**1**]	1.955	1.955	1.955			

Table 5.34: Geometrical Data Complexes 2 (COSMO)

$[L_i\text{Mo(CO)}_3]$	B-N1 [Å]	B-N2 [Å]	B-N3 [Å]	C=S1 [Å]	C=S2 [Å]	C=S3 [Å]	B-H/C [Å]
c[Tm]	1.547	1.547	1.547	1.714	1.713	1.714	1.225
c[Tm$_2$n$^{\text{tBu}}$]	1.580*	1.540	1.538	1.711	1.713	1.713*	1.221
c[Tmn$_2^{\text{tBu}}$]	1.568*	1.572*	1.529	1.709*	1.708	1.711*	1.216
c[Tn$^{\text{tBu}}$]	1.557	1.560	1.560	1.708	1.709	1.707	1.211
c[PhTm]	1.564	1.559	1.574	1.712	1.716	1.715	1.644
c[PhTn$^{\text{tBu}}$]	1.579	1.588	1.569	1.710	1.707	1.706	1.649

Table 5.35: Thermodynamical Data Dissociation 1

compound	E_{elec} [H]	E_{elec}^{SP} [H]	energy [kJ/mol]	ΔH [kJ/mol]	ΔS [kJ/mol·K]
Tm	-2012.75533	-2014.03390	785.67	788.15	0.68796
Tm_2n^{tBu}	-2168.47751	-2169.91643	1021.30	1023.78	0.77346
Tmn_2^{tBu}	-2324.19893	-2325.79931	1256.69	1259.17	0.86291
Tn^{tBu}	-2479.92075	-2481.68342	1492.48	1494.96	0.96607
m0	-662.34692	-662.76814	241.88	244.36	0.33979
py0	-818.05055	-818.62881	476.43	478.91	0.43533
Dm-	-1350.24568	-1351.11022	529.38	531.86	0.53975
Dmpy-	-1506.00786	-1507.03289	762.92	765.40	0.63995
Dpy-	-1661.73298	-1662.92080	998.93	1001.41	0.70064
m-	-662.41092	-662.84124	238.72	241.20	0.33813
py-	-818.13738	-818.73077	474.27	476.75	0.43481
Dm0	-1350.24145	-1351.10001	536.47	538.95	0.52938
Dmpy0	-1505.97699	-1506.99797	772.14	774.62	0.61384
Dpy0	-1661.68893	-1662.87349	1007.41	1009.89	0.70292
dDm0	-2700.49996	-2702.21276	1080.72	1083.20	0.89246

Table 5.36: Thermodynamical Data Dissociation 1.R1b

educt	product	E_{elec} [H]	E_{elec}^{SP} [H]	E_{elec} [kJ/mol]	E_{elec}^{SP} [kJ/mol]	energy [kJ/mol]
Tm	Dm-	0.16273	0.15554	427.24	408.36	-14.41
Tm_2n^{tBu}	Dmpy-	0.12273	0.11540	322.23	302.99	-16.50
Tm_2n^{tBu}	Dm-	0.18127	0.17740	475.93	465.76	-15.49
Tmn_2^{tBu}	Dpy-	0.11904	0.11036	312.53	289.76	-15.88
Tmn_2^{tBu}	Dmpy-	0.14052	0.13761	368.93	361.30	-17.34
Tn^{tBu}	Dpy-	0.13722	0.13380	360.28	351.30	-17.12

Table 5.37: Thermodynamical Data Dissociation 1.R2b

educt	product	E_{elec} [H]	E_{elec}^{SP} [H]	E_{elec} [kJ/mol]	E_{elec}^{SP} [kJ/mol]	energy [kJ/mol]
Tm	Dm0	0.10296	0.09265	270.33	243.26	-10.48
Tm_2n^{tBu}	Dmpy0	0.08960	0.07723	235.24	202.76	-10.44
Tm_2n^{tBu}	Dm0	0.09868	0.08565	259.08	224.87	-10.56
Tmn_2^{tBu}	Dpy0	0.09909	0.08458	260.15	222.06	-10.56
Tmn_2^{tBu}	Dmpy0	0.08456	0.07057	222.01	185.28	-10.28
Tn^{tBu}	Dpy0	0.09444	0.07915	247.96	207.81	-10.80
Tm	dDm0	-0.01707	-0.01274	-44.81	-33.45	7.78

Table 5.38: Thermodynamical Data Dissociation 1 (THF)

compound	E_{elec} [H]	E_{elec}^{SP} [H]	energy [kJ/mol]	ΔH [kJ/mol]	ΔS [kJ/mol·K]
PhTm	-2243.37631	-2244.88860	1004.41	1006.89	0.78417
PhTn$^{\text{tBu}}$	-2710.52961	-2712.52575	1709.12	1711.60	1.04547
tPhDm-	-1812.89763	-1814.24523	1060.70	1063.18	0.73934
tPhDpy-	-2124.38245	-2126.04979	1532.93	1535.41	0.92084
tDm-	-1582.26190	-1583.37533	842.72	845.20	0.63766
tDmpy-	-1738.03392	-1739.30645	1079.95	1082.43	0.73597
tDpy-	-1893.75146	-1895.18650	1313.53	1316.01	0.82820
THF	-232.01399	-232.26951	305.95	308.43	0.29961
tPhDm0	-1812.93302	-1814.23548	1072.07	1074.55	0.74739
tPhDpy0	-2124.35457	-2126.03912	1542.84	1545.32	0.91230
tDm0	-1582.30360	-1583.40835	854.29	856.77	0.64112
tDmpy0	-1738.02054	-1739.28737	1090.51	1092.99	0.71610
tDpy0	-1893.73272	-1895.16301	1325.18	1327.66	0.83771

Table 5.39: Thermodynamical Data Dissociation 1.R1b (THF)

educt	product	E_{elec} [H]	E_{elec}^{SP} [H]	E_{elec} [kJ/mol]	E_{elec}^{SP} [kJ/mol]	energy [kJ/mol]
Tm	tDm-	0.16050	0.15994	421.39	419.91	-7.02
Tm$_2$n$^{\text{tBu}}$	tDmpy-	0.11066	0.11135	290.54	292.34	-5.42
Tm$_2$n$^{\text{tBu}}$	tDm-	0.17904	0.18180	470.08	477.31	-8.10
Tmn$_2^{\text{tBu}}$	tDpy-	0.11455	0.11417	300.75	299.76	-7.23
Tmn$_2^{\text{tBu}}$	tDmpy-	0.12845	0.13356	337.24	350.65	-6.26
Tn$^{\text{tBu}}$	tDpy-	0.13274	0.13761	348.50	361.31	-8.47
PhTm	tPhDm-	0.14576	0.14474	382.69	380.01	-7.78
PhTn$^{\text{tBu}}$	tPhDp-	0.11061	0.11666	290.40	306.30	-5.71

Table 5.40: Thermodynamical Data Dissociation 1.R1b (THF)

educt	product	E_{elec} [H]	E_{elec}^{SP} [H]	E_{elec} [kJ/mol]	E_{elec}^{SP} [kJ/mol]	energy [kJ/mol]
Tm	tDm-	0.16050	0.15994	421.39	419.91	-7.02
Tm$_2$n$^{\text{tBu}}$	tDmpy-	0.11066	0.11135	290.54	292.34	-5.42
Tm$_2$n$^{\text{tBu}}$	tDm-	0.17904	0.18180	470.08	477.31	-8.10
Tmn$_2^{\text{tBu}}$	tDpy-	0.11455	0.11417	300.75	299.76	-7.23
Tmn$_2^{\text{tBu}}$	tDmpy-	0.12845	0.13356	337.24	350.65	-6.26
Tn$^{\text{tBu}}$	tDpy-	0.13274	0.13761	348.50	361.31	-8.47
PhTm	tPhDm-	0.14576	0.14474	382.69	380.01	-7.78
PhTn$^{\text{tBu}}$	tPhDp-	0.11061	0.11666	290.40	306.30	-5.71

Table 5.41: Thermodynamical Data Dissociation 1 (COSMO/THF)

compound	E_{elec} [H]	E_{elec}^{SP} [H]	energy [kJ/mol]	ΔH [kJ/mol]	ΔS [kJ/mol·K]
cPhTm	-2243.46074	-2244.97767	1007.030	1009.51	0.75124
cPhTn^{tBu}	-2710.59841	-2712.59885	1711.860	1714.34	1.00068
cTm	-2012.83973	-2014.12249	789.110	791.59	0.65911
cTm$_2$n^{tBu}	-2168.55644	-2170.00024	1024.510	1026.99	0.74995
cTmn$_2^{tBu}$	-2324.27360	-2325.88014	1260.300	1262.78	0.83514
cTn^{tBu}	-2479.99267	-2481.76125	1495.920	1498.40	0.92013
ctPhDm-	-1812.96944	-1814.31930	1060.55	1063.03	0.70736
ctPhDpy-	-2124.44758	-2126.11944	1537.24	1539.72	0.87111
ctDm-	-1582.33819	-1583.45577	847.18	849.66	0.60465
ctDmpy-	-1738.11082	-1739.40770	1083.95	1086.43	0.69673
ctDpy-	-1893.82592	-1895.26597	1319.39	1321.87	0.78258
cTHF	-232.01827	-232.27408	306.36	308.84	0.29396
cm0	-662.35784	-662.78013	243.17	245.65	0.33035
cpy0	-818.06006	-818.63755	479.14	481.62	0.41733
ctPhDm0	-1812.96944	-1814.28279	1060.47	1062.95	0.71057
ctPhDpy0	-2124.37090	-2126.03697	1543.46	1545.94	0.88176
ctDm0	-1582.32291	-1583.42996	855.54	858.02	0.60907
ctDmpy0	-1738.03716	-1739.30651	1090.67	1093.15	0.69933
ctDpy0	-1893.75222	-1895.18596	1326.69	1329.17	0.79146
cm-	-662.49683	-662.93009	240.93	243.41	0.33422
cpy-	-818.21805	-818.81502	477.29	479.77	0.42010
dDm0	-2700.53048	-2702.24598	1082.56	1085.04	0.84305

Table 5.42: Thermodynamical Data Dissociation 1.R1b (COSMO/THF)

educt	product	E_{elec} [H]	E_{elec}^{SP} [H]	E_{elec} [kJ/mol]	E_{elec}^{SP} [kJ/mol]	energy [kJ/mol]
cTm	ctDm-	0.16197	0.16067	425.24	421.84	-5.12
cTm$_2$n^{tBu}	ctDmpy-	0.10605	0.08649	278.43	227.08	-3.75
cTm$_2$n^{tBu}	ctDm-	0.17646	0.18100	463.31	475.20	-4.55
cTmn$_2^{tBu}$	ctDpy-	0.10810	0.10812	283.81	283.87	-4.10
cTmn$_2^{tBu}$	ctDmpy-	0.12099	0.10898	317.65	286.12	-3.57
cTn^{tBu}	ctDpy-	0.12495	0.13180	328.06	346.04	-3.75
cPhTm	ctPhDm-	0.15172	0.15232	398.34	399.92	-9.67
cPhTn^{tBu}	ctPhDp-	0.10904	0.11594	286.28	304.40	-1.84

Table 5.43: Thermodynamical Data Dissociation 1.R2b (COSMO/THF)

educt	product	E_{elec} [H]	E_{elec}^{SP} [H]	E_{elec} [kJ/mol]	E_{elec}^{SP} [kJ/mol]	energy [kJ/mol]
cTm	cdDm0	0.07880	0.06579	206.88	172.73	-15.80
cTm	ctDm0	0.03826	0.03651	100.44	95.86	1.00
cTm$_2$n^{tBu}	ctDmpy0	0.04071	0.03771	106.90	99.01	0.73
cTm$_2$n^{tBu}	ctDm0	0.03375	0.02934	88.62	77.03	1.96
cTmn$_2^{tBu}$	ctBpy0	0.04281	0.03817	112.40	100.21	0.96
cTmn$_2^{tBu}$	ctBmpy0	0.03665	0.03270	96.22	85.84	1.30
cTn^{tBu}	ctBpy0	0.04066	0.03435	106.75	90.19	1.70
cPhTm	ctPhDm0	0.01273	0.03887	33.43	102.06	-11.99
cPhTn^{tBu}	ctPhDp0	0.02773	0.02094	72.80	54.99	2.53

Table 5.44: Thermodynamical Data Dissociation 2 (THF)

compound	E_{elec} [H]	E_{elec}^{SP} [H]	energy [kJ/mol]	ΔH [kJ/mol]	ΔS [kJ/mol·K]
THF	-232.01399	-232.26951	305.950	308.43	0.29961
tDm0	-1582.30360	-1583.40835	854.29	856.77	0.64112
tDmp0y	-1738.02054	-1739.28737	1090.51	1092.99	0.71610
tDpy0	-1893.73272	-1895.16301	1325.18	1327.66	0.83771
tPhDm0	-1812.93302	-1814.23548	1072.07	1074.55	0.74739
tPhDpy0	-2124.35457	-2126.03912	1542.84	1545.32	0.91230
t$_2$Bm+	-1151.69865	-1152.63755	919.15	921.63	0.60320
t$_2$Bpy+	-1307.41329	-1308.51465	1155.29	1157.77	0.69453
t$_2$PhBm+	-1382.32366	-1383.49848	1136.92	1139.40	0.71046
t$_2$PhBpy+	-1538.05180	-1539.38773	1373.21	1375.69	0.77962
tBm-	-919.74909	-920.45241	588.27	590.75	0.49473
t$_2$Bpy-	-1307.56687	-1308.67861	1139.54	1142.02	0.73285
tPhBm-	-1150.40318	-1151.34235	807.12	809.60	0.60196
tPhBpy-	-1306.18562	-1307.28207	1045.5	1047.98	0.67063
tBm0	-919.78485	-920.47735	596.53	599.01	0.49309
t$_2$Bpy0	-1307.55769	-1308.66075	1147.31	1149.79	0.69097
t$_2$PhBm0	-1382.46959	-1383.64965	1129.78	1132.26	0.75135
t$_2$PhBpy0	-1538.19209	-1539.52973	1365.68	1368.16	0.79812
tDm-	-1582.26190	-1583.37533	842.72	845.20	0.63766
tDmpy-	-1738.03392	-1739.30645	1079.95	1082.43	0.73597
tDpy-	-1893.75146	-1895.18650	1313.53	1316.01	0.82820
tPhDm-	-1812.89763	-1814.24523	1060.70	1063.18	0.73934
tPhDpy-	-2124.38245	-2126.04979	1532.93	1535.41	0.92084

Table 5.45: Thermodynamical Data Dissociation 2.R1 (THF)

educt	product	E_{elec} [H]	E_{elec}^{SP} [H]	E_{elec} [kJ/mol]	E_{elec}^{SP} [kJ/mol]	energy [kJ/mol]
tDm0	tBm0	0.17183	0.16286	451.13	427.58	-15.88
tDmpy0	tBm0	0.18513	0.18120	486.07	475.75	-17.55
tDmpy0	t$_2$Bpy0	0.12993	0.12798	341.13	336.02	-7.27
tDpy0	t$_2$Bpy0	0.13848	0.14296	363.57	375.34	-7.39
tPhDm0	t$_2$PhBm0	0.13051	0.08720	342.66	228.93	-6.36
tPhDpy0	t$_2$PhBpy0	0.12592	0.15008	330.60	394.05	-6.68
tDm0	t$_2$Bm+	0.20802	0.19907	546.15	522.65	-2.37
tBmpy0	t$_2$Bm+	0.19850	0.18855	521.16	495.04	-3.04
tBmpy0	t$_2$Bpy+	0.21033	0.20098	552.21	527.68	-2.45
tDpy0	t$_2$Bpy+	0.19604	0.18709	514.71	491.21	-1.57
tPhDm0	t$_2$PhBm+	0.21244	0.16527	557.77	433.90	-2.38
tPhDpy0	t$_2$PhBpy+	0.17938	0.19013	470.97	499.18	-1.31
tDm0	tBm-	0.50228	0.48041	1318.73	1261.32	-23.68
tBmpy0	tBm-	0.54089	0.51745	1420.10	1358.58	-28.67
tBmpy0	t$_2$Bpy-	0.41543	0.40274	1090.72	1057.39	-14.58
tDpy0	t$_2$Bpy-	0.44928	0.43641	1179.59	1145.79	-18.02
tPhDm0	tPhBm-	0.47761	0.41760	1253.96	1096.41	-22.61
tPhDpy0	tPhBpy-	0.43839	0.43956	1150.99	1154.05	-23.77

Table 5.46: Thermodynamical Data Dissociation 2.R2 (THF)

educt	product	E_{elec} [H]	E_{elec}^{SP} [H]	E_{elec} [kJ/mol]	E_{elec}^{SP} [kJ/mol]	energy [kJ/mol]
tDm-	tBm0	0.06613	0.05674	173.64	148.96	-7.47
tBmpy-	tBm0	0.11169	0.09832	293.24	258.14	-9.15
tBmpy-	t$_2$Bpy0	0.07931	0.07397	208.23	194.20	0.13
tDpy-	t$_2$Bpy0	0.07038	0.06448	184.79	169.30	2.10
tPhDm-	t$_2$PhBm0	0.03112	0.02385	81.72	62.61	1.85
tPhDpy-	t$_2$PhBpy0	0.06697	0.05879	175.84	154.35	1.07
tDm-	tBm-	0.16590	0.15477	435.56	406.36	-12.57
tBmpy-	tBm-	0.23428	0.22522	615.10	591.33	-15.25
tBmpy-	t$_2$Bpy-	0.13413	0.12921	352.16	339.23	-4.48
tDpy-	t$_2$Bpy-	0.14803	0.14859	388.65	390.12	-3.51
tPhDm-	tPhBm-	0.14753	0.13473	387.35	353.75	-11.70
tPhDpy-	tPhBpy-	0.14628	0.13891	384.06	364.71	-11.00

Table 5.47: Thermodynamical Data Dissociation 2 (COSMO/THF)

compound	E_{elec} [H]	E_{elec}^{SP} [H]	energy [kJ/mol]	ΔH [kJ/mol]	ΔS [kJ/mol·K]
cTHF	-232.01827	-232.27408	306.36	308.84	0.29396
ctDm0	-1582.32291	-1583.42996	855.54	858.02	0.60907
ctDmpy0	-1738.03716	-1739.30651	1090.67	1093.15	0.69933
ctDpy0	-1893.75222	-1895.18596	1326.69	1329.17	0.79146
ctPhDm0	-1812.96944	-1814.28279	1060.47	1062.95	0.71057
ctPhDpy0	-2124.37090	-2126.03697	1543.46	1545.94	0.88176
cm0	-662.35784	-662.78013	243.17	245.65	0.33035
cpy0	-818.06006	-818.63755	479.14	481.62	0.41733
ct$_2$Bm0	-1151.79962	-1152.74865	912.82	915.30	0.57564
ct$_2$Bpy0	-1307.57687	-1308.68307	1151.03	1153.51	0.6516
ct$_2$PhBm0	-1382.47952	-1383.66200	1132.91	1135.39	0.70536
ct$_2$PhBpy0	-1538.21502	-1539.55523	1368.62	1371.10	0.74719
cm-	-662.49683	-662.93009	240.93	243.41	0.33422
cpy-	-818.21805	-818.81502	477.29	479.77	0.4201
ct$_2$Bm+	-1151.76111	-1152.70109	921.25	923.73	0.57006
ct$_2$Bpy+	-1307.47005	-1308.57251	1157.16	1159.64	0.65385
ct$_2$PhBm+	-1382.38790	-1383.56429	1139.45	1141.93	0.6657
ct$_2$PhBpy+	-1538.10438	-1539.44231	1375.19	1377.67	0.75208
cm+	-662.12938	-662.55064	243.51	245.99	0.33419
cpy+	-817.79446	-818.38159	475.15	477.63	0.43281
ct$_2$Bm-	-1151.87536	-1152.84150	907.19	909.67	0.61117
ct$_2$Bpy-	-1307.64160	-1308.75946	1143.91	1146.39	0.68279
ct$_2$PhBm-	-1150.50412	-1151.44134	810.89	813.37	0.57801
ct$_2$PhBpy-	-1306.26013	-1307.36108	1049.18	1051.66	0.64276
ctDm-	-1582.33819	-1583.45577	847.18	849.66	0.60465
ctDmpy-	-1738.11082	-1739.40770	1083.95	1086.43	0.69673
ctDpy-	-1893.82592	-1895.26597	1319.39	1321.87	0.78258
ctPhDm-	-1812.96944	-1814.31930	1060.55	1063.03	0.70736
ctPhDpy-	-2124.44758	-2126.11944	1537.24	1539.72	0.87111

Table 5.48: Thermodynamical Data Dissociation 1.R1 (COSMO/THF)

educt	product	ΔH [kJ/mol]	ΔS [kJ/mol·K]	$\Delta_r H$ [kJ/mol]	ΔG [kJ/mol]	K^{298}
cTm	ctDm-	-5.12	-0.01807	416.72	422.11	$1.11 \cdot 10^{-74}$
cTm$_2$n^{tBu}	ctDmpy-	-3.75	-0.01683	223.33	228.35	$9.83 \cdot 10^{-41}$
cTm$_2$n^{tBu}	ctDm-	-0.02	-0.02193	475.18	481.72	$4.00 \cdot 10^{-85}$
cTmn$_2^{tBu}$	ctDpy-	-0.02	-0.54184	283.85	445.40	$9.21 \cdot 10^{-79}$
cTmn$_2^{tBu}$	ctDmpy-	-3.57	-0.01504	282.55	287.03	$5.15 \cdot 10^{-51}$
cTn^{tBu}	ctDpy-	-3.75	-0.01418	342.29	346.52	$1.95 \cdot 10^{-61}$
cPhTm	ctPhDm-	-9.67	-0.00749	390.25	392.48	$1.72 \cdot 10^{-69}$
cPhTn^{tBu}	ctPhDp-	-1.84	-0.00620	302.56	304.41	$4.64 \cdot 10^{-54}$

Table 5.49: Thermodynamical Data Dissociation 2.R1b (COSMO/THF)

educt	product	E_{elec} [H]	E_{elec}^{SP} [H]	E_{elec} [kJ/mol]	E_{elec}^{SP} [kJ/mol]	energy [kJ/mol]
ctDm0	ct$_2$Bm0	0.18371	0.17526	482.33	460.15	-5.91
ctDmpy0	ct$_2$Bm0	0.19575	0.19439	513.94	510.36	-5.07
ctDmpy0	ct$_2$Bpy0	0.12072	0.11739	316.95	308.21	-2.83
ctDpy0	ct$_2$Bpy0	0.13356	0.13942	350.66	366.04	-2.88
ctPhDm0	ct$_2$PhBm0	0.15034	0.11474	394.73	301.25	9.25
ctPhDpy0	ct$_2$PhBpy0	0.11409	0.11827	299.53	310.52	-2.06
ctDm0	ct$_2$Bm+	0.08323	0.07286	218.52	191.31	0.28
ctDmpy0	ct$_2$Bm+	0.07627	0.06449	200.24	169.32	1.51
ctDmpy0	ct$_2$Bpy+	0.08855	0.07799	232.48	204.75	1.06
ctDpy0	ct$_2$Bpy+	0.08238	0.07251	216.30	190.38	1.40
ctPhDm0	ct$_2$PhBm+	0.10298	0.06249	270.36	164.06	13.55
ctPhDpy0	ct$_2$PhBpy+	0.06673	0.05373	175.20	141.07	2.66
ctDm0	ct$_2$Bm-	0.33643	0.31190	883.30	818.90	-11.20
ctDmpy0	ct$_2$Bm-	0.38561	0.35750	1012.43	938.63	-14.69
ctDmpy0	ct$_2$Bpy-	0.28445	0.27050	746.82	710.19	-9.61
ctDpy0	ct$_2$Bpy-	0.33443	0.31900	878.05	837.53	-13.99
ctPhDm0	ct$_2$PhBm-	0.33594	0.29081	882.02	763.53	-6.07
ctPhDpy0	ct$_2$PhBpy-	0.31631	0.29430	830.46	772.70	-19.13

Table 5.50: Thermodynamical Data Dissociation 2.R2 (COSMO/THF)

educt	product	ΔH [kJ/mol]	ΔS [kJ/mol·K]	$\Delta_r H$ [kJ/mol]	ΔG [kJ/mol]	K^{298}
ctDm-	ct$_2$Bm0	0.21	0.01125	134.38	131.02	$1.11 \cdot 10^{-23}$
ctBmpy-	ct$_2$Bm0	-0.20	0.00505	309.89	308.38	$9.34 \cdot 10^{-55}$
ctBmpy-	ct$_2$Bpy0	1.65	-0.00487	181.79	183.24	$7.87 \cdot 10^{-33}$
ctDpy-	ct$_2$Bpy0	2.57	-0.00484	112.76	114.20	$9.82 \cdot 10^{-21}$
ctPhDm-	ct$_2$PhBm0	6.93	0.03826	10.32	-1.09	$1.55 \cdot 10^{0}$
ctPhDpy-	ct$_2$PhBpy0	2.31	0.00222	63.42	62.76	$1.01 \cdot 10^{-11}$
ctDm-	ct$_2$Bm-	-3.18	0.04291	280.94	268.15	$1.05 \cdot 10^{-47}$
ctBmpy-	ct$_2$Bm-	-3.98	0.03781	528.26	516.99	$2.64 \cdot 10^{-91}$
ctBmpy-	ct$_2$Bpy-	-3.23	0.02245	370.09	363.40	$2.15 \cdot 10^{-64}$
ctDpy-	ct$_2$Bpy-	-2.70	0.02358	372.86	365.83	$8.04 \cdot 10^{-65}$
ctPhDm-	ct$_2$PhBm-	-4.01	0.20100	252.86	192.93	$1.58 \cdot 10^{-34}$
ctPhDpy-	ct$_2$PhBpy-	-6.44	0.18898	310.73	254.39	$2.70 \cdot 10^{-45}$

Table 5.51: Thermodynamical Data Dissociation 2.R2b (COSMO/THF)

educt	product	E_{elec} [H]	E_{elec}^{SP} [H]	E_{elec} [kJ/mol]	E_{elec}^{SP} [kJ/mol]	energy [kJ/mol]
ctDm-	ct$_2$Bm0	0.06000	0.05110	157.53	134.17	0.21
ctDmpy-	ct$_2$Bm0	0.11141	0.11811	292.51	310.09	-0.20
ctDmpy-	ct$_2$Bpy0	0.05538	0.06861	145.41	180.14	1.65
ctDpy-	ct$_2$Bpy0	0.04927	0.04197	129.35	110.19	2.57
ctPhDm-	ct$_2$PhBm0	0.01136	0.00129	29.81	3.39	6.93
ctPhDpy-	ct$_2$PhBpy0	0.03278	0.02328	86.05	61.11	2.31
ctDm-	ct$_2$Bm-	0.12325	0.10822	323.60	284.12	-3.18
ctDmpy-	ct$_2$Bm-	0.19367	0.20272	508.48	532.24	-3.98
ctDmpy-	ct$_2$Bpy-	0.12965	0.14219	340.39	373.32	-3.23
ctDpy-	ct$_2$Bpy-	0.14254	0.14305	374.23	375.56	-2.70
ctPhDm-	ct$_2$PhBm-	0.10749	0.09784	282.21	256.87	-6.49
ctPhDpy-	ct$_2$PhBpy-	0.12739	0.12080	334.46	317.17	-8.92

Table 5.52: Dissociation Tm

B-N1 [Å]	E [H]	E_{rel} [H]	E_{rel} [kJ/mol] [kJ/mol]	E^{SP} [H]	E_{rel}^{SP} [H]	E_{rel}^{SP} [kJ/mol]
1.35	-2012.73219	0.02314	60.75	-2014.01210	0.02180	57.23
1.40	-2012.74324	0.01208	31.73	-2014.02267	0.01123	29.49
1.50	-2012.75402	0.00131	3.44	-2014.03278	0.00112	2.93
1.56	-2012.75533	0.00000	0.00	-2014.03390	0.00000	0.00
1.60	-2012.75474	0.00058	1.53	-2014.03325	0.00065	1.72
1.80	-2012.74274	0.01258	33.04	-2014.02127	0.01263	33.16
2.00	-2012.72624	0.02909	76.37	-2014.00527	0.02863	75.16
2.20	-2012.71334	0.04199	110.24	-2013.99250	0.04140	108.69
2.40	-2012.70426	0.05106	134.06	-2013.98452	0.04938	129.65
2.60	-2012.69818	0.05714	150.03	-2013.97952	0.05438	142.78
2.80	-2012.69386	0.06146	161.37	-2013.97610	0.05780	151.76
3.00	-2012.69071	0.06462	169.65	-2013.97356	0.06034	158.43
3.20	-2012.68799	0.06733	176.79	-2013.97133	0.06257	164.29
3.50	-2012.68537	0.06996	183.68	-2013.96910	0.06480	170.13
3.80	-2012.68462	0.07070	185.63	-2013.96867	0.06523	171.25

Table 5.53: Dissociation cTm

B-N1 [Å]	E [H]	E_{rel} [H]	E_{rel} [kJ/mol] [kJ/mol]	E^{SP} [H]	E_{rel}^{SP} [H]	E_{rel}^{SP} [kJ/mol]
1.35	-2012.81724	0.02249	59.04	-2014.10137	0.02112	55.45
1.40	-2012.82824	0.01149	30.17	-2014.11186	0.01063	27.90
1.50	-2012.83863	0.00109	2.87	-2014.12158	0.00091	2.39
1.55	-2012.83973	0.00000	0.00	-2014.12249	0.00000	0.00
1.60	-2012.83902	0.00071	1.85	-2014.12170	0.00079	2.07
1.80	-2012.82617	0.01356	35.60	-2014.10902	0.01347	35.36
2.00	-2012.80851	0.03122	81.97	-2014.09207	0.03042	79.87
2.20	-2012.79374	0.04598	120.73	-2014.07822	0.04427	116.23
2.40	-2012.78371	0.05602	147.08	-2014.06849	0.05400	141.77
2.60	-2012.77790	0.06183	162.33	-2014.06358	0.05891	154.68
2.90	-2012.77255	0.06718	176.37	-2014.05967	0.06282	164.93
3.20	-2012.76856	0.07117	186.86	-2014.05650	0.06599	173.26
3.50	-2012.76586	0.07387	193.94	-2014.05412	0.06837	179.49

Table 5.54: Dissociation ctTm

B-N1 [Å]	E [H]	E_{rel} [H]	E_{rel} [kJ/mol] [kJ/mol]	E^{SP} [H]	E_{rel}^{SP} [H]	E_{rel}^{SP} [kJ/mol]
1.35	-2244.84690	0.02587	67.92	-2246.38227	0.02220	58.29
1.40	-2244.85992	0.01285	33.74	-2246.39315	0.01132	29.73
1.50	-2244.87020	0.00257	6.74	-2246.40280	0.00167	4.39
1.55	-2244.87277	0.00000	0.00	-2246.40447	0.00000	0.00
1.60	-2244.87167	0.00109	2.87	-2246.40422	0.00026	0.67
1.80	-2244.85585	0.01692	44.42	-2246.38926	0.01522	39.95
2.10	-2244.83363	0.03914	102.77	-2246.36667	0.03781	99.26
2.40	-2244.81436	0.05840	153.34	-2246.34895	0.05552	145.76
2.70	-2244.81870	0.05407	141.95	-2246.35000	0.05447	143.01
3.00	-2244.82680	0.04597	120.69	-2246.35885	0.04563	119.79
3.30	-2244.83119	0.04158	109.16	-2246.36428	0.04019	105.52
3.60	-2244.83297	0.03980	104.50	-2246.36710	0.03737	98.11
3.80	-2244.83381	0.03895	102.27	-2246.36847	0.03600	94.52

Table 5.55: Dissociation ctDm

B-N1 [Å]	E [H]	E_{rel} [H]	E_{rel} [kJ/mol] [kJ/mol]	E^{SP} [H]	E_{rel}^{SP} [H]	E_{rel}^{SP} [kJ/mol]
1.35	-1582.30328	0.01962	51.52	-1583.41135	0.01861	48.86
1.40	-1582.31343	0.00947	24.87	-1583.42105	0.00891	23.41
1.50	-1582.32233	0.00058	1.51	-1583.42946	0.00051	1.33
1.54	-1582.32291	0.00000	0.00	-1583.42996	0.00000	0.00
1.60	-1582.32143	0.00147	3.87	-1583.42845	0.00151	3.97
1.80	-1582.30601	0.01689	44.36	-1583.41344	0.01653	43.39
2.10	-1582.27672	0.04618	121.26	-1583.38576	0.04420	116.06
2.40	-1582.25497	0.06793	178.35	-1583.36595	0.06401	168.06
2.70	-1582.24212	0.08079	212.10	-1583.35528	0.07468	196.08
3.00	-1582.24237	0.08054	211.46	-1583.35475	0.07521	197.46
3.30	-1582.24149	0.08142	213.76	-1583.35446	0.07550	198.24
3.60	-1582.24034	0.08256	216.77	-1583.35371	0.07625	200.20
3.80	-1582.23961	0.08330	218.71	-1583.35285	0.07711	202.46

Table 5.56: Dissociation PhTm

B-N1 [Å]	E [H]	E_{rel} [H]	E_{rel} [kJ/mol] [kJ/mol]	E^{SP} [H]	E^{SP}_{rel} [H]	E^{SP}_{rel} [kJ/mol]
1.35	-2243.35422	0.02717	71.33	-2244.86743	0.02652	69.62
1.40	-2243.36623	0.01515	39.79	-2244.87901	0.01494	39.22
1.50	-2243.37871	0.00268	7.03	-2244.89079	0.00315	8.28
1.59	-2243.38139	0.00000	0.00	-2244.89395	0.00000	0.00
1.60	-2243.38120	0.00018	0.48	-2244.89302	0.00093	2.44
1.80	-2243.37280	0.00859	22.55	-2244.88449	0.00946	24.84
2.10	-2243.35567	0.02571	67.51	-2244.86761	0.02634	69.15
2.40	-2243.34389	0.03750	98.45	-2244.85749	0.03645	95.71
2.70	-2243.33669	0.04470	117.36	-2244.85196	0.04199	110.25
3.00	-2243.33191	0.04948	129.91	-2244.84846	0.04549	119.43
3.30	-2243.32833	0.05306	139.32	-2244.84545	0.04849	127.32
3.60	-2243.32595	0.05543	145.54	-2244.84297	0.05097	133.83

Table 5.57: Dissociation tPhDm

B-N1 [Å]	E [H]	E_{rel} [H]	E_{rel} [kJ/mol] [kJ/mol]	E^{SP} [H]	E^{SP}_{rel} [H]	E^{SP}_{rel} [kJ/mol]
1.35	-1812.91410	0.01888	49.57	-1814.25498	0.01767	46.38
1.40	-1812.92377	0.00921	24.19	-1814.26394	0.00871	22.86
1.50	-1812.93247	0.00051	1.34	-1814.27222	0.00043	1.13
1.54	-1812.93298	0.00000	0.00	-1814.27265	0.00000	0.00
1.60	-1812.93155	0.00143	3.75	-1814.27122	0.00142	3.74
1.80	-1812.91599	0.01700	44.62	-1814.25622	0.01643	43.14
2.10	-1812.88608	0.04691	123.15	-1814.22799	0.04466	117.25
2.40	-1812.86291	0.07007	183.97	-1814.20682	0.06582	172.82
2.70	-1812.84811	0.08487	222.84	-1814.19376	0.07889	207.13
3.00	-1812.83890	0.09408	247.01	-1814.18591	0.08673	227.72
3.30	-1812.83185	0.10113	265.52	-1814.17960	0.09305	244.31
3.80	-1812.83239	0.10060	264.12	-1814.18006	0.09259	243.09

Table 5.58: Dissociation cTn^{tBu}

B-N1 [Å]	E [H]	E_{rel} [H]	E_{rel} [kJ/mol] [kJ/mol]	E^{SP} [H]	E^{SP}_{rel} [H]	E^{SP}_{rel} [kJ/mol]
1.30	-2479.95224	0.04043	106.14	-2481.72281	0.03844	100.92
1.40	-2479.98025	0.01242	32.60	-2481.74957	0.01167	30.64
1.50	-2479.99123	0.00144	3.78	-2481.75996	0.00128	3.37
1.56	-2479.99267	0.00000	0.00	-2481.76125	0.00000	0.00
1.60	-2479.99213	0.00054	1.42	-2481.76076	0.00049	1.28
1.80	-2479.97998	0.01268	33.30	-2481.74900	0.01225	32.16
2.10	-2479.95523	0.03744	98.29	-2481.72534	0.03591	94.27
2.40	-2479.93694	0.05573	146.31	-2481.70880	0.05244	137.69
2.70	-2479.92950	0.06317	165.84	-2481.70408	0.05717	150.10
3.00	-2479.93128	0.06138	161.17	-2481.70708	0.05416	142.21
3.30	-2479.93687	0.05580	146.50	-2481.71240	0.04884	128.24
3.60	-2479.93866	0.05401	141.80	-2481.71482	0.04643	121.90
3.80	-2479.93859	0.05408	141.99	-2481.71532	0.04593	120.58

Table 5.59: Dissociation ctDpy

B-N1 [Å]	E [H]	E_{rel} [H]	E_{rel} [kJ/mol] [kJ/mol]	E^{SP} [H]	E^{SP}_{rel} [H]	E^{SP}_{rel} [kJ/mol]
1.35	-1893.71902	0.02282	59.91	-1895.15432	0.02182	57.29
1.40	-1893.72999	0.01185	31.11	-1895.16488	0.01125	29.55
1.50	-1893.74050	0.00134	3.52	-1895.17485	0.00129	3.38
1.56	-1893.74184	0.00000	0.00	-1895.17614	0.00000	0.00
1.60	-1893.74139	0.00045	1.19	-1895.17575	0.00039	1.02
1.80	-1893.72917	0.01267	33.27	-1895.16407	0.01207	31.68
2.10	-1893.70420	0.03764	98.83	-1895.14061	0.03553	93.28
2.40	-1893.68628	0.05557	145.89	-1895.12477	0.05137	134.87
2.70	-1893.67413	0.06771	177.77	-1895.11413	0.06200	162.79
3.00	-1893.66925	0.07260	190.60	-1895.10902	0.06711	176.21
3.30	-1893.68977	0.05207	136.71	-1895.12665	0.04949	129.94
3.60	-1893.69321	0.04863	127.68	-1895.13028	0.04586	120.41
3.80	-1893.69371	0.04813	126.37	-1895.13115	0.04499	118.13

Table 5.60: Polynomial fit parameters

	a1	a2	a3	a4	a5	a6	a7
ctTm	-16.31	974.94	-1632.11	1252.53	-566.20	152.07	-18.48
cTn^{tBu}	-4.39	905.16	-1691.71	1572.56	-861.48	259.22	-32.34
ctTn^{tBu}	-19.59	1176.54	-2679.80	3111.15	-2022.31	677.92	-90.22
ctDn^{tBu}	10.85	944.81	-2376.98	3058.44	-2101.73	712.46	-93.31

Table 5.61: Thermodynamical Data Tautomerism I

tautomer	E_{elec} [H]	E^{SP}_{elec} [H]	energy [kJ/mol]	ΔH [kJ/mol]	ΔS [kJ/mol·K]
mSH	-662.97	-663.39	266.22	268.70	0.35976
mNH	-662.99	-663.41	274.54	277.02	0.34554
cmSH	-662.98	-663.40	266.72	269.20	0.34598
cmNH	-663.00	-663.42	275.48	277.96	0.33741
n^{tBu}SH	-818.697	-819.28	500.94	503.42	0.44438
n^{tBu}NH	-818.71	-819.29	511.62	514.10	0.44142
cn^{tBu}SH	-818.70	-819.29	502.4	504.89	0.42904
cn^{tBu}NH	-818.72	-819.30	513.12	60	0.4232

Table 5.62: Thermodynamical Data Tautomerism II

equilibrium	E_{elec} [H]	E^{SP}_{elec} [H]	E_{elec} [kJ/mol]	E^{SP}_{elec} [kJ/mol]	energy [kJ/mol]
mSH − mNH	-0.02060	-0.01827	-54.10	-47.97	8.32
cmSH − cmNH	-0.02492	-0.02384	-65.44	-62.59	8.76
n^{tBu}SH − n^{tBu}NH	-0.01611	-0.01340	-42.30	-35.19	10.68
cn^{tBu}SH − cn^{tBu}NH	-0.01830	-0.01692	-48.04	-44.43	10.72